



**UCGE Reports
Number 20197**

Department of Geomatics Engineering

**A Feasibility Study for Real-Time Detection and
Georeferencing of Forest Fire Hot Spots**

(URL: <http://www.geomatics.ucalgary.ca/links/GradTheses.html>)

by

David Bruce Wright

May 2004



UNIVERSITY OF
CALGARY

UNIVERSITY OF CALGARY

A Feasibility Study for Real-Time Detection and Georeferencing
of Forest Fire Hot Spots

by

David Bruce Wright

A THESIS

SUBMITTED TO THE FACULTY OF GRADUATE STUDIES
IN PARTIAL FULFILMENT OF THE REQUIREMENTS FOR THE
DEGREE OF MASTER OF SCIENCE

DEPARTMENT OF GEOMATICS ENGINEERING

CALGARY, ALBERTA

May, 2004

© David Bruce Wright 2004

Abstract

This research explores the issues involved in developing a real-time system for the detection and georeferencing of forest fire hot spots. The system integrates a wide area differential GPS receiver, an inertial measurement unit and thermal video camera. The research discusses the specific issues encountered with synchronizing the georeferencing information with the thermal video images. Thermal imaging concepts are presented, with specific discussion of the issues related to the identification, extraction, and tracking of forest fire hot spots. System testing indicates that the real-time identification, extraction and tracking of hot spots, combined with real-time positioning from WADGPS allowed for the automatic georeferencing of targets to within 2 m at survey altitudes near 350 m. With the feasibility of this system confirmed from these results, specific issues encountered with the development of real-time software on a Windows 2000 platform highlight the non-deterministic or soft real-time characteristics of Windows 2000. Although this research has provided promising results, further testing and acquisition of thermal imaging during realistic forest fire conditions is required to confirm consistent and repeatable results.

Acknowledgements

I would first like to express my sincerest gratitude to Dr. Naser El-Sheimy. His patience, support, and guidance have been invaluable. He knew when to push and when to sit back; and through all of it, he was supportive while letting me complete this thesis my way.

Many thanks have to go to my colleagues and friends. To Cameron Ellum, Thilanka Galappaththi, Andrew Hunter, Michael Kern, and Anastasia Salycheva for our many discussions and conversations.

Special thanks go to Joyce Metcalfe and Kelly Wright for pointing out my many grammatical inconsistencies and for our many conversations.

Finally thanks are given to my family. To my brother and sister-in-law for their unquestioned support. Most of all, my deepest gratitude and thanks goes to my parents - for their love, support, guidance, and encouragement through out the years. All I am, I owe to them.

Table of Contents

Approval Page	ii
ABSTRACT	iii
ACKNOWLEDGEMENTS	iv
LIST OF FIGURES	ix
LIST OF TABLES	xi
NOTATION CONVENTIONS, COORDINATE FRAMES AND ACRONYMS	xii
CHAPTER 1	
INTRODUCTION	1
1.1 Forest Fire Characteristics	4
1.2 Overview of Forest Fire Detection Methodology	5
1.3 Research Objective	7
1.4 Thesis Outline	8
CHAPTER 2	
GEOREFERENCING	11
2.1 Georeferencing Concepts	11
2.2 General Direct Georeferencing System Model	14
2.2.1 Camera Position and Orientation	15
2.2.2 Thermal Imager Geometric Camera Model	17
2.3 Unknown Parameter Determination	23
2.3.1 Thermal Camera Geometric Calibration	23
2.3.2 Boresight Alignment	27
2.3.3 Lever Arm Offset Determination	29
2.4 3D Space Intersection	30

2.5	Wide Area Differential GPS: WAAS And OmniStar	31
2.6	Inertial Motion Unit : IMU	33
2.7	Georeferencing Summary	34
CHAPTER 3		
THERMAL IMAGING BACKGROUND		35
3.1	Black Body Radiation	36
3.2	Heat Transfer Terminology And Definitions	40
3.2.1	Absorptivity And Absorptance	40
3.2.2	Reflectivity And Reflectance	40
3.2.3	Transmissivity And Transmittance	40
3.2.4	Angle Of Incidence	41
3.2.5	Emissivity And Emittance	41
3.2.6	Black Vs. Grey Vs. Real Bodies	41
3.2.7	Energy Conversion	42
3.2.8	Solar Gain	42
3.2.9	Thermal Equilibrium	43
3.3	Thermal Imagers	44
3.3.1	Wavelength Selection Issues	45
3.4	Thermal Image Processing	46
3.4.1	Thermal Image Systematic Errors	47
3.5	Thermal Imaging Background Summary	54
CHAPTER 4		
FOREST FIRE DETECTION FROM THERMAL IMAGERY		55
4.1	Hot Spot Characteristics	55
4.1.1	Thermally Imaged Fire Spatial Characteristics	56
4.2	Image Processing Terminology	58
4.3	Thermal Image Systematic Error Corrections	60
4.4	Initial Feature Identification	63
4.4.1	Feature Extraction	64
4.5	Feature Tracking And Enhanced Feature Identification	66
4.5.1	Pixel Motion Estimation	68
4.5.2	Feature Cross Referencing And Tracking	71
4.6	Hot Spot Evaluation	74

4.7	Forest Fire Detection from Thermal imagery Summary	76
CHAPTER 5		
REAL TIME SYSTEM INTEGRATION		
5.1	Real-time Systems Overview	77
5.1.1	Real-time Definitions	78
5.1.2	Real-time Systems Specification and Design	80
5.1.3	Real-time Image Processing Issues	82
5.1.4	Synchronization Issues	84
5.1.5	System Speed	88
5.2	Hot Spot Detection System Development	88
5.2.1	System Integration Overview	89
5.2.1.1	Software Operating System	90
5.2.2	System Software Design	93
5.2.3	System Synchronization	93
5.2.3.1	Video To Georeferencing Data Synchronization	94
5.2.3.2	Storage Synchronization	96
5.3	System Structure and Data Flow	99
5.3.1	Video Modules	100
5.3.1.1	Video Processing Sub Module	101
5.3.2	Remaining System Modules	103
5.4	System Integration Summary	106
CHAPTER 6		
TESTS AND RESULTS		
6.1	Equipment Configuration and Test Environment	107
6.2	WADGPS / IMU Results	111
6.3	Camera Geometric Calibration and Alignment Results	117
6.4	Real-Time System Performance Results	120
6.4.1	Video Sub-System Performance	120
6.4.2	WADGPS/IMU Georeferencing Sub-System Capture Performance	124
6.5	Image Processing Performance	127
6.6	3D Space Intersection Results	130
6.7	Testing and Results Summary	136

CHAPTER 7	
SUMMARY AND RECOMMENDATIONS	137
7.1 Conclusions	138
7.2 Specific Contributions	139
7.3 Recommendations	139
REFERENCES	140

List of Figures

Figure 2-1: Diagram of Equation 2-1 Parameter Relationships	14
Figure 2-2: Diagram of Equation 2-2 Parameter Relationships	15
Figure 2-3: Camera Perspective Center to Hot Spot Relationship.....	17
Figure 2-4: Positive Image Plane.....	19
Figure 2-5: Negative and Positive Radial Distortion Examples.....	20
Figure 2-6: Decentering Distortion Example	20
Figure 2-7: Sample Camera Calibration Image	26
Figure 3-1: Black Body Radiation Across Applicable Wavelengths	36
Figure 3-2: Relative Power by Temperature and IR Band	39
Figure 3-3: Basic Frame by Frame Image Statistics.....	49
Figure 3-4: Systematic Frame Pixel Intensity Profile	50
Figure 3-5: Thermal Images of Controlled Temperature Bath	51
Figure 3-6: Difference In Low Temperature Thermal Images	51
Figure 3-7: Thermal Imager Pixel Histogram Distribution	52
Figure 3-8: Systematic Image Noise Examples	53
Figure 4-1: Hot Spot Characteristic Diagram.....	57
Figure 4-3: Background Correction Method 1.....	61
Figure 4-4: Background Correction Method 2.....	62
Figure 4-5: Final Image Processing for Feature Identification	64
Figure 4-6: Feature Extraction Logic Kernel	65
Figure 4-7: Sample Frames Representing Hot Spot Motion Through Frame	68
Figure 4-8: Pixel Motion Estimate Due to Speed and Flying Height	70
Figure 4-9: Feature Track Comparisons.....	72
Figure 4-10: Feature Correspondence Correlation Tests.	73
Figure 4-11: Small Partially Obscured Hot Spot Tracks	75
Figure 5-1: Forest Fire Hot Spot Detection System Overview	89
Figure 5-2: Synchronization Timing Chart	94
Figure 5-3: Queue / Sync. Thread Internal Structure.....	96
Figure 5-4: Serial Port Capture - Save - Parse Flow	97
Figure 5-5: Video Module Flow.....	100
Figure 5-6: Image Processing Flow Modification.....	102
Figure 5-7: Remainder of System Data Flow Diagram	103
Figure 5-8: Cross Reference Thread Internal Structure.....	105
Figure 6-1: Examples of Target Hot Spots	109

Figure 6-2: Tree Canopy Coverage of the Test Hot Spots	110
Figure 6-3: Night Flight 3D Position Error	112
Figure 6-4: Day Flight 3D Position Error	112
Figure 6-5: Night Test Flight Path with 3D Error Range by Location	113
Figure 6-6: Day Test Flight Path with 3D Error Range by Location	114
Figure 6-7: Night Flight Post Processed to Real-time Attitude Comparison	116
Figure 6-8: Day Flight Post Processed to Real-time Attitude Comparison	116
Figure 6-9: Multi-Frame Storage Test Results.....	121
Figure 6-10: Storage Non Deterministic Behavior	121
Figure 6-11: Actual Frame Times and Video Slips	122
Figure 6-12: Lost and Duplicated Video Frames	123
Figure 6-13: Comparison between Video Timing Signal and GPS Mark Time .	126
Figure 6-14: Comparison between VTS Frame to Frame Time Difference and MT Frame to Frame Time Difference	126

List of Tables

Table 2-1: Post-Mission and Real-time Mapping System Differences	13
Table 2-2: IMU Performance Accuracy	34
Table 3-1: Thermal Wavelength Definitions	37
Table 4-1: Pixel Motion Estimate Due to Attitude Variations	70
Table 5-1: Polling Rate for Serial Data	98
Table 5-2: Outline of Capture Thread Internal Data Flow	99
Table 5-3: Image Processing Function Computational Order	102
Table 6-1: Geo-Referencing System and Camera Mount	108
Table 6-2: Critical Computer System Specifications	108
Table 6-3: Hot Spot Co-ordinates	109
Table 6-4: 3D Error Statistics (meter)	115
Table 6-5: Attitude Error Statistics (degrees.)	117
Table 6-6: Camera Calibration Results	118
Table 6-7: Lever Arm Offset Values	118
Table 6-8: Boresight Calibration Results with Sample Alignment Images	119
Table 6-9: Video Capture and Save Statistics	124
Table 6-10: Georeferencing Sub-System Capture Statistics	125
Table 6-11: Image Processing Performance	128
Table 6-12: Tracking and Georeferencing Performance (millisecond)	129
Table 6-13: Night Test Calculated Position Errors, meters Using Post Processed Georeferencing Data.	131
Table 6-14: Re-Calibrated Boresight Alignment	132
Table 6-15: Night Test Calculated Position Errors, meters Using Post Processed Georeferencing Data and Re-Calibrated Boresight.	133
Table 6-16: Night Test Calculated Position Errors, meters Using WAAS Georeferencing Data and Re-Calibrated Boresight	134
Table 6-17: Day Test Calculated 2D Horizontal Position Errors, meters	135

Notation Conventions, Coordinate Frames and Acronyms

Notation Conventions

- Vectors are represented with boldface lower case letters: \mathbf{r}
- Matrices are represented with boldface upper case R: \mathbf{R}
- The coordinate frames used in a vector relationship or matrix transformation are specified as from the subscript frame to the superscript frame: \mathbf{r}_p^M indicates the vector of object point (P) in the mapping (M) frame. \mathbf{R}_c^b Indicates that the rotation matrix \mathbf{R} is for transforming vectors from the camera (c) frame to the body (b) frame.
- *Vector* means components of a vector: x_p^C , y_p^C , and z_p^C are the components of vector $\mathbf{r}_p^C = [x_p^C \quad y_p^C \quad z_p^C]^T$.
- Rotation Matrix $\mathbf{R} = \mathbf{R}_z \mathbf{R}_y \mathbf{R}_x$: \mathbf{R}_z is the rotation matrix around the z axis, \mathbf{R}_y around the y axis, and \mathbf{R}_x is around the x axis.

Coordinate Frames

- Mapping Frame:
Consists of the geodetic longitude, latitude and height or altitude. Standard mapping convention. Standard GPS output based on WGS-84 ellipsoid.

- Earth Centered Earth Fixed (ECEF) Frame:
 - Origin at center of mass of the Earth.
 - X-axis orthogonal to the z-axis, on the mean Greenwich meridian plane
 - Y-axis completes the right handed 3D Cartesian coordinate system.
 - Z-axis aligned through the mean spin axis of the Earth.

- Local Tangential Plane:
 - Origin at locally selected mapping frame point.
 - X-axis: Local Tangential east.
 - Y-axis: Local Tangential north.
 - Z-axis: Local Altitude.

- Body Frame of Aircraft:
 - Origin at center of center of rotation of Inertial motion unit.
 - X-axis: points to the right hand side of IMU when looking forward along length of aircraft.
 - Y-axis: points forward of the IMU along the longitudinal or length of aircraft.
 - Z-Axis: points upward or vertical from the IMU relative to the local tangential plane.

Acronyms

- 2D Two Dimensional
- 3D Three Dimensional
- AHRS Attitude And Heading Reference System
- ATT Attitude Log
- BBQ Barbecue

- BDS Novatel Black Diamond System
- CPU Central Processing Unit
- DGPS Differential Global Positioning System
- FAA Us Federal Aviation Administration
- FIFO First In First Out
- FOV Field Of View
- GCP Ground Control Point
- GIS Geographical Information System
- GPS Global Positioning System
- HDD Hard Disk Drive
- HZ Hertz
- I/O Input / Output
- IMU Inertial Measurement Unit
- IR Infrared
- LWIR Long wave Infrared
- m² Metres Squared
- MHz Megahertz
- MMS Mobile Mapping System
- MMSS Mobile Multi Sensor System
- ms Milliseconds
- MT Mark Time Log
- MWIR Mid Wave Infrared
- NIR Near Infrared
- NT New Technology - Original Term For Microsoft Windows 32 Bit Operating Systems
- NTSC National Television Standards Committee
- O() Magnitude Order Of Operations
- OMNI Omnistar

- OS Operating System
- PIII Pentium Three
- RAM Random Access Memory
- RMSE Root Mean Square Error
- RS-170 Video Standard
- SatLoc Commercial Wadgps Receivers
- SI Space Intersection Function
- SWIR Short Wave Infrared
- um micrometre
- UML Unified Modeling Language
- USB-2 Universal Serial Bus Generation, Second Generation
- UTC Universal Time Code
- VTS Video Timing Signal
- WAAS Wide Area Augmented System
- WADGPS Wide Area Differential Global Positioning System
- WDM Windows Driver Model

Chapter 1

Introduction

Mobile Mapping Systems (MMS) have become an emerging trend in mapping applications because they allow a task-oriented implementation of geodetic concepts at the measurement level (Schwarz and El-Sheimy, 1996). Major progress has been made in Mobile Multi-Sensor Systems (MMSS) over the last few years in terms of sensor resolution, data rate and operational flexibility. Thus, the use of multiple sensors in mapping and Geographic Information Systems (GIS) applications has become very attractive. Examples of mobile multi-sensor systems can be found in airborne remote sensing (Mostafa, 1999)(Skaloud, 1999), airborne laser scanning (Krabil and Wright, 2000)(Morin and El-Sheimy, 2002), mobile mapping vans and trains (Benning and Tussems, 1998)(Blaho and Toth, 1995)(El-Sheimy, 1996)(Graefe, et al, 2001)(Li, et al, 2001), and portable mobile mapping systems (Ellum, 2001)(Hunter, 2002). These systems have a common feature, as the sensors necessary to solve a specific problem are mounted on a common platform. Accurate synchronization of the data streams allows for the solution of the mapping problem by using data from one integrated measurement process only. The post-mission integration of results from a

number of disjoint measurement processes avoids inherent errors and results in greater conceptual clarity, task-oriented system design and data flow optimization. In most cases, it also offers the potential for real-time solution, which is becoming more important in many applications.

After data are collected using a vehicle (van, airplane or ship), information of interest is processed off site and extracted in the post-mission mode of operation, resulting in a high degree of accuracy in determining both position (≤ 0.1 m "RMSE") and attitude (≈ 0.02 degrees "RMSE"). The position accuracy is accomplished by using the precise GPS carrier phase in differential mode, known as DGPS. DGPS uses two GPS receivers, one in static mode over a known control point and the second on the vehicle (Santerre and St-Pierre, 1999)(Teunissen and Kleusberg, 1999). The attitude accuracy is accomplished by tightly coupling DGPS and INS data through Kalman filtering (Shin and El-Sheimy, 2002)(Farrell and Barth, 1999).

In many remote-sensing applications, there is no need for real-time processing of the data. Therefore, post-mission processing is adequate. However, many emerging remote sensing applications, specifically forest fire fighting, require real-time mapping rather than the highest possible accuracy. Understanding the size, location, and speed of advance of the fire front is critical to optimal allocation of fire fighting resources and maintaining fire crew safety. Investigations of major wild-land fire accidents involving loss of life often indicate

that insufficient or untimely information about the location and speed of advance of the fire imperilled the fire crews (Holtz, 2001). Development of a real-time forest fire hot spot detection system would save the lives of many forest fire fighters.

Problem Statement and Motivation

World-wide, forests and other wooded areas cover about 40 percent of the Earth's land area and generate substantial goods and services of benefit to humanity. Canada, for example, has an area of over 997 million hectares, of which nearly 418 million hectares are forested, representing about ten percent of the world's forests (CNFDP Area statistics, 2003). Over fifty-eight percent (CNFDP Area statistics, 2003) of Canada's forest is commercially productive, contributing in excess of \$44 billion (CNFDP Economic Statistics, 2003) to the economy annually. Wild-land fires in Canada, however, are a threat to this resource. On average, 8,900 fires burn over two million hectares annually (CNFDP Forest Fire Statistics, 2003), of which 602,000 hectares are commercially productive forest. This is equivalent to over 70 million m³ of productive forest or nearly a third of the annual average harvest of 163 million m³ (CNFDP Forest Fire Statistics, 2003). In addition, fire management costs average \$384 million per year, or 22% of Canada's forest management budget (CNFDP Expenditure Statistics, 2003). Moreover, fire related financial losses amount to more than \$5.07 billion per year (CNFDP Forest Fire Statistics, 2003).

The economic importance of the forest industry in Canada has generated extensive research into understanding and modeling forest fire behaviour to facilitate the prediction and evaluation of fire potential.

1.1 Forest Fire Characteristics

Several variables affect the size, spread, and eventual destructive costs of fires. A great deal of time and energy is spent in the suppression of fires, and the faster they are detected, the better. Success in pre-suppression planning and actual suppression of wildfires is directly related to how well forest management agencies understand and predict fire (ASRD Forest Protection, 2004)(Martell, 2001). For the purpose of this thesis though, general thermal forest fire characteristics have been reviewed to extend the understanding of the detection requirements.

Common terms used in describing fire behaviour and characteristics (ASRD Wildfire Behaviour, 2004) include:

- Smouldering - fire burning without flame and barely spreading
- Creeping - fire spreading slowly over the ground, generally with low flame
- Running - fire rapidly spreading and with a well-defined head
- Torching (Synonym: Candle or Candling) - – igniting and flaring up, usually from bottom to top, of the foliage of single or small clumps of trees

- Spotting - fire-producing firebrands carried by the surface wind, a fire whirl, and/or convection column that fall beyond the main fire perimeter resulting in spot fires
- Crowning - fire ascending into the crowns of trees and spreading from crown to crown

Certain fire behaviours are easy to observe, but some can be difficult to detect and allow apparently innocuous fires to grow into dangerous and damaging infernos on a moment's notice. A smouldering or creeping fire may remain undetected for several days or even weeks after initial ignition, yet can quickly grow to become a running or spotting fire from a change in the wind speed or direction.

1.2 Overview of Forest Fire Detection Methodology

A principal goal of forest fire detection is to find and report fires when they are still small. A small fire is easier to contain and suppress, mitigating both costs and losses. Detection methodologies include indirect or direct systems (ASRD Wildfire Detection, 2004)(Martell, 2001 pp. 558-563). Indirect systems rely on the public to report any signs of fire that are observed. It is in the public's best interest to help protect society from the potentially destructive force of a forest fire. The costs of public awareness programs are minimal. Such programs are aimed at teaching the public about the dangers of fire and how to report fire sightings.

Direct systems, including lookout towers, lightning detection systems and patrol aircraft are employed by forest management agencies to monitor large forested areas. Positioning of lookout towers is guided by general fire risk factors. High-risk areas are determined through the use of fire behaviour models incorporating weather history, topography, forest structure and fuel complex information. Towers are then positioned to optimize continuous monitoring of high-risk areas identified within the forest. Analysis of current weather conditions enables forestry management agencies to augment existing lookout towers by dispatching patrol aircraft. Aircraft are also used in areas where towers are not feasible. Patrols look for specific fire indicators, such as smoke and flame, and generally cover wide areas with each patrol pass.

Once a fire has been detected and a suppression campaign has started, the fire perimeter must be monitored carefully to prevent certain fire behaviours, such as spotting and smouldering, from starting new fires. Fire perimeter mapping and post-suppression surveying are two areas where thermal imaging technology is utilized effectively. Post-suppression surveys, through low-level air patrols of the fire perimeter using a thermal imager, ensure that contained and controlled fires have not jumped firebreaks. Higher altitude flights are used to map the fire perimeter and a mosaic of the area is done from the thermal images. Documenting the location of hot spots outside the firebreaks is time consuming

and potentially inaccurate. There is clearly a need to timely, accurate reporting of new hot spots from the survey.

1.3 Research Objective

The main objective of this thesis is the development of a real-time forest fire hot spot detection system, combining a thermal video camera, an integrated WADGPS and IMU georeferencing unit, and a video logging and processing computer into a system that can be readily mounted into a patrol aircraft.

This system will:

- Automatically identify forest fire hot spots during night and day operations using thermal imaging technology.
- Locate hot spots within 10 meters, from an aircraft or a helicopter platform, using the georeferenced thermal images.
- Report and document these results in real time, which in this case is 1 minute.

To achieve this research objective, the following tasks needed to be addressed:

- Selection of thermal imager and video capture hardware.
- Development of custom multimedia capture and process software. The video data and georeferencing data must be synchronized precisely to streamline the three-dimensional (3D) space intersection processing of the identified hot spots. This also requires storage of all collected data in a single system.

- Adaptation of a geometric camera calibration methodology to the thermal imager.
- Investigation of factors affecting the final accuracy of the integrated system.
- Testing of the prototype system under day and night operating conditions using controlled surveyed target fires in a lightly forested environment to observe obscuration effects.

1.4 Thesis Outline

A discussion of georeferencing concepts leading to the direct georeferencing system model begins in Chapter 2. The accuracy of each component of the model is described and error sources and any calibration and alignment requirements are detailed. The application specific photogrammetric issues are presented, starting with the general camera model. The geometric calibration approach used for the thermal imager is shown, with an example of the actual calibration images from the thermal imager. The boresight alignment process and the 3D space intersection process are described. Background information on the WADGPS and IMU systems used is also provided, including accuracy expectations.

Chapter 3 starts with a discussion of heat transfer concepts, leading to those specifically related to thermal imaging. These concepts are used to explain some of the benefits and limitations of the different thermal imaging technologies

leading to the selection of the particular thermal imaging camera that was used in the hot spot detection system.

Chapter 4 applies the specific heat transfer concepts and thermal imaging issues presented in Chapter 3 to explain some of the issues related to forest fire detection. Various thermal images are included to highlight these specific issues. From the application specific thermal imaging issues, the specific image processing requirements and methodology to address those issues is presented, as well as the remaining data processing requirements to prepare the extracted image feature data for integration with the geo-processing requirements presented in Chapter 2.

In Chapter 5, a general overview of real-time systems and real-time system design issues is presented first. With this general information, the system integration issues are discussed in more detail. A system synchronization methodology is presented and then any special issues of the various system components are discussed. Special emphasis is given to the software integration and any hardware or software specific issues that required additional consideration to adapt the various modules to work in a real-time framework for the final system.

In Chapter 6, the testing and analysis of results are presented. The system testing took place over a control test area in Calgary on July 30 and 31, 2002. The test area was a public picnic area in which controlled fires were set in

surveyed fire and barbecue pits. An analysis of the WADGPS / IMU performance and overall real-time system performance, thermal image segmentation and georeferenced fire results are presented. The performance of the real-time WADGPS and IMU results are compared to the post processed DGPS and IMU results. The calibration results for the boresight alignment and lever-arm offset are also presented. Then an analysis of the real-time performance of the system is done. Two critical areas were specifically examined: the integrity of the captured data and synchronization quality and the image processing and georeferencing processing time requirements. Finally the results of the 3D space intersection process on the automatically extracted hot spot feature tracks are compared to the actual surveyed positions.

The final summary of the research work is presented in Chapter 7. This includes any conclusions and specific contributions of the research, as well as recommendations for further research and development directions.

Chapter 2

Georeferencing

This chapter starts with a general overview of georeferencing imaging sensors and continues with a detailed model of the direct georeferencing approach. The specific model components are presented, along with a description of how the various unknown model parameters are obtained, including discussion on the error sources and accuracy expectations. Finally, the computations required to determine a fully georeferenced hot spot are presented.

2.1 Georeferencing Concepts

Georeferencing is the process of relating specific information to the real world coordinate system. Georeferencing of specific features from photos and images requires the determination of the camera position, orientation and geometric characteristics. These are defined as the camera external orientation (3 positions and 3 orientations) at the time of exposure and the internal orientation parameters (focal length, coordinates of principal point, and lens distortion).

The traditional approach to georeferencing is referred to as Indirect georeferencing. The proper georeferencing of aerial images by indirect methods requires knowledge of the position of predetermined ground control points (GCPs) and identifiable tie points in the images. This approach was dictated by

the technology available. Observed GCPs are used to determine the exterior orientation of the images, which requires that a complete ground control survey has been completed for the area and that the GCPs are readily identifiable by some image processing mechanism. The survey, placement and maintenance of these GCPs is both time consuming and expensive, and also must be already in place before the aerial survey takes place.

Conversely, direct georeferencing measures the position and attitude, or alignment, of the images through the mounting of the navigation sensors, such as GPS and an inertial motion unit (IMU), in the vehicle. The accuracy and synchronization of both these components with the camera is critical to the desired result, which is the recording of the position and orientation of the camera for every image. Direct georeferencing is becoming more common as the cost of high quality and high accuracy GPS and IMU systems decreases. In addition, the removal of maintenance costs associated with GCPs has led to the development of more mobile multi-sensor mapping systems. Examples include Ellum's (2001) personal portable system and El-Sheimy's (1996) ground-based vehicle system, both of which also mount all sensor components (camera, IMU, GPS) on a common rigid platform.

Some specific issues that differentiate a typical direct georeferencing mapping system from the real-time mapping system required for this research are briefly outlined in Table 2-1. The differences outlined in Table 2-1 lead to interpreting

the direct georeferencing system model, as presented by Ellum (2001) and El-Sheimy (1996), in specific parts that separate the real-time data processing requirements from the fixed or pre-processed data.

Table 2-1: Post-Mission and Real-time Mapping System Differences

	Typical Mapping Requirements	Forest Fire Hot Spot Detection System Real-time Requirements
Setup Time	Not critical.	2 Hours or less.
Reporting Time	Hours to Days	1 minute or less.
Position	DGPS in post mission processing with high accuracy requirements: cm level.	Real-time WADGPS with medium accuracy requirements: meter level
Orientation	Post-mission processing with high accuracy requirements: 0.05 - 0.1 degrees	Real-time with medium to high accuracy requirements: 0.5 - 1 degree
Image Quality	Analog Film to High Resolution digital (Multi Megapixel) stills	Thermal Imagery at: 320 width X 240 height X 10 bit resolution.
Image Rate	Altitude dependent rate based on 60% forward overlap.	20+ images / second with high forward overlap.
Image Measurements	Post mission with full utilization of future extraction techniques and dedicated image processing system.	Real-time hot spot identification and extraction.

2.2 General Direct Georeferencing System Model

The geometric relationship between a camera, an inertial measurement unit (IMU), and a GPS antenna for an airborne mobile multi-sensor system (MMSS) is shown in Figure 2-1.

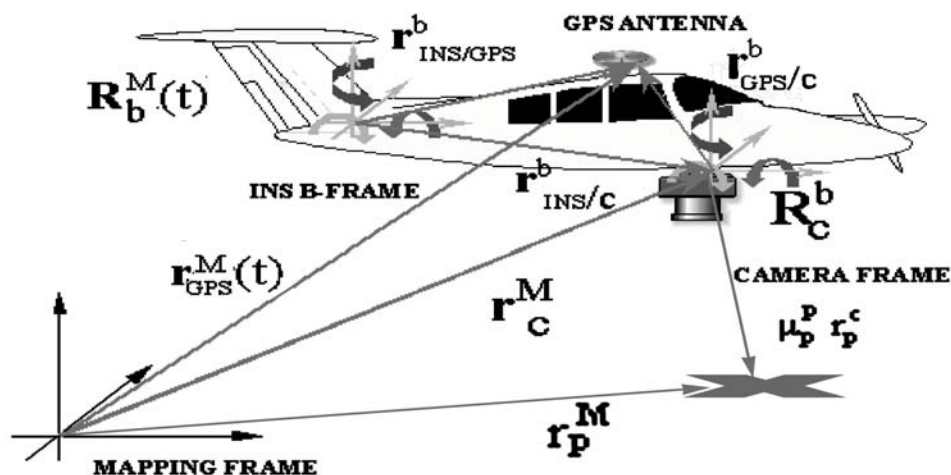


Figure 2-1: Diagram of Equation 2-1 Parameter Relationships

The key co-ordinates for this research are related by

$$\mathbf{r}_p^M = \mathbf{r}_{GPS}^M(t) - \mathbf{R}_b^M(t) \mathbf{R}_c^b (\mathbf{r}_{GPS}^c - \mu_p^p \mathbf{r}_p^c) \quad \text{Equation 2-1}$$

Where:

\mathbf{r}_p^M	: X, Y, Z position vector of the feature point in mapping frame	Desired result
$\mathbf{r}_{GPS}^M(t)$: Real-time GPS position vector in mapping frame	Estimated in real time
$\mathbf{R}_b^M(t)$: attitude matrix between the body frame and mapping frame	Estimated in real time
\mathbf{R}_c^b	: rotation matrix between the camera frame and body frame	Estimated through calibration

$\mathbf{r}_{\text{GPS}}^c$: GPS to Camera lever arm vector	fixed and externally measured
μ_p^p	: Image point scale factor	Unknown, to be determined
\mathbf{r}_p^c	: image point	point extracted in real time through image processing
T	: time of exposure	

2.2.1 Camera Position and Orientation

From the definition of the real-time requirements for the forest fire hot spot detection system (presented in Chapter 1) and the overall physical system configuration (presented in Chapter 5), there is a specific approach to providing the real-time direct georeferencing information. The first part is to determine the camera position $\mathbf{r}_c^M(t)$ and its orientation $\mathbf{R}_c^M(t)$ at the image exposure time (t), as depicted in Figure 2-2

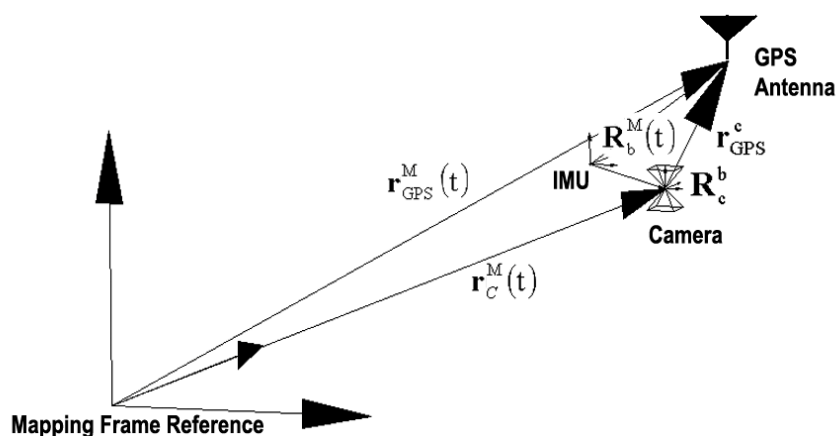


Figure 2-2: Diagram of Equation 2-2 Parameter Relationships

Figure 2-2 shows just the portion of Equation 2-1 that determines the perspective centre of the camera and can be expressed as:

$$\mathbf{r}_c^M(t) = \mathbf{r}_{GPS}^M(t) - \mathbf{R}_c^M(t) \mathbf{r}_{GPS}^c \quad \text{Equation 2-2}$$

Where:

$\mathbf{r}_c^M(t)$: X, Y, Z position vector of the camera perspective center in mapping frame.

$\mathbf{R}_c^M(t)$: $= \mathbf{R}_b^M(t) \mathbf{R}_c^b$: camera attitude rotation matrix w.r.t. the mapping frame.

The IMU provides the real-time body to mapping frame attitude $\mathbf{R}_b^M(t)$, and in all situations there will be a slight misalignment between the IMU and the camera imaging plane. The process of correcting this misalignment is typically called the boresight alignment and the amount of misalignment is defined by \mathbf{R}_c^b .

The final component is the physical position offset between the GPS antenna and the camera perspective center. This component is called the lever arm offset and is defined by \mathbf{r}_{GPS}^c . Both of these terms are fixed parameters that can be obtained through calibration, which will be discussed in Section 2.3.2 and 2.3.3. Once these two parameters are known, then the perspective center of the camera can be determined in real time quite simply by applying Equation 2-2.

2.2.2 Thermal Imager Geometric Camera Model

The second part involves the relationship between the camera, the actual image obtained by the camera system, and the final object position, as depicted in Figure 2-3.

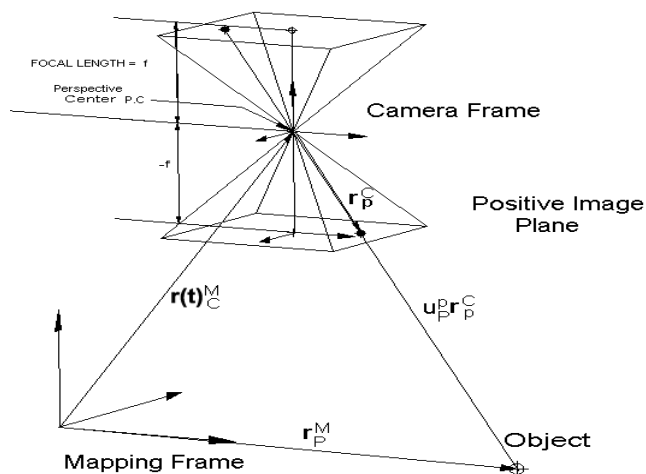


Figure 2-3: Camera Perspective Center to Hot Spot Relationship

Figure 2-3 shows the portion of Equation 2-1 relating the camera perspective centre to the final hot spot location in the mapping frame and can be expressed as:

$$\mathbf{r}_p^M = \mu_p^p \mathbf{R}_C^M(t) \mathbf{r}_p^c + \mathbf{r}_C^M(t) \quad \text{Equation 2-3}$$

Each of these parameters have been presented previously, with $\mathbf{r}_C^M(t)$ obtained from Equation 2-2, and $\mathbf{R}_C^M(t)$ coming from the IMU real-time attitude and the

boresight alignment. The remaining components, the image point vector \mathbf{r}_p^c and the image point scale μ_p^p , still need to be determined.

The image point x_p^i, y_p^i in Figure 2-3 is related to the point vector $\mathbf{r}_p^c = [x_p^c \quad y_p^c \quad -f]^T$ through an intermediate point \bar{x}, \bar{y} by a transformation from the image frame to the camera frame. The image point x_p^i, y_p^i is referenced to the top left corner of the image (which is the standard convention found on computer systems), and is transformed to the camera frame by the relationship to the principal point x_o, y_o expressed by:

$$\bar{x} = x_p^i - x_o, \quad \bar{y} = y_o - y_p^i \quad \text{Equation 2-4}$$

which is a translation in the x axis, and a reflection and translation in the y axis respectively,.

Even though the image point \bar{x}, \bar{y} is aligned from the image to the overall mapping frame, there are image corrections that are still required to complete the relationship between x_p^i, y_p^i and x_p^c, y_p^c , allowing the final determination of the actual hot spot location \mathbf{r}_p^M .

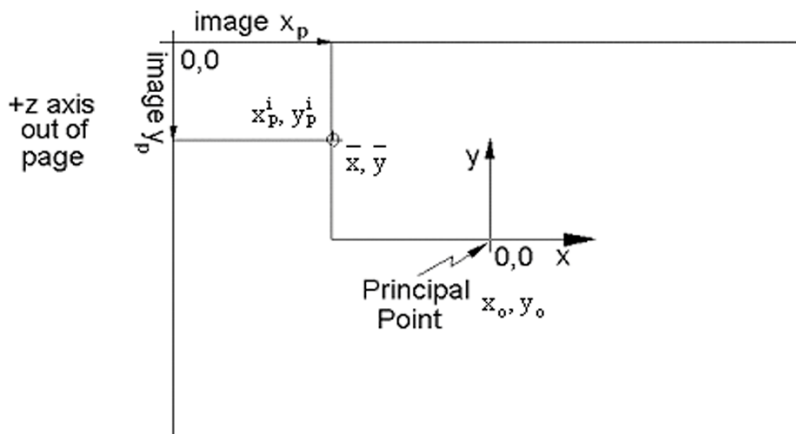


Figure 2-4: Positive Image Plane

A thermal imaging camera can be treated geometrically like any other camera. The images exhibit geometric distortions caused by the optical path that must be corrected before a 3D space intersection computation can be done, and consists of radial distortion components δx_r and δy_r , decentering distortion components δx_d and δy_d , and the in-plane distortion component δx_f .

Radial distortion is a symmetric distortion about the principal point of the image. This causes a displacement of the imaged point from its theoretically correct position, which is effectively a change in the angle between the incoming ray of light and the ray of light incident on the imaging sensor. Radial distortion causes straight lines to appear curved in the resulting image, as depicted in Figure 2-5. Note that normally only the k_1 and k_2 coefficients are significant, and $k_0=0$, as this component is also effectively handled by the calibration of the principal point and focal length (Ellum, 2001)(Mikhail et.al., 2001).

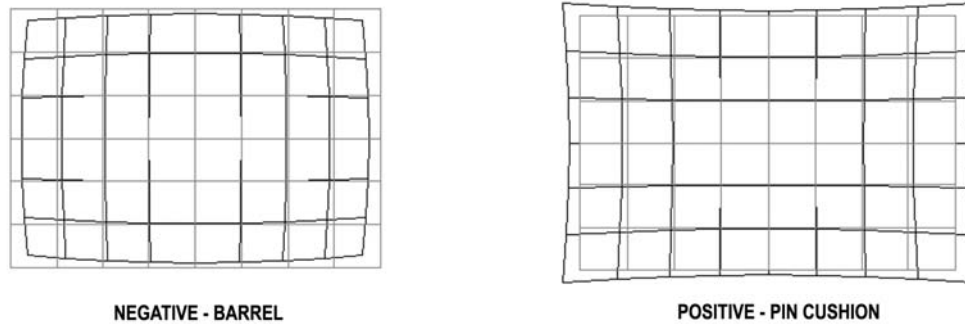


Figure 2-5: Negative and Positive Radial Distortion Examples

Decentering distortions are more an artifact of errors in the assembly and rotational symmetry of the multiple lens components typical of a modern compound lens (Ellum, 2001)(Mikhail et.al., 2001). The overall effect is depicted in Figure 2-6.

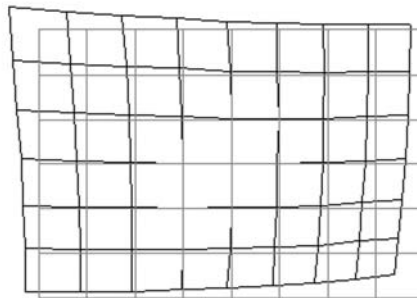


Figure 2-6: Decentering Distortion Example

Affinity and shear are aspects of in-plane distortion that are typical characteristics of the capture medium. Affinity is effectively a difference in scales between the x and y axis, and shear describes the non-orthogonality between axes. Note that these terms are only applied to one axis, due to the cross axis nature of this distortion. For any digital imaging system, the geometric integrity of

the image sensor is very high from the high geometric consistency inherent in modern semiconductor manufacturing technology, such that the actual in-plane distortions are negligible.

The general model for the corrected image points is expressed by:

$$x_p^C = \bar{x} + \delta x, \quad y_p^C = \bar{y} + \delta y \quad \text{Equation 2-5}$$

where:

f	:	focal length
\bar{x}, \bar{y}	:	transformed image point
x_p^i, y_p^i	:	actual image point
x_o, y_o	:	principal point
$\delta x, \delta y$:	distortion components

The distortion components $\delta x, \delta y$ are models consisting of several sub-components such that:

$$\delta x = \delta x_r + \delta x_d + \delta x_f, \quad \delta y = \delta y_r + \delta y_d \quad \text{Equation 2-6}$$

including radial distortion components:

$$\delta x_r = \frac{\bar{x} \delta r}{r}, \quad \delta y_r = \frac{\bar{y} \delta r}{r} \quad \text{Equation 2-7}$$

Radial to image X-Y relationship:

$$r = \sqrt{\bar{x}^2 + \bar{y}^2} \quad \text{Equation 2-8}$$

Radial distortion error:

$$\delta r = k_0 r + k_1 r^3 + k_2 r^5 + k_3 r^7 \dots \quad \text{Equation 2-9}$$

where:

$k_0, k_1, k_2, k_3 =$ Radial distortion coefficients

Decentering distortion components:

$$\begin{aligned} \delta x_d &= p_1 \left(r^2 + 2\bar{x}^2 \right) + 2p_2 \bar{x}\bar{y} \\ \delta y_d &= p_2 \left(r^2 + 2\bar{y}^2 \right) + 2p_1 \bar{x}\bar{y} \end{aligned} \quad \text{Equation 2-10}$$

where:

$p_1, p_2 =$ Decentering distortion coefficients

Affinity and shear (in-plane) component:

$$\delta x_f = b_1 \bar{x} + b_2 \bar{y} \quad \text{Equation 2-11}$$

where:

$b_1, b_2 =$ Affinity and shear coefficients

Once the image point vector \mathbf{r}_p^c is determined from the actual image point x_p^i, y_p^i , there is the question of the image point scale μ . Scale can be simply expressed as:

$$\mu_p^p = \frac{f}{H - h} \quad \text{Equation 2-12}$$

where:

$H - h =$ flying height above terrain

If the system is being used over very flat terrain, then Equation 2-12 would give a good value for the scale and a solution for Equation 2-3 could be determined, as there are now three unknowns with three equations. In reality, the terrain will not be flat and the image point scale μ_p^p will be unknown. The image point scale can be determined by other means, which will be presented in Section 2.3.

2.3 Unknown Parameter Determination

Throughout Section 2.2, there have been several parameters introduced that are unknown and must be determined before the system can be effectively utilized. The key parameters to determining the remaining unknowns are related to the geometric distortions of the actual image; and as such, the geometric calibration technique for the camera will be discussed first, followed by the boresight alignment and lever arm offset determination. Finally, the process of 3D space intersection for estimating the object point coordinates \mathbf{r}_p^M and image point scale μ_p^p will be presented.

2.3.1 Thermal Camera Geometric Calibration

As previously stated, a thermal camera can be treated geometrically as any other camera, which allowed for the simple application of existing calibration methods to determine the radial distortion coefficients k_1, k_2 , decentering distortion

coefficients p_1, p_2 , affinity and shear coefficients b_1, b_2 , focal length f , and the principal point x_0, y_0 .

The only unique requirement to the method used is to ensure that the material used for target has a strong thermally observable difference from the general background, through a significant emissivity differential. This term is discussed further in Chapter 3.

The calibration method selected was developed to allow for a planar calibration rig instead of a 3D calibration rig as typically used for photogrammetric camera calibration. Zhang (2002), Heikkila and Silven (1997), Bouguet (1999), among others, present techniques for geometric camera calibration by using a planar rig. Bouguet has also developed a freely available Matlab toolbox (Bouguet, 2004) for geometric calibration of any camera. This toolbox, and the general method outlined by its documentation, was used to calibrate the thermal imager used for this research. Although the specific details of these approaches are beyond the scope of this research, the general idea behind them is as follows: By having a consistent geometric calibration pattern (in this case a square grid), certain constraints and estimates can be introduced into the mathematical models. These constraints allow for the use of a planar calibration rig instead of a 3D calibration rig. Because of the fixed, known shape of the grid, the pose (the position and orientation of the grid) can be estimated from projective geometry and a rigid body transformation, which in combination with prior knowledge of the

grid dimensions, provides a 3D pattern relative to the image plane. It is considered known by Bouguet (1999) that the optical center or principal point cannot be estimated using a planar calibration rig, although this information can be extracted if using a 3D rectangular parallelepiped. The Matlab Toolkit (Bouguet, 2004) actually does allow for extraction of all intrinsic parameters, which suggests that the combination of multiple planar calibration images with different poses can effectively be considered a 3D calibration rig. The primary result is that all of the camera's intrinsic orientation parameters can be determined using a very simple 2D calibration rig. There are further constraints and conditions involved but the above description gives a very general overview. For a complete description, see Bouguet's thesis (1999), Chapters 2 and 3.

Following the method described in the Matlab toolbox tutorial (Bouguet, 2004), a checkerboard pattern was created on a metal plate utilizing thermal insulation tape to satisfy the requirement for a thermally identifiable grid. This test pattern was heated from the front for a short period of time. The metal itself is highly reflective of thermal wavelengths, and the tape is not. So with a warm or cold environment, the grid is visible without any heating. Heating causes a greater contrast. With the different heat capacities and emissivities of the tape and metal, the checkerboard pattern is distinctly visible allowing for a large set of images to calibrate the camera to be acquired, similar to the image shown in Figure. 2-7.

The image in Figure 2-7 is a representative calibration sample. The actual calibration process included 45 images of the calibration grid, which statistically improved the quality of the results.

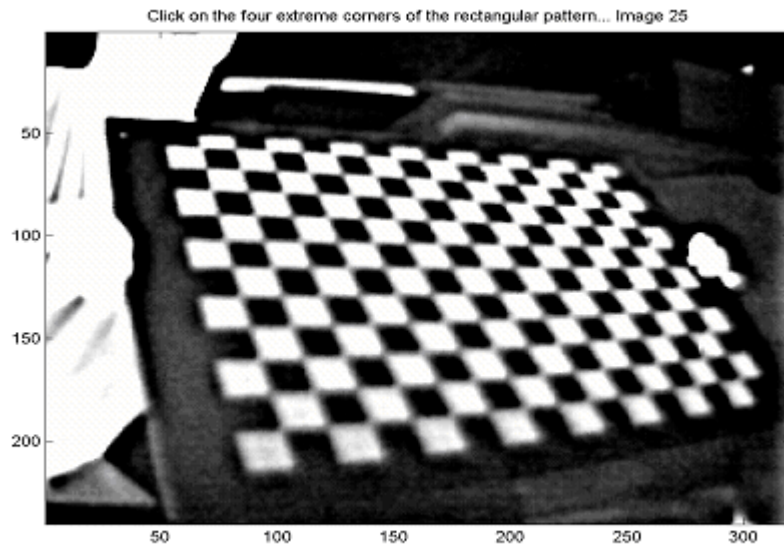


Figure 2-7: Sample Camera Calibration Image

The confidence interval for various parameters is directly related to the degrees of freedom in the final calculations. The *degrees of freedom* is determined from the number of unknowns and the number of equations or data samples. For the camera calibration, there are effectively 10 camera parameters as unknowns $(f, x_0, y_0, k_1, k_2, k_3, p_1, p_2, b_1, b_2)$ with 165 x-y points per image. The actual grid orientation or pose is estimated for each image, as is the image scale from prior knowledge of the grid dimensions, which is effectively an additional 4 unknowns per image. So the degree of freedom is expressed as $165 \cdot 3 \cdot N$ equations $-14 \cdot N$

unknowns, with N = number of images. With more images, the degrees of freedom increase by a factor of 481 per image, improving the confidence interval. An improvement in the confidence interval means a narrower range of values around the mean value determined by the least square minimization.

There are a couple of potential error sources in this calibration process. These come in part from the capture method, which in this case is the image data being from an interlaced video system. This causes blurring of the image data. Other sources of error include the automated corner extraction process used and the geometric integrity of the target grid. It is noted by Smith and Brady (1998) that there are some localization problems with the Harris corner detector used by the toolbox (Bouguet, 2004), which can add potential errors, although this appears to be only for more complex corners, such as a "T". Since the grid relied on the different rate of cooling of the metal and thermal tape, the actual temperature threshold was shifting as the whole target grid cooled.

2.3.2 Boresight Alignment

The calibration of the camera boresight alignment is essential to correct for any misalignment between the camera frame and the IMU body frame. The boresight parameters are used in converting the IMU attitude angles to the standard photogrammetric rotation angles. This requires knowledge of the coordinates of at least 3 ground points across multiple images and trajectories. Recalling Equation 2.2, $\mathbf{r}_c^M(t) = \mathbf{r}_{GPS}^M(t) - \mathbf{R}_b^M(t) \mathbf{R}_c^b \mathbf{r}_{GPS}^c$, to calibrate for \mathbf{R}_c^b ,

knowledge of all remaining components is required across multiple images. A minimum of three specific control points for $\mathbf{r}_c^M(t)$ were set up. For the best results, post processed GPS position $\mathbf{r}_{GPS}^M(t)$ and IMU body frame orientation $\mathbf{R}_b^M(t)$ are available, leaving the boresight alignment \mathbf{R}_c^b and the lever arm vector \mathbf{r}_{GPS}^c unknown. The vector \mathbf{r}_{GPS}^c can be initially estimated as $(0,0,0)^T$, or the initial measured value can be used.

Through application of proper least squares minimization techniques, the boresight alignment problem can be solved quite simply, provided there are enough control points and images. The University of Calgary's WinBundle software (Ellum, 2001) includes the functionality to do the boresight alignment, and is used in this research.

Basically, for each control point there are three equations with four unknowns (the three boresight rotations and one image point scale per image). Therefore, there is a requirement for the control point to be observed in at least 2 images, giving six equations for 3+N unknowns, with N = number of images. With three control points per image, there are then 3+3*N unknowns from 9*N equations, giving 9*N-(3+3*N) degrees of freedom. Besides the degrees of freedom obtained, another reason for three control points is the non-linear nature of the rotation matrix, which can have multiple solutions to a single point observation without additional information to constrain the solution. Three control points

define a plane, and then the solution is aligning a plane to a plane. Also, multiple images reduce the sensitivity of the final result to any image point errors that occur, which can potentially be quite large. As discussed previously with camera calibration, the more images used in the calibration procedure, the greater the overall confidence interval of the results.

The accuracy of this result is dependent upon the post-processed attitude of the IMU, the surveyed position of the target hotspots, and the image quality. Additional issues also involve the narrow angles and field of view of the camera, as discussed by Mostafa (1999). The results are presented in Chapter 6.

2.3.3 Lever Arm Offset Determination

Invariably there is going to be an offset in position between the GPS or IMU module and the camera perspective center. This can be determined in a couple of ways. The simplest way is to measure the offsets; and depending on the desired and expected accuracy for the system, this may be more than adequate. The alternative is to numerically determine the values, which can be solved using an approach similar to that taken for the boresight alignment, using least squares minimization techniques.

For the system test flights, there was a survey available for the offset between a mounted GPS antenna and the camera perspective centre in the remote sensing aircraft. A measurement was then made between the surveyed antenna and the test antenna, with the test camera aligned in two dimensions with the analog

remote sensing camera body. Realistically for this thesis, the measured values for the lever arm offsets are more than satisfactory because of the overall system accuracy obtainable. There are also geometric issues to be considered that support using the measured values. Mostafa (1999) went into some depth in analyzing the effect of camera pixel dimensions on the precision of heights. This effect is shown by Mostafa (1999) to be significantly greater than horizontal errors and even attitude effects. This would have an even greater effect than shown in his work due to the smaller overall image dimensions of the thermal camera compared to the camera used in his work.

2.4 3D Space Intersection

The process of space intersection, or triangulation, is relatively simple once all components are aligned within the aircraft. This is assuming that the image points are correctly extracted and the boresight alignment of the camera to the body frame is done correctly.

Again, the basic equation for this is Equation 2-3 $\mathbf{r}_p^M = \mu_p^P \mathbf{R} \mathbf{r}_p^c + \mathbf{r}_C^M$

Where:

$\mathbf{R} = \mathbf{R}_b^M(t) * \mathbf{R}_c^b$: body attitude and Bore Sight alignment

\mathbf{r}_p^c : distortion corrected x, y hot spot image coordinate within a specific thermal image at time (t). (from Equation 2-5)

\mathbf{r}_C^M : X, Y, Z coordinate of the camera perspective center in the mapping frame at time (t) (from Equation 2-2)

\mathbf{r}_p^M : X, Y, Z position vector of the desired hot spot feature point in the mapping frame

From Equation 2-3, there are 4 unknowns: μ and the three components of \mathbf{r}_p^M with all other components are known. Since there are 4 unknowns in 3 equations, a second image is required to allow for solving all the unknowns. This gives $3 \cdot N - (3 + N)$ degrees of freedom. In reality, more than 2 images are desired to help minimize imaging error effects as commented previously based on the increase in degrees of freedom provided. In field operation, the number of images and image points are unknown, but the identity of each hot spot will have been cross-referenced from frame to frame already. This is explained further in Chapter 4.

The derivation of the least squares minimization matrices for the 3D space intersection process is relatively simple (El-Sheimy, 2000). Also, the horizontal components are expected to be significantly more accurate than the vertical or height component as discussed in the previous section discussing the lever arm determination. The final results for this processing are presented and discussed in Chapter 6.

2.5 Wide Area Differential GPS: WAAS And OmniStar

The backbone of a direct georeferencing system is the navigation system integrating GPS and an Inertial Measurement Unit (IMU) system. In the recent past, a tried and true approach to accurately georeference any imager in real

time required a differential GPS due to the limitations to the real-time accuracy of any stand alone GPS available. A wide area differential GPS (WADGPS) reduces the complexity for the end user by providing a readily available correction service with low user expense and time. There are two systems that were evaluated in this research: WAAS and OmniStar.

The Wide Area Augmented System (WAAS) is an initiative of the US Federal Aviation Administration (FAA) that is designed to provide an improved real-time, single frequency GPS based position as well as system integrity information (FAA 2003). The system improves both the horizontal and vertical accuracy, with accuracy's within 1-2 m horizontally and 2-3 m vertically (FAA 2003)(Cannon et.al. 2002). The WAAS system coverage area includes most of North and South America at this time, although various complimentary systems are being developed such that the area becomes worldwide.

OmniStar is commercial Wide Area Differential system and is marketed as a sub-meter level of service (OmniStar 2003). Tests done with an OmniStar DGPS system in static operation gave results slightly higher than this (Cannon et.al. 2002), although it is also noted that the test area is on the edge of the OmniStar satellite coverage. WADGPS provide the $\mathbf{r}(t)_{GPS}^M$ to the direct georeferencing system model. Results from testing both WAAS and OmniStar are presented in Chapter 6.

2.6 Inertial Measurement Unit (IMU)

An IMU is a device that detects 3 accelerations and 3 rotations of the device relative to a specific inertial reference frame, which is the earth. The rotations are determined from the detection of angular velocities by gyroscopes, and the accelerations are obtained directly from accelerometers. The primary component of interest in this research is the actual physical orientation of the device with respect to the inertial or mapping frame, which can be obtained from the angular velocities by integrating over time to determine the orientation changes of the body from the initial reference orientation. There are various technologies and classification of IMU units that provide different accuracies. Generally, the cost of an IMU unit increases proportionally with the desired accuracy. Integrated GPS/IMU systems help to reduce the expense required to obtain high quality position and orientation data. GPS and IMU are complementary systems that support each other's weaknesses. The GPS will give the IMU system consistent position information that helps to stabilize the IMU results, and the IMU system provides the GPS reasonable inertial information during GPS errors and blockages. This is an area of significant research (Petrovello et. al., 2003) (Salychev et.al., 2000)(Skaloud, 1999) and is beyond the scope of this thesis. For this thesis work, a Novatel Black Diamond System (BDS) was used with Attitude specifications as shown in Table 2-2.

Table 2-2: IMU Performance Accuracy

Pitch	0.015°
Roll	0.015°
Azimuth	0.05°
Acceleration RMS	0.03 m/s ²
Time Accuracy	50 ns

Note that attitude information from the IMU must be translated to the mapping frame orientation, although this will be incorporated into the final boresight alignment. The IMU provides the attitude values for the rotation matrix $\mathbf{R}_b^M(t)$ to the direct georeferencing system model. Results from testing this component of the system for this thesis are presented in Chapter 6.

2.7 Georeferencing Summary

This chapter has presented all the necessary photogrammetric models and explanations for the implementation of any georeferenced camera system. Some of the error sources were also discussed briefly. The next chapter presents the basic terminology required to understand the essence of thermal imaging and some systematic issues observed with the thermal imager used in this research.

Chapter 3

Thermal Imaging Background

Thermal imaging is a very specialized field that is not fully understood by the general public and even the technical community if they haven't been exposed to it. In some cases the terms *thermal imaging* and *infrared imaging* are used interchangeably and carelessly, leading to misunderstandings about the type of equipment required to do proper thermal imaging. This chapter discusses the meaning of thermal imaging, why thermal imaging and infrared imaging are sometimes used interchangeably, and how the infrared and thermal spectrums are generally defined. General heat transfer concepts are presented, specifically those that apply to thermal imaging and affect the performance of thermal imaging systems. Also included is a brief discussion on the reasoning used to select the specific thermal imaging technology for this study. In order to correctly interpret thermal images, a basic understanding of all the mechanisms of how the object generates, receives, transfers and emits thermal energy is important. In addition to the thermal imaging background, general systematic issues observed in the thermal video from tests under day and night conditions are pointed out. Note that most of the definitions and equations in this chapter are available in

any decent physics text, and are presented here to reinforce the concepts that specifically apply to thermal imaging.

3.1 Black Body Radiation

Heat transfer is the movement of heat energy from one object to another. There are three modes in which this energy can be transferred: conduction, convection and radiation (Holtz, 2001). In most cases, heat energy is transferred by a combination of these three modes. Thermal imaging is observing radiation mode energy transfer. The radiation is more specifically called thermal radiation, which is often confused with infrared radiation but is, in reality, a subset of the infrared spectrum. Thermal radiation is best explained using the basic theory of black-body radiation. This effectively relates the radiated energy at a specific wavelength for a given temperature as shown Figure 3-1.

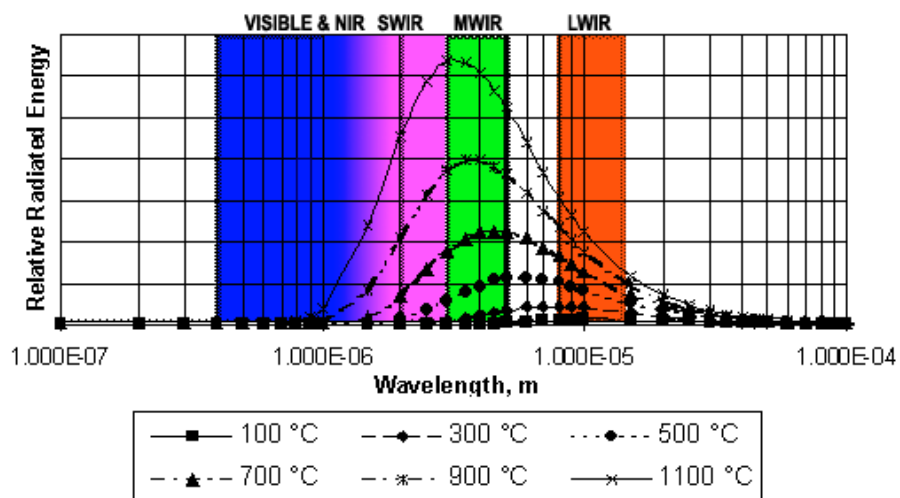


Figure 3-1: Black Body Radiation Across Applicable Wavelengths

Different wavelength ranges of the spectrum shown in Figure 3-1 are generally referenced by the terms listed in Table 3-1. Figure 3-1 was developed from Planck's Law for Black-Body Radiation (Holtz, 2001) which can be stated as:

$$u(T, f) = 8\pi hf^5 / \left(c^3 \left(e^{(hf/kT)} - 1 \right) \right) = \text{Joule/sec/m}^2/\text{m} \quad \text{Equation 3-1}$$

where:

T	Temperature (Kelvin)	
λ	Wavelength (m)	
f	Frequency (hz)	c / λ
c	Speed of light	2.99792458×10^8 metres sec^{-1}
k	Boltzman Constant	1.3807×10^{-23} Joule K^{-1}
h	Planck's Constant	6.626×10^{-34} Joule sec.

Table 3-1: Thermal Wavelength Definitions

Visible	Part of light spectrum "Visible" to human eyes.	0.4-0.7 μm
IR	Infrared: part of the electromagnetic spectrum with a wavelength longer than for visible light, but shorter than radio waves.	0.7-100 μm
NIR	"Near" infrared: part of infrared spectrum closest to visible light	0.7-1.0 μm
SWIR	"Short Wave" infrared	1-3 μm
MWIR	"Mid Wave" infrared	3-5 μm
LWIR	"Long Wave" infrared	8-12 μm

Equation 3-1 represents the ideal case, which is a useful representation for discussion purposes. By looking closer at the spectrum shown in Figure 3-1, it becomes clear why different wavelengths are better than others for detecting thermal characteristics. Even at a moderately hot temperature (1000 K), there is little “visible” light, but significant thermal radiation. Even IR films and normal digital cameras with IR sensitivity do not detect what are considered to be the thermal bands, since what they actually detect is in the NIR band.

This is also can be explained by Wien's Law (Holtz, 2001):

$$\lambda_{\max} = \frac{2898}{T} = \text{peak energy wavelength in } \mu\text{m} \quad \text{Equation 3-2}$$

Where:

T = Absolute Temperature in Kelvin

Wien's Law allows us to calculate the wavelength at which the peak maximum energy is emitted for a specific temperature. Of more use is the effective radiated energy or power (Watts/m²) within a particular range of wavelengths. By integrating the energy per wavelength across a particular IR band, the relative power in that IR band can be determined. Figure 3-2 shows the results of this calculation.

Note that the four infrared bands shown in Figure 3-2 do not cover the entire thermal spectral range and as such do not total 100% of the blackbody radiation.

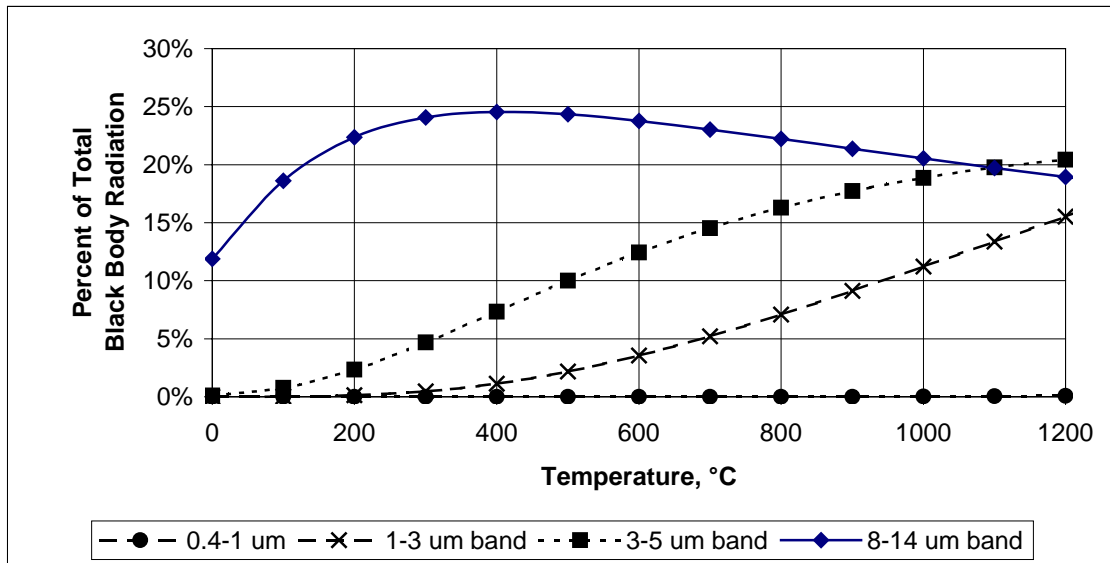


Figure 3-2: Relative Power by Temperature and IR Band

The total emitted energy is defined by the Stefan-Boltzmann Law (Holtz, 2001):

$$q = \sigma T^4 \quad \text{emitted energy} \quad \text{Equation 3-3}$$

Where:

$$\sigma \quad \text{Stefan-Boltzmann Constant} \quad = 5.67 \times 10^{-8} \frac{J}{sm^2 K^4}$$

T Absolute Temperature (Kelvin)

This covers the entire thermal radiation spectrum, not just the thermal IR bands.

Of particular interest is the 8-12 um bandwidth, which dominates the radiation in the lower temperatures. This is why it is important to be detecting these wavelengths in thermal imaging for broad temperature range detection at the typical environmental conditions. As the temperature increases, the shorter wavelengths start to dominate the radiated energies, going into what is the visible

spectrum. There are other reasons, to be discussed later, why the LWIR band was selected for this research.

3.2 Heat Transfer Terminology And Definitions

With a clearer understanding of what wavelengths are detected by thermal imaging, there are some additional terms that need to be defined to help explain thermal imaging issues, including the following (Holtz, 2001):

3.2.1 Absorptivity And Absorptance

Absorptivity is simply the proportion of the incident energy on an object that is absorbed by an ideal material. Absorptance is the absorptivity of a real object. Different objects have different absorptance at different spectral wavelengths.

3.2.2 Reflectivity And Reflectance

Reflectivity is simply the proportion of incident energy on an object that is reflected by an ideal material. Reflectance is the reflectivity of a real object. Different objects have different reflectance at different spectral wavelengths.

3.2.3 Transmissivity And Transmittance

Transmissivity is simply the proportion of incident energy that passes through an ideal material. Transmittance is the transmissivity of a real object. Different objects have different transmittance at different spectral wavelengths.

3.2.4 Angle Of Incidence

Something that most of us have probably observed at one time or another is an apparent reflection from an asphalt road. This is because the reflectance of materials is a function of viewing angle. Asphalt, although rough and coarse textured becomes reflective to heat when viewed at an angle near 90°. This is the case for many materials that must be always factored into any thermal evaluation.

3.2.5 Emissivity And Emittance

Although Planck's law is useful to gain an understanding of the thermal radiation wavelengths, most objects emit only a fraction of all the radiation that it suggests. This fraction is the emissivity, or:

$$\varepsilon = \frac{M_{ACTUAL}}{M_{Blackbody}} = \text{Actual Energy Emitted} / \text{Theoretical Energy Emitted}$$

and varies with wavelength, temperature, shape and angle of incidence. Emittance is the actual amount of energy radiating from an object.

3.2.6 Black Vs. Grey Vs. Real Bodies

In reality, there is no ideal black body. It is a useful concept for explaining how thermal energy interacts with matter. A black body is a perfect absorber, such that the object doesn't reflect or transmit thermal energy. A grey body may reflect or transmit thermal energy as well as absorb energy, and also has the same spectral distribution as a black body. A real body is one that may reflect or

transmit thermal energy, and also has an emissivity that will vary with the wavelength and temperature of the object.

There are many issues involved in determining the source of the thermal energy in a thermal image for a particular scene that need to be understood to effectively isolate the thermal phenomena of interest. Some of the other issues become apparent from evaluation of the thermal images obtained for the specific application.

3.2.7 Energy Conversion

Energy is stored or available in various forms, such as in the molecular structure of a material, the motion of the object, or the temperature of the object. This energy can be transferred to other objects by convection, conduction or radiation. During the process of conversion, the mechanism of storing the energy may change. In particular, burning wood is the process of converting molecular or chemical energy stored in the molecular structure of the wood to other lower energy molecular structures as well as releasing thermal energy in the form of radiation.

3.2.8 Solar Gain

Solar gain is the overall heating effect of the sun's radiant energy on specific objects. Because they have different emissivity, absorptance and reflectance properties, different materials heat up at different rates during the day. This heating effect is called solar gain.

3.2.9 Thermal Equilibrium

The Law of Conservation of Energy requires that the sum of energy flowing into and out of a system is the same and that the total energy must be constant. The emittance of an object is equal to the total sum of transmittance, absorptance, and reflectance; although for most objects and materials, the transmittance is 0 in the infrared part of the spectrum (Holtz, 2001). Note that emissivity and emittance tend to be used indiscriminately in literature. Also, when an object is at thermal equilibrium with its environment, then the object's absorptance must equal the emittance. These observations lead to many additional comments about materials, such as good absorbers are good emitters or that poor absorbers must be good reflectors. This can also be interpreted to mean that objects cannot be studied in isolation. Every surrounding object is also emitting and absorbing radiation and influencing the surrounding environment. Thermal equilibrium is the state in which various objects in contact with each other are at the same temperature, with no further heat energy flow between them. Heat transfer is the process of bringing the various objects to a state of thermal equilibrium.

Transient heat transfer is the situation that arises when objects are in a constant state of temperature change, such as that caused by solar gain effects and the day and night cycle. Thermal energy is absorbed during the day from solar gain,

and is emitted back to the environment at night to achieve a state of thermal equilibrium.

Steady state heat transfer occurs in the situation when an object is receiving or generating a constant amount of energy that is being transferred to surrounding objects and the environment at a constant rate. A fire can be an example of this situation, where the combustion process is releasing energy at a high rate to the surrounding environment.

3.3 Thermal Imagers

A thermal imager is a general term used for an imaging device that can detect thermal energy as discussed previously when defining blackbody radiation. Actual thermal imagers use different detector materials based on the spectral sensitivity range of the thermal imager desired, and this spectral sensitivity can be further controlled by the selection of specific optical characteristics of the lens and filters. Early thermal detection methods required that the actual detector element was cryogenically cooled to 77 Kelvin just to allow the detector to work, although advances in technology now have systems that are considered *uncooled* even though they are actually thermoelectrically cooled to a range of 225 Kelvin to 250 Kelvin. One main difference is that the newer *uncooled* systems are lighter and considered more reliable. The actual market for thermal imagers has primarily been the military market, although commercial uses now include industrial, residential, medical, automotive, resource and environmental

conservation and monitoring applications. An excellent paper by A. Rogalski (Rogalski, 2002), discusses the history and gives a general review of infrared detection technologies.

3.3.1 Wavelength Selection Issues

A study done in 1989 (referenced by West and Gregor, 1999) concluded that long wave thermal systems are better for outdoor applications. The study was looking specifically at the effects of solar reflections during daytime use, and states that 'solar reflections were not apparent with the long wave system in *almost all situations*. The goal of this study was for evaluating which thermal bandwidth was more suited to outdoor use for thermal inspections. In the MWIR region of the spectrum, there is a significant spectral absorption band by atmospheric carbon dioxide that doesn't exist in the LWIR range. Rogalski and Chrzanowski (2002) present several of the differences between the MWIR and LWIR. Specifically, there is quantitative evidence to the negligible effect of reflected sunlight in the 8-13 um LWIR band compared to the significant effect in the 3-5 um MWIR. Holtz (2001, pp. 109-10) also points out that solar radiation is 6 times higher in MWIR than black-body radiation, also indicating reflections or sun glints can be a problem in MWIR. In LWIR, reflections are almost negligible. Other factors include better transmission of LWIR through mist and smoke. Holtz (p. 82, 2001) discusses that particle sizes affect scattering more so in MWIR than

in LWIR and even supports that LWIR can provide better range performance in smoke and moderate haze than a MWIR system.

This would strongly suggest that a LWIR system would be best for detecting fires during daylight hours. This doesn't mean that all reflections are eliminated, just a significant portion.

With a LWIR system, lower temperatures on a surface can be detected; but to accurately detect high temperatures as well, higher pixel depth or resolution is required. A MWIR system is very good at detecting high temperatures and has a better overall contrast for a similar temperature change (pp. 113-114, Rogalski and Chrzanowski ,2002); yet it unfortunately suffers from more solar reflection problems, as discussed above. A MWIR system also suffers from poorer atmospheric transmission under poor weather conditions change (pp. 113-114, Rogalski and Chrzanowski ,2002). In the end, the decision was made to use a thermal imaging camera that could function in both the MWIR and LWIR spectral range and utilized optics designed for the LWIR band.

3.4 Thermal Image Processing

The goal of any image processing is to simplify the extraction of the particular feature of interest; or as Russ (2002) states, *preparing images for measurement of the features and structures present*. This process starts by correcting for any camera artifacts and limitations, such as periodic noise from clock signals,

motion blur effects from interlaced video or other quantifiable non-linearities in the image capture process. (Russ, 2002)(Perry et Al. 2001).

Once the images have been corrected, the initial identification of possible features of interest can be done. As such, the image processing module is a multi-step process, with the first level of processing designed to correct for any systematic errors and the next, to quickly identify possible features of interest. These possible features need to be tracked or correlated from frame to frame, with basic statistics of the feature track also logged. Finally, an evaluation of the complete feature track is done to determine the validity of this feature as a hot spot. General Image processing terminology and the specific data flow selected for this research are presented in greater detail in Chapter 4. The real-time considerations and modifications to the image processing methodology selected are presented in Chapter 5.

3.4.1 Thermal Image Systematic Errors

As stated above, any quantifiable non-linearities need to be corrected for, which can also be referred to as systematic errors. Figure 3-3 and Figure 3-4 highlight an observed systematic error and also help to understand the range of values that can be expected from the thermal images. In Figure 3-3, there is a wide range between the minimum and maximum value within the thermal image frames. The maximum intensity is generally below a value of 500, even when the aircraft is on the ground at the beginning and end of the graphs. The frames with

strong heat sources show up very clearly with maximum intensity spikes above 500, but the relatively consistent difference between the maximum and average frame intensities may be hiding smaller hot spots, depending on the cause of the range between the minimum and maximum values within the frame. During the actual flight, the general maximum intensity statistics drops below 300 for both the day and night flights, with the occasional high intensity spikes that coincide with hot spots. The general trend of the average and maximum intensity to have a consistent difference (over a short range of frames) is what initially suggested a systematic issue with the imager.

Also note that the early part of the night flight, shown in Figure 3-3, has both more noise and a higher intensity, which can be attributed to two things. The first is the higher temperature during the daylight hours causing significant solar gain effects, such that the ground is still cooling off. The later part of the night flight is very similar to the day flight values for overall range. The second is that, at the beginning and end of the flights, the camera is much closer to the ground, indicating an expected relationship between distance and sensitivity.

Figure 3-4 is the average pixel intensity observed for every image frame captured, and indicates that there is an overall background change that appears to be primarily dependent on the row within the image. The broad range between the minimum and maximum values within the frame is not random, but instead something systematic within the imaging system. This must be accounted for in

any image-processing algorithm to help in extracting small, low-intensity hot spots, which is a requirement for the system.

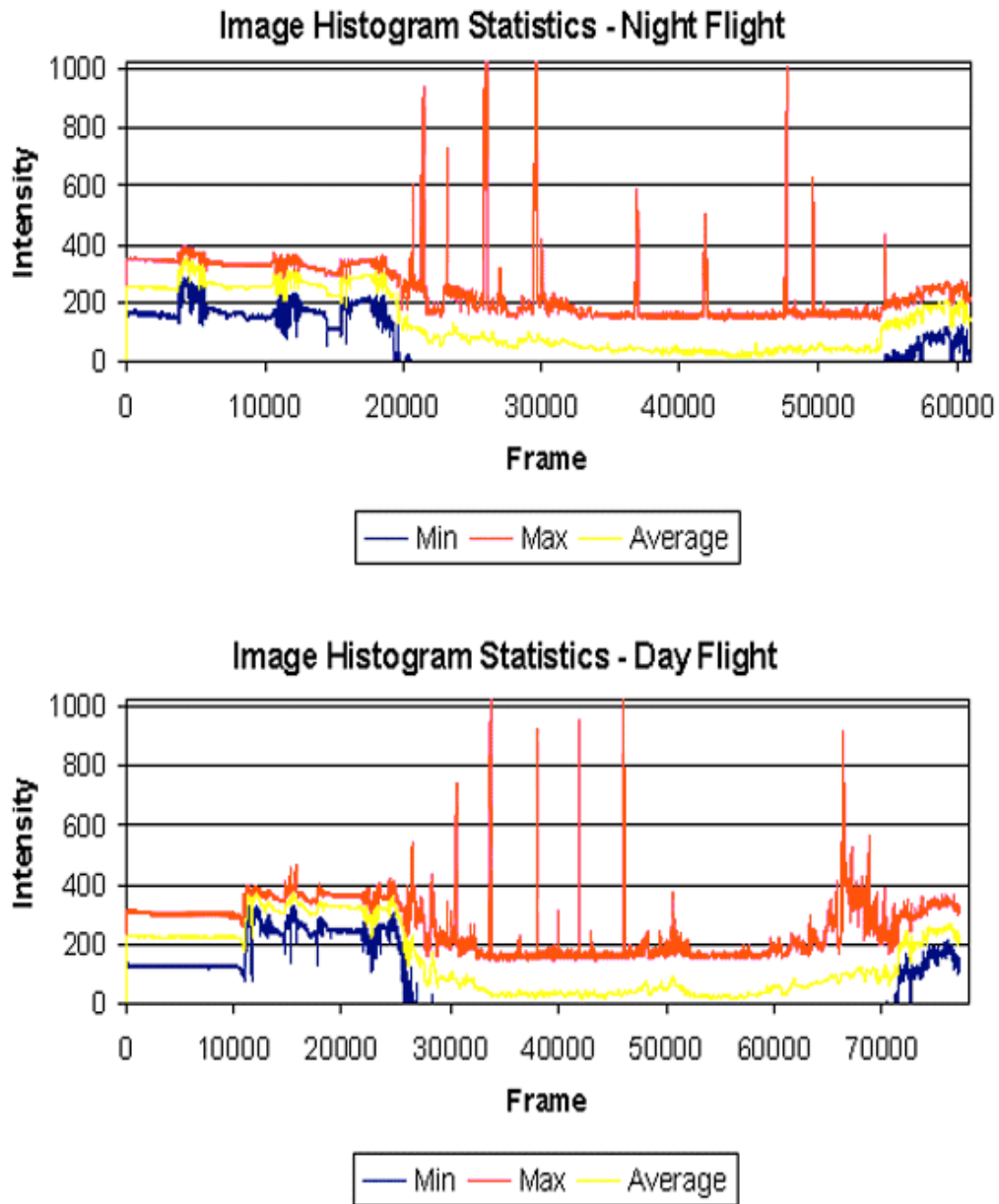


Figure 3-3: Basic Frame by Frame Image Statistics

The spiking occurring along the average data line of Figure 3-4 is consistent with an overall grid that appears in every image. This noise appears to come from the camera - frame grabber interface, which is probably clock noise.

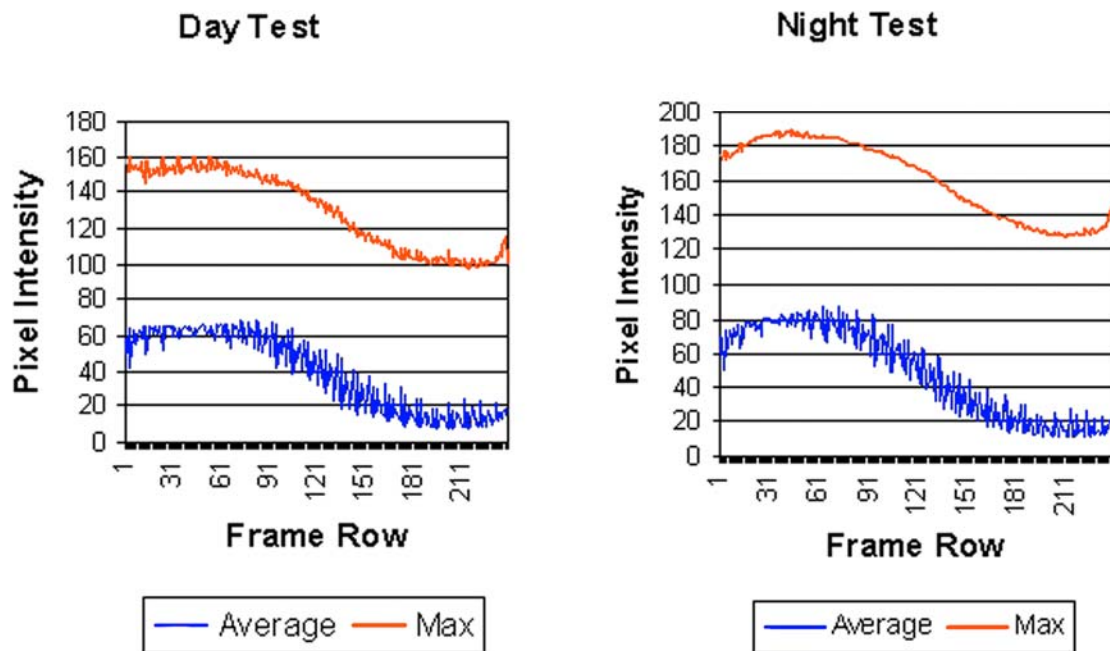


Figure 3-4: Systematic Frame Pixel Intensity Profile

The above observations lead to the requirement for further testing of the thermal imager to determine its basic sensitivity characteristics.

Imaging a water bath at different temperatures did this. The bath was in an insulated container with continuous water circulation and mixing provided by an underwater pump. The initial temperature was an ice bath, and adding boiling water to the bath generated each temperature increase. For each temperature increase, the difference from frame to frame was determined until it became constant. The idea for this approach originated from a presentation by Ryan

(2002), in which a temperature controlled water bath was used to check the calibration of non-contact temperature monitors used in their work on the calibration of thermal satellite data.

The two lowest temperature images and their difference are presented in Figure 3-5 and Figure 3-6.

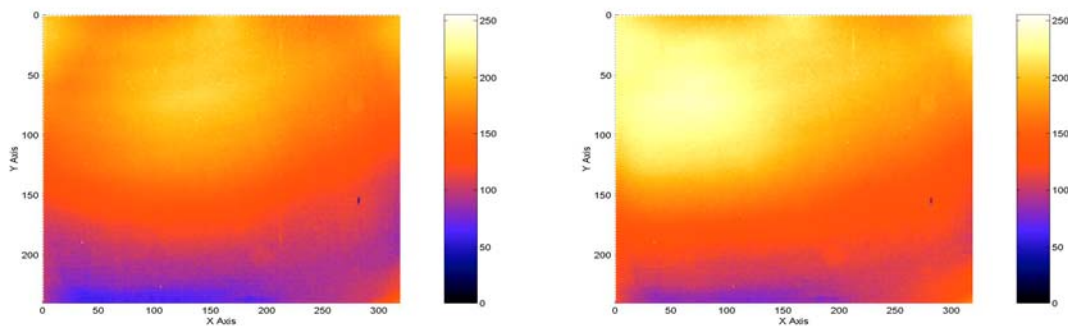


Figure 3-5: Thermal Images of Controlled Temperature Bath

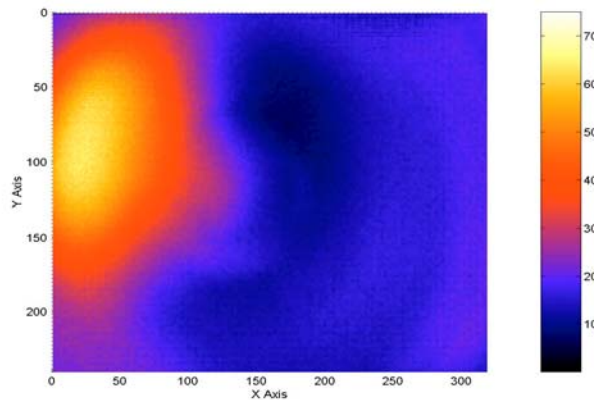


Figure 3-6: Difference In Low Temperature Thermal Images

From this test, it was determined that each pixel of the thermal imager has a different sensitivity at different intensities, or effectively a different calibration curve.

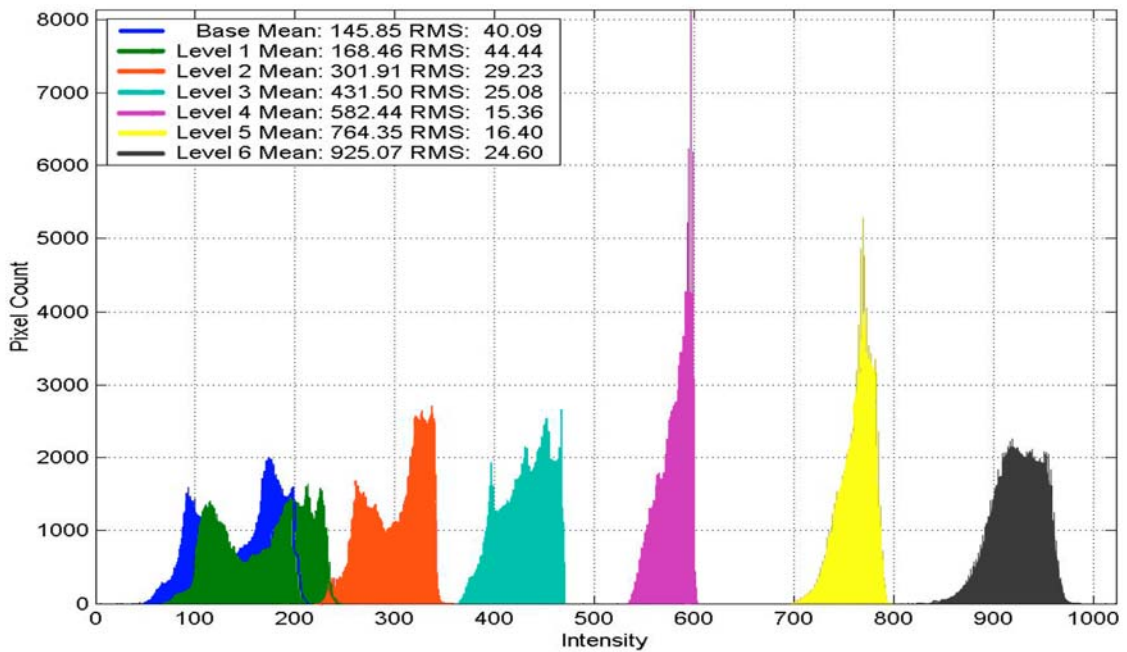


Figure 3-7: Thermal Imager Pixel Histogram Distribution

Figure 3-7 presents the constant temperature images seen in Figure 3-5 as an overall image histogram, and includes 5 higher temperatures. At low temperatures, there is a wider range in the pixel intensities than at the mid-range temperatures. The histogram increases again as the average intensity increases.

The purpose of the above test was to obtain a relative or qualitative understanding of the sensitivity characteristic for the imager, instead of a quantitative or actual calibration. The complete calibration of the imager requires

other factors such as the actual distance between the imager and object, and is beyond the scope of this thesis.

A final error that is observed is that some pixels in the imager appear to lose sensitivity below a certain value, or have a fixed intensity. Every pixel around these pixels may be greater than 50 or even 100 in value, yet this individual pixel drops to zero. This occurs along the top portion of the images in this application, as shown in Figure 3-8, Enlargement 1. There are also some "bad" pixels that appear to stay at one value for most every image, as indicated in Figure 3-8, Enlargement 2 and 3.

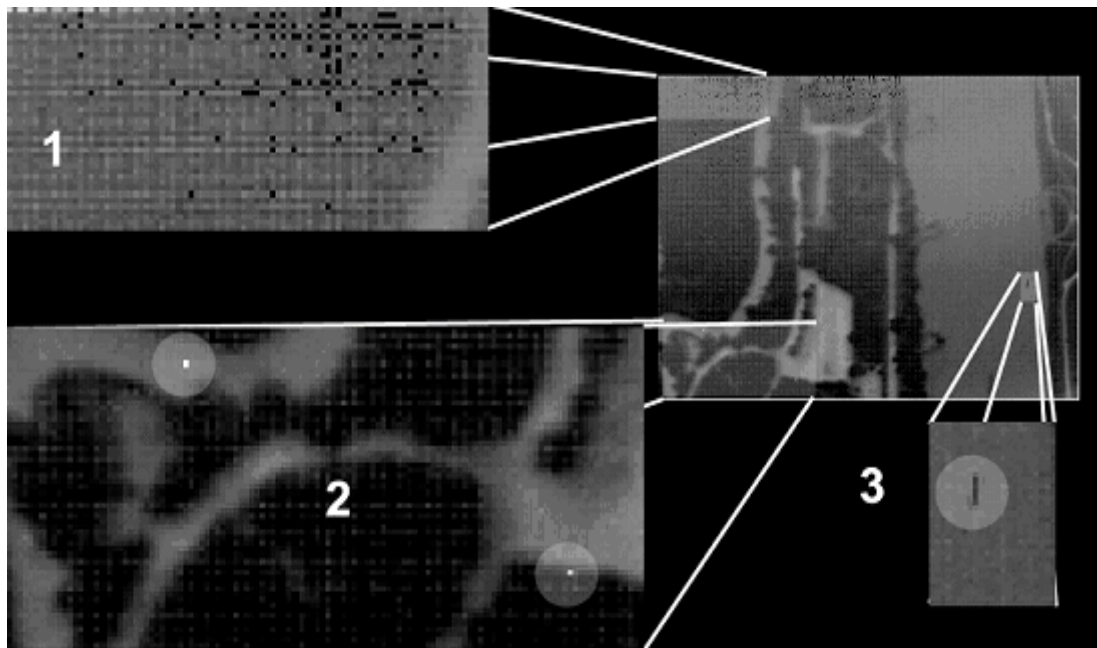


Figure 3-8: Systematic Image Noise Examples

The reason for it occurring is not clear. It isn't the purpose of this thesis to determine these problems, but instead to note them and work around them as best as possible.

3.5 Thermal Imaging Background Summary

This chapter has presented some of the applicable terminology and background to understanding what thermal imaging is, and what effects must be considered to allow for the accurate and consistent location of hot spots. These factors include the background behind the selection of the type and wavelength sensitivity of the thermal imager. Also, systematic issues that must be accounted for and resolved within the initial stages of the image processing methodology are highlighted.

Chapter 4

Forest Fire Detection from Thermal Imagery

With the background in thermal imaging presented in Chapter 3, specific thermal images and image sequences of controlled fires under day and night conditions are introduced with general qualitative explanations of the thermal issues involved. Then the spatial and temporal processing requirements and approaches to identify and locate the desired fire hot spots are presented.

4.1 Hot Spot Characteristics

Once corrections for systematic errors in the images have been made, factors affecting the accurate detection of forest fire hot spots have to be considered. Currently, most if not all thermal imaging flight surveys are done early in the morning, either before sunrise or immediately after sunrise. This is not only dictated by flight regulations for some of the pilots, but also by purely practical aspect of thermal imaging issues involving the MWIR type of thermal imagers currently used by the forestry department.

The process of transient heat transfer, in which the ground, trees, roads, rocks, and all other objects are moving towards thermal equilibrium, has had the greatest amount of time to eliminate the effects of solar gain from the previous day. As such, the primary, higher intensity, thermal radiation sources are going

to be from the forest fire hotspots. Once the sun rises, the sun starts heating various materials at different rates; and some materials start reflecting the sunlight, making the images harder to interpret correctly. The problem is that it is desirable to detect hotspots in day or night conditions, because waiting for night conditions can allow easily controlled small hot spots to become significant and costly fires.

4.1.1 Thermally Imaged Fire Spatial Characteristics

Radiated heating takes a lot more time than convection and conductive heating and is dependent on several factors, including the absorption rate, the heat capacity of the object, and the distance between the objects, among others. Thermal imaging detects fire by the radiated energy. With a small forest fire at the base of trees and surrounded by several trees, the radiation is absorbed by these surrounding trees and not transmitted through. This leads to the fire "hot spots" being obscured occasionally by the surrounding forest.

Also note there is a blooming effect around the fires. Occurring as a result of the immediately surrounding air being heated, this blooming effect can cause an incorrect determination of the hotspot center within the image when combined with the actual hot spot being obscured. Figure 4-1 is used to help explain these two characteristics.

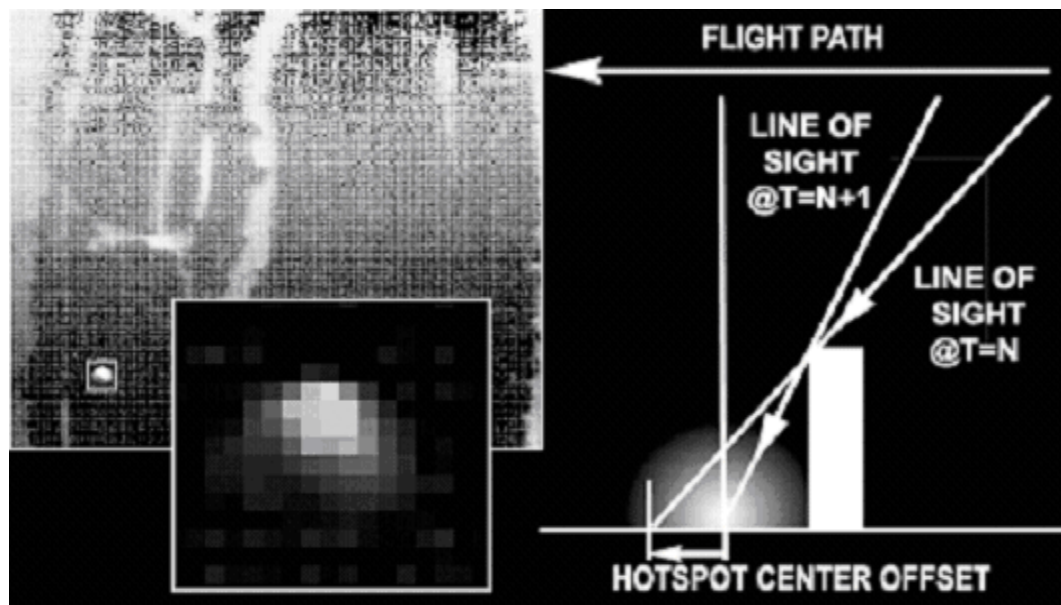


Figure 4-1: Hot Spot Characteristic Diagram

The inset image is an enlargement of the hotspot from the background image. The background has been enhanced for clarity while the inset is the actual pixel values. At the flying altitude from which this image was taken the fire pit here would only be 1 pixel in size, but the hot spot from the fire in that pit is several pixels in size because of this blooming effect. The right side of Figure 4-1 shows the effect of the hot spot being obscured. The imager can see some of the heated air around the fire, but not the exact center of the unobscured hot spot. As a clearer path to the hot spot occurs, a brighter hot spot is imaged. This will cause some error in the actual center for the hot spot. By monitoring the location of the brightest pixel within the identified hot spot, it may be possible to weight the 3D space intersection process and to potentially separate actual hot spots from strong reflections and low level thermal sources such as roads or rock.

The effect of an obscured hot spot is shown in the following excerpt from a video sequence, as depicted in Figure 4-2.

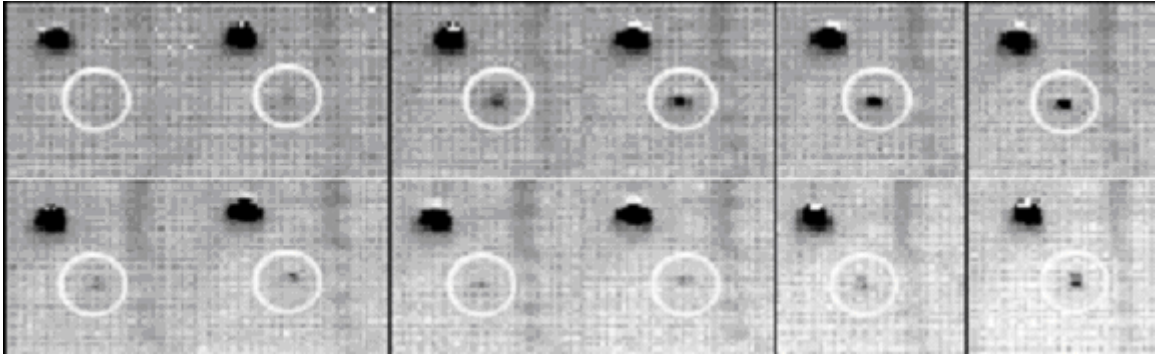


Figure 4-2: Extracted Sub Image Highlighting Obscured Hot Spot Effect

Note that these are inverted images, such that hotspots are black. These are 5 frame intervals going across for display purposes. This will cause a flickering effect.

4.2 Image Processing Terminology

Before going any further, the basic terminology used in explaining the image processing algorithms are defined as follows.

- Kernel - a 2D array that defines a particular set of mathematical or logical, spatially consistent operations. These mathematical operations can be either integer or floating-point operations. For faster computations, integer- and logic-based kernels are highly desirable.

- Convolution - the process in which the above kernel is shifted through the image matrix one pixel at a time, and the same operations defined in the kernel are performed at every pixel within the image.
- Pixel Neighborhood - the immediately surrounding pixels to the target pixel to within a certain distance.
- Connectivity - the alignment of the pixels within the pixel neighborhood. 4 connectivity refers to neighboring pixels that are in contact with the target pixel and aligned either vertically or horizontally to it. 8 connectivity includes all the 4 connectivity pixels and also any other pixels in contact with the target pixel that are diagonally aligned pixels to it.
- Thresholding - the process of partitioning of an image into regions. This is also called segmentation. Adaptive thresholding is useful when there is uneven illumination, and variable thresholding is where a function is fitted to a specific background.
- Object - the final desired feature that must be isolated from the background. To be effective in object - background separation, the images must have sufficient contrast and the threshold intensity levels are known. Object and feature are used interchangeably throughout this thesis.

There are also various levels of computation involved in image processing dependent on the types of operations desired. These operations include:

- Point level operations - where the output is directly determined from an operation on single pixels. Operations such as thresholding, image addition and subtraction are examples of point level operations.
- Local level operations - where the output is dependent on the neighborhood of the input pixel. Smoothing or blurring, and edge detection are examples of local level operations.
- Global level operations - where the output depends on the whole picture. Histograms and Fourier transforms are examples of global level operations.
- Object level operations - generally the next step after the image processing. These include feature tracking and process control.

With the above definitions, the thermal image processing will be presented. Additional issues related to processing speed will be discussed in Chapter 5.

4.3 Thermal Image Systematic Error Corrections

The systematic errors presented in Chapter 3 have a dramatic effect on the final results, necessitating a correction. The random noise and bad pixels observed are actually very easy to eliminate with a simple local operation called a median filter, which replaces the bad pixels with the value of the middle pixel from a sorted list of the surrounding neighborhood. This is proven to be very effective at eliminating this type of 1 pixel noise, while maintaining the overall sharpness of the image (Russ, 2002).

The second issue is the removal or equalization of the background. Two simple approaches are evaluated that involve monitoring a general image characteristic and using it to modify that specific image frame before extracting the desired features.

As shown previously in Figure 3-4, there is a fairly consistent shape and movement to the vertical profile of the images. This is the average value of all pixels within one row of the image. The approach is to subtract this average from every pixel in that row, with all negative values becoming zero. This gives a partial correction to the background variation as shown in Figure 4-3.

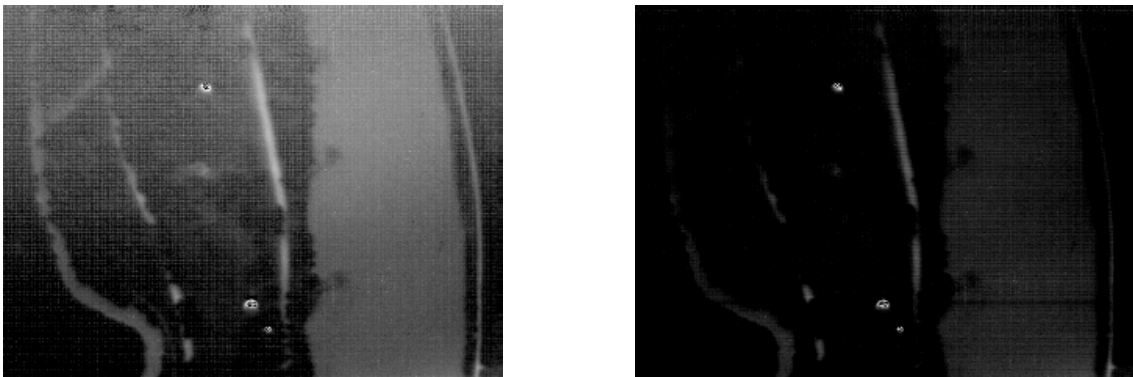


Figure 4-3: Background Correction Method 1

The problem with this method was that whenever there was a strong horizontal characteristic such as a road or trail, the feature would disappear. This could be corrected by instead using the characteristic curve only and shifting this up or down based on the mean of the image. A benefit from this approach is that the erroneous pixels may not need to be corrected first.

A second method is to use an image of a known constant object as the background and subtract this from the entire image, with an adaptive adjustment based on the difference between the mean of the image and the mean of the background. As previously noted in Chapter 3, the thermal imager has an inconsistent sensitivity at different average intensities, but very good results can be achieved by using a background image, as shown in Figure 4-4.

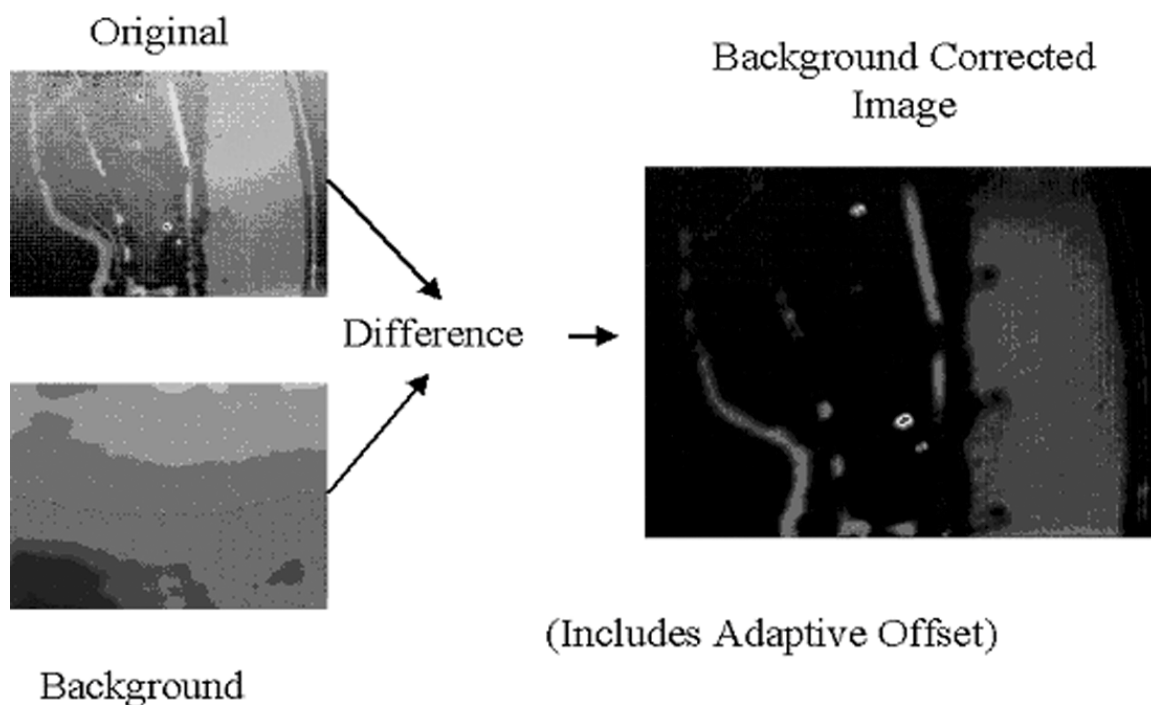


Figure 4-4: Background Correction Method 2

As with the first method, this approach also does a good job of correcting the background variation. By basing the selected background on similar intensity levels, a decent correction is obtained for this stage. The benefit of this is that it

is quick, and doesn't suffer any problems from a strong horizontal feature. Also, by using an uncorrected background image, any of the consistently bad pixels are automatically eliminated. The background image can be determined from the tests of the thermal imager with a controlled temperature bath as discussed in Section 3.4.1, or by using a large body of water imaged from a similar altitude, as the reference background.

There are other potential methods to identify and remove the variable background, specifically by using Fourier transforms. By transforming the image to its frequency domain equivalent and then filtering out higher frequency data and transforming it back to the spatial domain, a low frequency image similar to the background can be obtained. This was not explored at this time simply because of numerical complexity of this global operation, compared to a simple subtraction or point level operation. A potential benefit of using a Fourier transform and other global type operations is that other periodic noise artifacts could also be removed by designing an appropriate frequency domain filter, which can be explored in future work.

4.4 Initial Feature Identification

Once the image has been corrected for any systematic errors, the features can be identified by a simple threshold operation, as shown in Figure 4-5.

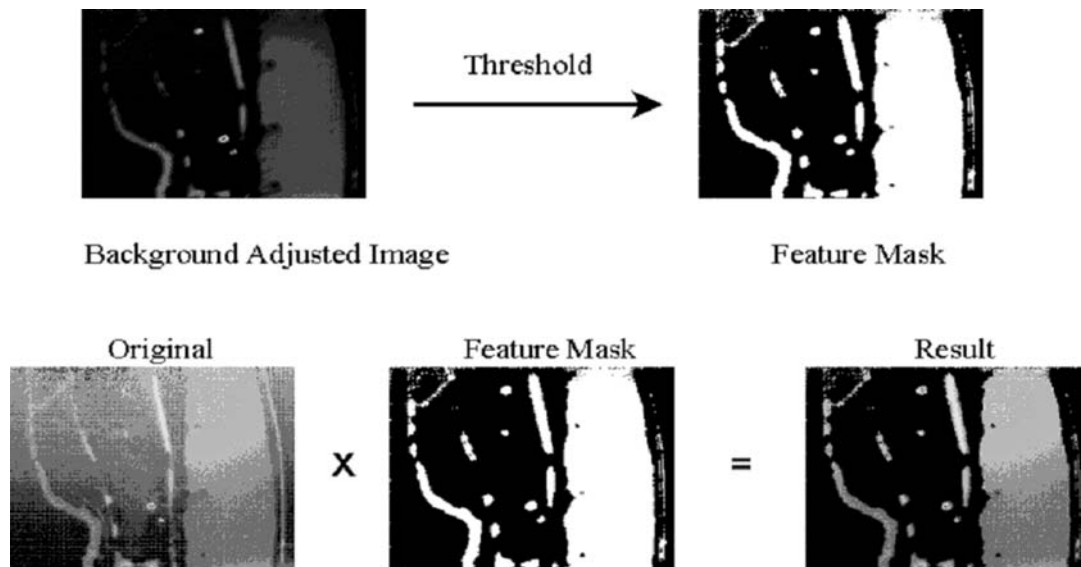


Figure 4-5: Final Image Processing for Feature Identification

The threshold selected is dependent upon the desired final results. In this case, a very low threshold is used to identify any feature that was brighter or warmer than the average background. Using a higher threshold would only identify the hottest points, which would definitely be fires, but may miss enough details to locate the point accurately in later processing. This will be explained in more detail in Section 4.5.

4.4.1 Feature Extraction

The feature extraction process is another very well defined process (Jain et.al., 1995). This can include many parameters about the feature, including position, size, orientation, perimeter, compactness, minimum and maximum limits, and maximum values, to name just a few. The actual process of component labeling

is a relatively simple sequential algorithm, as presented in (Jain et.al., 1995), although the basic principles are outlined next. With the potential features identified above, the position, size and location of the hottest pixel is determined by convolution through the image with a simple 2 X 3 logic kernel, as shown in Figure 4-6.

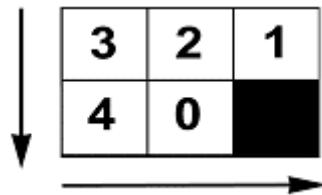


Figure 4-6: Feature Extraction Logic Kernel

Basically, if the target cell (0) is part of a feature, then a check of the surrounding cells (1, 2, 3, and 4) is done to determine if it is adjacent to a previously labeled feature or that it is a new one. Only the past cells need to be checked, as the feature label is inserted into the *image* to allow for further object or feature identification. Cells 1 through 4 have already been processed and contain a feature label that is passed forward to further cells as the kernel passes through the image. If none of its neighbors have a label, then give this pixel a new label. If any of the previous pixels have a label, then that label is copied into the target pixel. Note that the lowest label value is used. In either case, add the pixel coordinates to a running summation of coordinates for that label, as well as to the pixel count for that label. This gives both a centre of gravity for the object feature

and an area for it. Once the entire image is processed, any labels that were combined by the process have their results combined as well.

An additional required function is to locate the *hottest* point within the identified feature since the feature center of gravity may not be the hottest part of the identified area. This is due to the obscuring effects discussed in 4.1.1. This is done by incorporating a maximum value check into the logic kernel, then recording the magnitude and location of that local peak within the feature object information structure. This was also done to test a personal hypothesis. This hypothesis is that a hot spot will have a varying maximum due to the obscuration effects and its maximum and variation are needed to indicate that it is fire across a larger range of image frames. This will be discussed more in Section 4.6.

4.5 Feature Tracking And Enhanced Feature Identification

The tracking of the features from frame to frame can become a numerical nightmare. There are several different approaches and issues to be considered as outlined next to help reduce the complexity.

The actual process of identifying the same object or feature across multiple images or frames is called the correspondence process (Jain et.al., 1995)(LaPlante, 1996). The actual method used in this correspondence process involves the matching of feature characteristics of consistent objects, or critical points, lines or other significant features. If this involves a large number of features, then the process can become very computationally expensive (Jain et

.al.,1995)(LaPlante, 1996). Various methods have been developed to reduce this problem by effectively limiting the number of features to try to correlate. An estimate for both direction and magnitude can help restrict the possible matches to improve the overall correspondence process. Using multi-resolution methods and coarse- to fine-grain approximations to find the optical flow or using time varying edge detection and difference imaging can obtain these estimates. Typically, it can be assumed that the scalar velocity of a given point will be relatively unchanged, as will the direction. A desired feature should have strong path coherence, which is when there is no dramatic change between frames from having a high enough sampling rate (Jain et.al., 1995). Strong path coherence typically assumes the same number of feature points available from frame to frame and that no features are missing, which isn't always the case. The motion estimation process is augmented dramatically with the inclusion of the WADGPS / IMU data for every frame as there is a direct correspondence between changes in position and attitude to the optical flow in the video frames. This can be directly incorporated into the correspondence process.

An evaluation of the overall camera-object relationship and aircraft configuration indicates that there is primarily a Y axis planar motion, with limited X and Z motion for the camera. In addition, the object of interest is stationary and relatively fixed in location, although occasionally occluded. In the worst case, it may be visible for only 1 frame before being blocked again for a number of

frames. Figure 4-7 displays the motion of the above hotspots through the video frames.

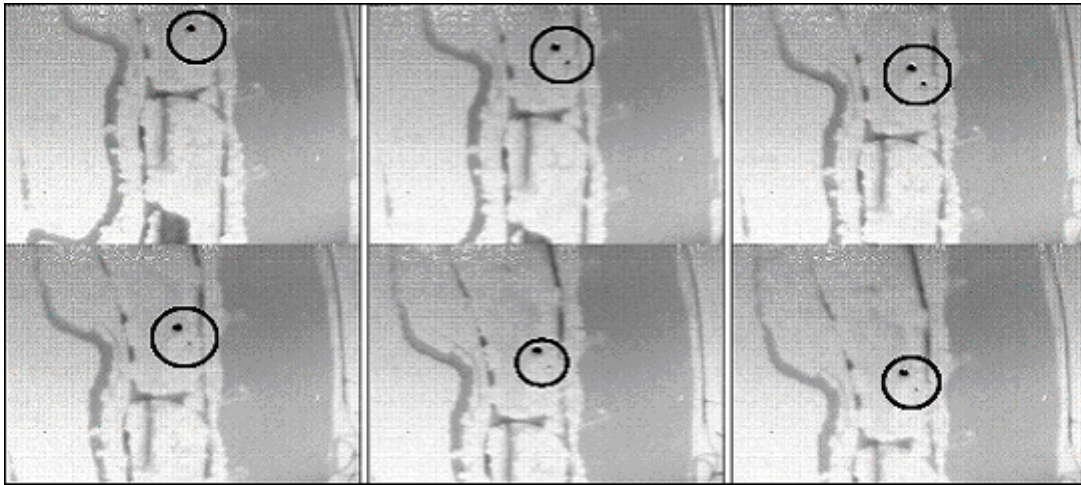


Figure 4-7: Sample Frames Representing Hot Spot Motion Through Frame

Note the image flow through the frame is from the top to bottom of the frame, and stays in approximately the same area horizontally, as expected for a fixed wing aircraft. In a helicopter-based system, the actual relative image motion can vary horizontally and vertically very quickly, such that the effective scale may change as the helicopter changes altitude, although that is not evaluated further here.

4.5.1 Pixel Motion Estimation

Motion estimation is the determination of spatial change over temporal changes. The first step in tracking the hot spots from frame to frame is to develop an estimate of the potential or effective pixel motion that could occur. This involves both the camera characteristics and the overall motion and flight characteristics. These include the effective height, flight speed, crab angle and attitude variation

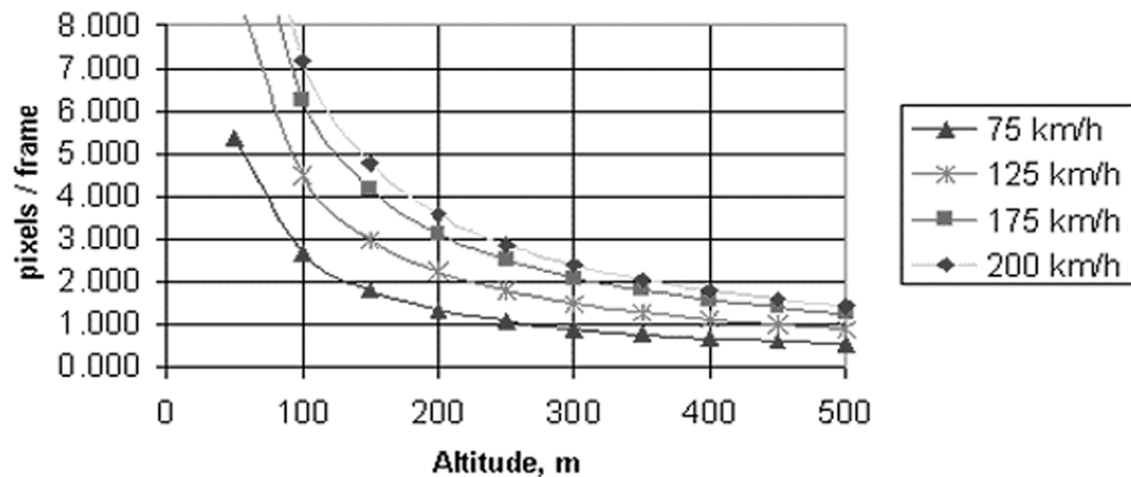
of the system, as well as the effective field of view of the camera. On a frame-by-frame basis, there is a direct correspondence between the change in roll (dr) and change in image x coordinate (dx), as there is with change in pitch (dp) and change in image y coordinate (dy). The crab angle, or difference between actual motion vector and the body orientation will have a slight affect on both x and y, adding additional variation to both dx and dy . The majority of the image flow will occur from the position changes of the aircraft instead of the attitude. There is a direct correspondence between dy and the forward motion of the aircraft, just as dx corresponds to any side to side motion. Finally, the actual pixel motion due to attitude variations is independent and unrelated to height, but pixel motion due to speed is directly related to the height as a result of the change in scale with height.

For example, In a remote sensing application, the attitude of the aircraft is generally controlled very tightly such that the variations are minimal, although a range will be considered here. Table 4-1 shows the pixel motion range estimates due to attitude variations, and Figure 4-8 shows the pixel motion range estimates due to height and flight speed. In Table 4-1, the pixel variation range is determined from the focal length and the actual pixel dimensions of the thermal imager for the roll and pitch variation, while the pixel variation range due to the azimuth is calculated at the edge of the image. This approach gives a worst case estimate of the pixel motion.

Table 4-1: Pixel Motion Estimate Due to Attitude Variations

Angle Type	Degrees	X	Y
		Pixel Variation	
Roll:	0.5	2.61	0.00
Pitch:	0.5	0.00	2.61
Azimuth:	0.5	1.38	1.38
Total:		3.99	3.99

**Pixel Translational Motion
@ 29.97 frames/s**

**Figure 4-8: Pixel Motion Estimate Due to Speed and Flying Height**

For example, If an aircraft is flying at 300 meters altitude with a speed of 125 km/h, the expected range of pixel motion would be in a range of 1.5 pixels/frame

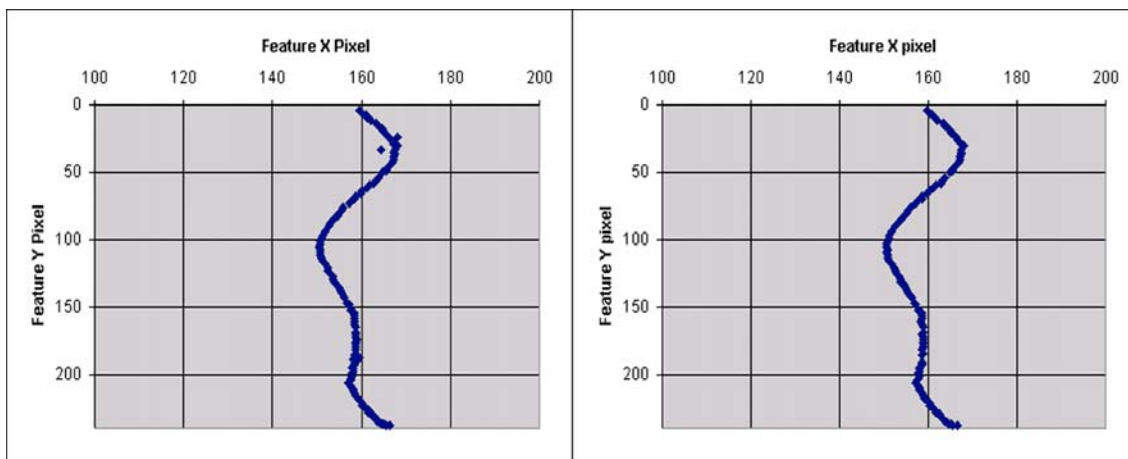
forward (due to forward and pitch motion) with nearly 4 pixels in all directions. The crab angle will determine a trend in the motion through the images. For example, a crab angle of up to 10 degrees either way will cause a shift in the x pixel coordinate of $(0.17 \text{ pixel}) / (\text{pixel y motion})$.

All of these parameters are readily available except for the flying height, which is normally defined in a flight plan. The speed can be determined from the GPS data, and the crab angle can be determined from the heading information from the IMU and the actual heading from the GPS data. The forward pixel motion may also be determined from recently tracked hot spots, which will also provide an estimate to the actual image scale.

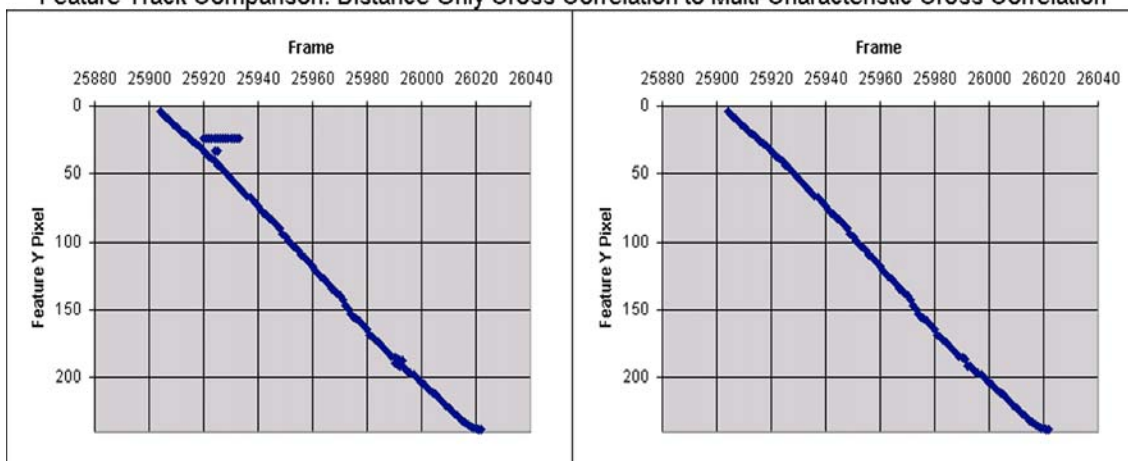
4.5.2 Feature Cross Referencing And Tracking

Figure 4-9 identifies characteristics used to correctly track a particular feature, and highlight the problem with using the closest feature for cross-referencing. If an erroneous feature is connected to a particular feature track, the error is continued through to the next frames. This can be seen with the small line of feature points on the X and Y pixel tracks, although it is not as obvious from the X-Y Feature Track diagram.

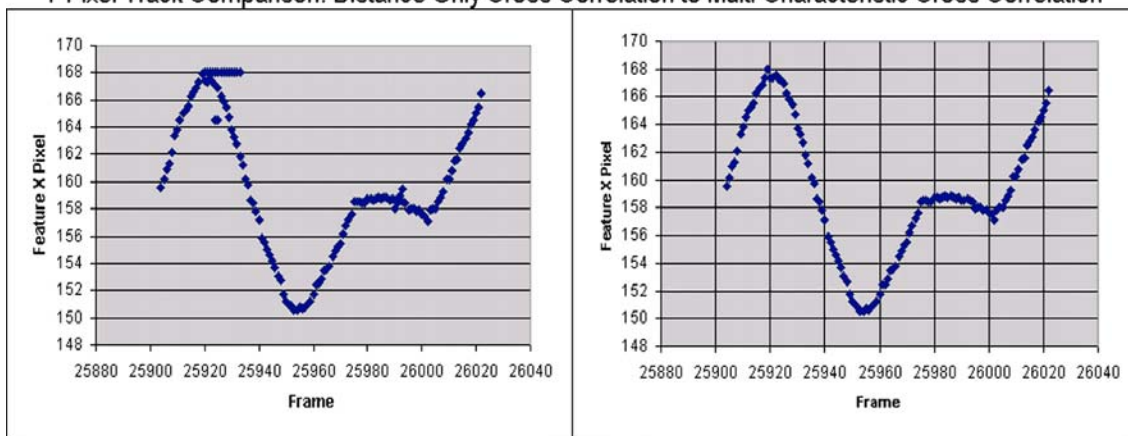
Figure 4-10 shows other possible correlations to test the correctness of the correspondence and cross-referencing procedure. As can be seen, both the Natural Log of Area ($\text{Ln}(\text{Area})$) plot and the correlation of the Delta X to Delta Roll show very distinctive correlations from frame to frame that can be exploited.



Feature Track Comparison: Distance Only Cross Correlation to Multi-Characteristic Cross Correlation

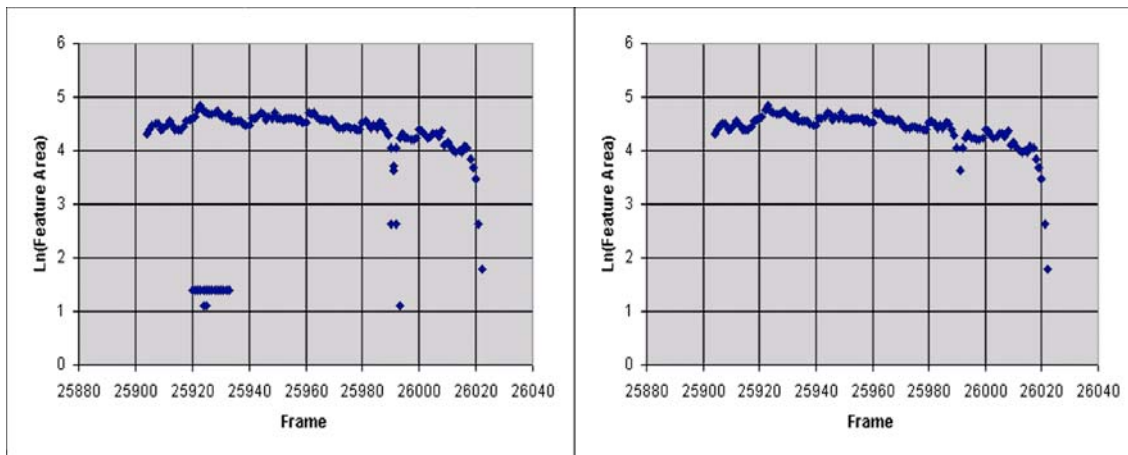


Y Pixel Track Comparison: Distance Only Cross Correlation to Multi-Characteristic Cross Correlation

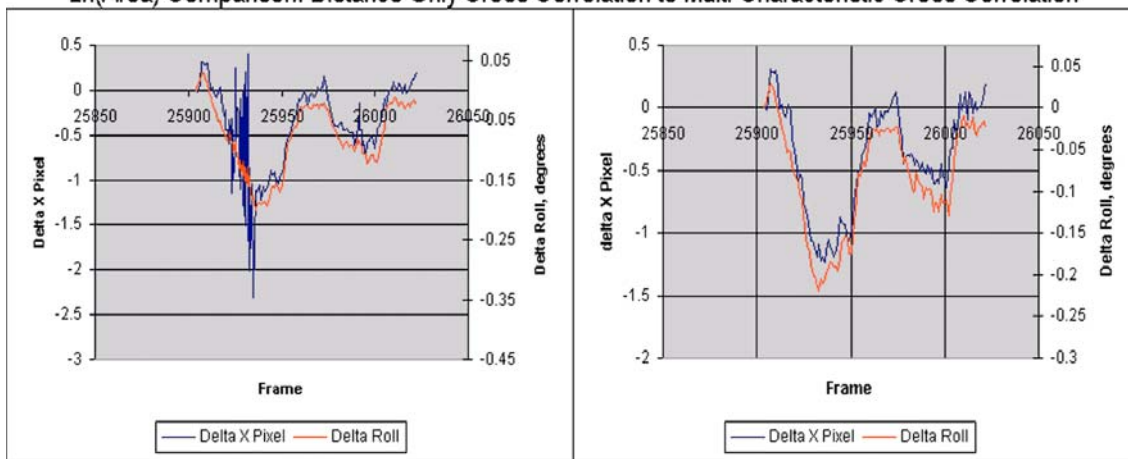


X Pixel Track Comparison: Distance Only Cross Correlation to Multi-Characteristic Cross Correlation

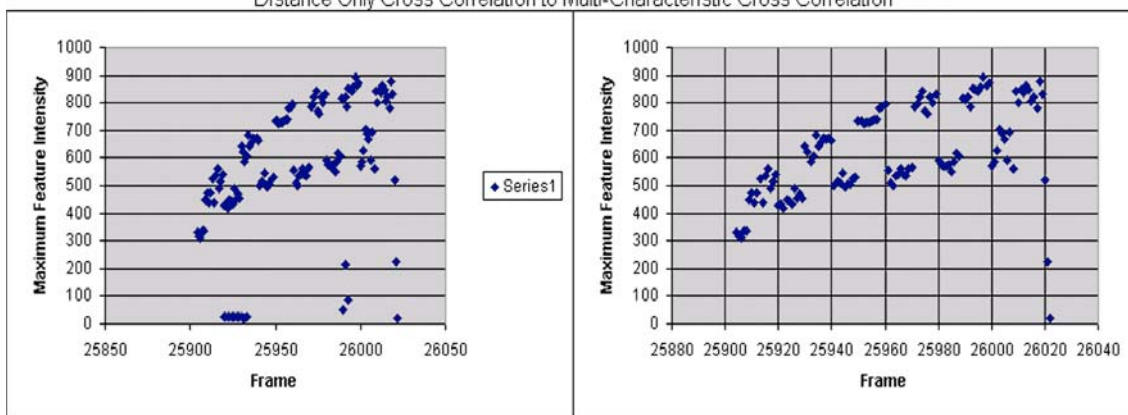
Figure 4-9: Feature Track Comparisons



Ln(Area) Comparison: Distance Only Cross Correlation to Multi-Characteristic Cross Correlation



Delta X Delta Roll Comparison:(5 Frame Running Average)
Distance Only Cross Correlation to Multi-Characteristic Cross Correlation



Maximum Feature Intensity Comparison
Distance Only Cross Correlation to Multi-Characteristic Cross Correlation

Figure 4-10: Feature Correspondence Correlation Tests.

These errors actually occur when multiple features within one frame are found to be within the particular target distance, and as such, the additional correlations can help decide between multiple cross-referencing solutions within a frame.

4.6 Hot Spot Evaluation

Once the extracted features are cross-referenced from frame to frame, the magnitude of the hottest pixel can be evaluated to determine if that feature had a wide range of values or a flat, relatively consistent value. The lower right graph within Figure 4-10 shows the maximum feature Intensity. There is a regular pattern or oscillation with the maximum Intensities, which actually corresponds to regular 1/2 frame slip, or odd / even field change for the interlaced video signal. This occurred in capturing the video and coincides with the timing of the synchronization signal used as the GPS mark time input.

This feature track is definitely of a hot spot, as the maximum intensity is well above the general maximum intensity statistic for day or night, even with the aircraft still on the ground as previously discussed in Section 3.4.1 and shown in Figure 3-3.

Figure 4-11 is included to show the purpose for using a low threshold for segmenting the images. By tracking the lower intensity features, they may occasionally manage to have a maximum intensity that separate them significantly enough from the background for them to be considered hot spots.

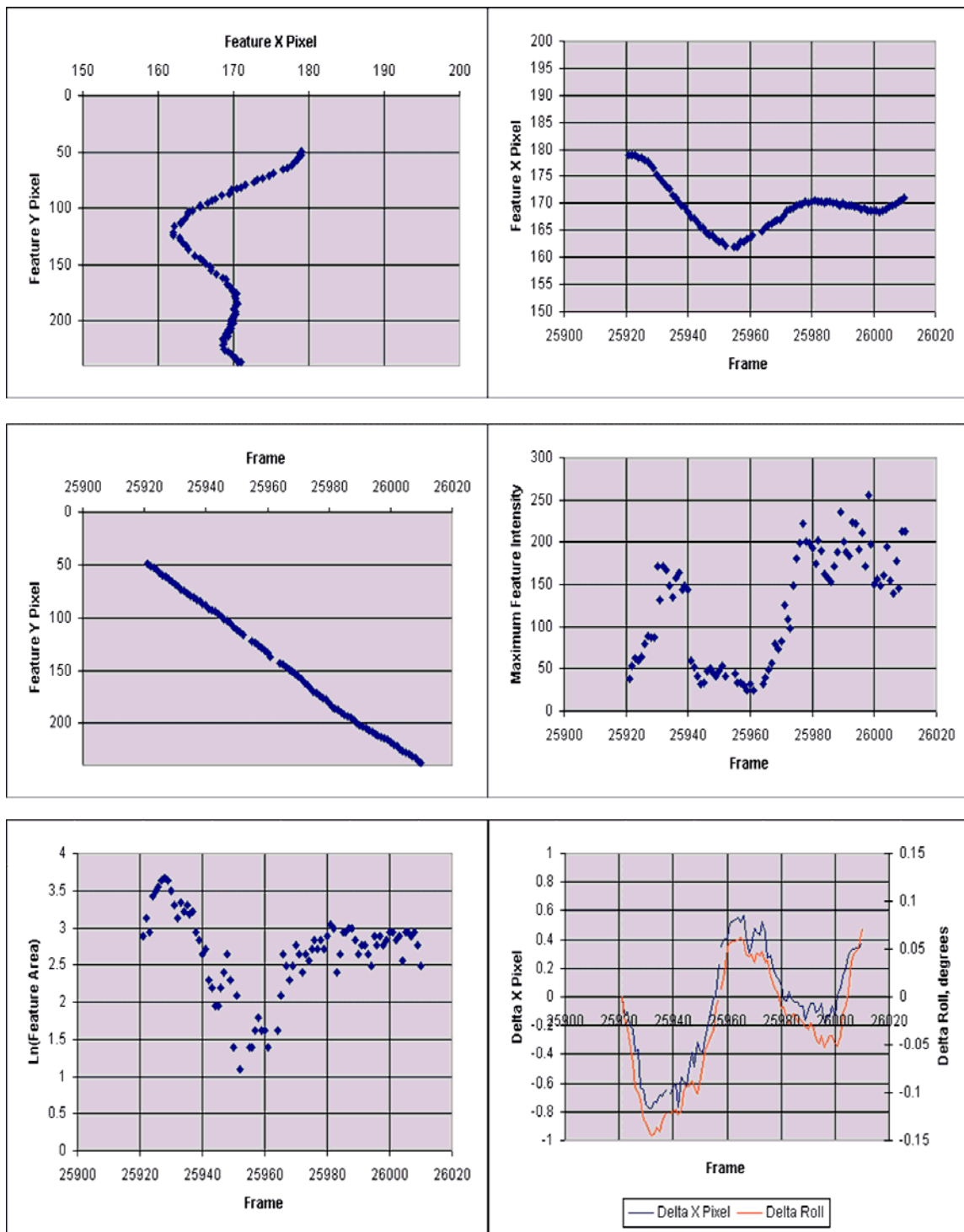


Figure 4-11: Small Partially Obscured Hot Spot Tracks

All of the desired correspondence features are there over a long track, but only the last third of the actual features exceed a threshold intensity of 200. By tracking this feature when it has a low intensity, a longer track is available to help provide a wider angle for the space intersection process.

4.7 Forest Fire Detection from Thermal imagery Summary

This chapter has presented the general methods used in the identification of forest fire hot spots. This started with a general introduction of image processing terminology which is then used to explain the different steps of the image processing. This includes how systematic imaging errors can be corrected for, then how the potential hot spot features are isolated and identified. Once the potential features are identified, the cross referencing and correlation process used to correctly identify a specific feature track was presented. Finally the actual validation of a forest fire hot spot was presented by the simple evaluation of the maximum feature intensities along the length of the entire feature track.

Chapter 5

Real-time System Integration

This chapter will discuss the different hardware and software components of the overall system, and how they are interconnected. The first section presents some of the issues related to the development of real-time systems. This includes a brief discussion of specification and design issues, definitions and general programming issues and considerations related to real-time imaging. The second section presents how these were applied in the development of the forest fire hot spot detection system.

5.1 Real-time Systems Overview

A real-time system controls and monitors some physical process in a timely manner (Douglass, 1999) and can be defined as a system that must satisfy some explicit bounded response time to a specific set of inputs. LaPlante (1997) among others (Douglass, 1999)(Labrosse, 2002) point out that real-time systems are ones where the actual response times must be constrained and thus predictable and is as important as the correctness of the output.

5.1.1 Real-time Definitions

Before going into further discussion about real-time systems, some definitions of key terminology are required for clarity.

- Deterministic Behavior - describes a system whose time evolution can be predicted exactly.
- Responsiveness – describes how fast the system reacts to the external sensor inputs.
- Predictability - describes the extent to which the characteristics of a system can be known ahead of time.
- Task (or thread) - a program that thinks it has the computer CPU all to itself and performs its own specific functions.
- Task Switching – occurs when the multi-tasking kernel decides to run a different thread. They add overhead but simplify the design by allowing the application to be divided into multiple tasks.
- Task Priorities –the importance of a particular task or thread.
- Static Priorities – exist when all the tasks and their timing constraints are known at the time of compilation.
- Multi-tasking - the process of scheduling and switching the CPU between several sequential tasks. This allows for the maximum utilization of the CPU and provides for modular construction of applications

- Concurrency - the simultaneous execution of multiple sequential chains of actions, by either a single or multiple processors. Pseudo concurrency is when a system has a single processor available to handle the multi-tasking process. True concurrency is when a system has multiple processors to handle the multiple tasks.
- Kernel - the part of the multi-tasking system responsible for the management of the tasks and the computer CPU usage. There are co-operative multitasking kernels, where the tasks co-operate with each other by running until it voluntarily gives up control. The problem is that this type of kernel is non-deterministic. There are also pre-emptive kernels, which are used when system responsiveness is important. The highest priority task is always given control when it is ready to run. Task level response is minimized and deterministic.

Many authors consider there are degrees of real-time systems, depending on how critical the outcome is. Three terms were found in literature (Douglass, 1999)(Labrosse, 2002)(LaPlante, 1997) for defining the degrees of real time. These are hard, firm, and soft.

A hard real-time system has performance requirements that must be met. All tasks must run correctly and on time, and are characterized by the severe consequences that may result if correct logic and time properties are not met. A

heart monitor that misses a random heart beat event can lead to an incorrect diagnosis or response.

Soft real-time systems are on the other end of the spectrum. They may have an average execution time constraint, but late data may still be good data. The time constraints may dictate that the tasks are performed as fast as possible, but without a specific deadline. In soft real-time systems, the performance is degraded but not destroyed by failing to meet a response time constraint (LaPlante, 1997).

A firm real-time system is one in which sufficient average performance is maintained at all times. The system developed for this thesis would fall into this category, in that late data isn't necessarily a problem, but there is a specific time deadline that must be met.

5.1.2 Real-time Systems Specification and Design

The initial requirement definition for a real-time system can be very simple and yet deceiving. It starts from a simple definition of the input and output requirements and leaves the rest of the system as a simple black box of unknown quantities. The actual performance budget is determined from this black-box perspective and propagates into performance requirements and budgets for every individual action (LaPlante, 1997). The temporal behaviour is the hardest and most important aspect of specification and design in a real-time

system, as it defines when everything must happen and in what order for the system to work.

The system specification details what the software will do and in what environment it will function; whereas, the design tells us how the software and hardware will do it. In reality, there is a fuzzy line between the specification and design of a system, and can even be an iterative approach. There is really no singular, perfect technique, although there is significant work on formalizing the approach, such as real-time Unified Modelling Language (UML), following along the UML standards developed for general software engineering.

There are many issues that must be resolved for the design of a real-time system. The selection or availability of hardware and software greatly affect the development of a cost-effective solution. Also, the involvement of both hardware and software engineers during the selection of hardware and software will significantly help in determining the best balance. For example, some hardware may be limited to a specific platform and operating system or have proprietary drivers such that it dictates how the rest of the system must be put together.

One of the goals in the design of real-time systems is to maximize the tolerance of the system to faults, which is achieved through careful design and rigorous testing. As such, testing is an even more critical aspect in the development process, in that it is meant to do more than just flush out any errors. The design must ensure that the software meets its requirements as specified, which is more

than simple black box testing (LaPlante, 1997). Black box testing simply provides the inputs to generate specific outputs, but doesn't always test all possible control paths and possibilities, and is generally data driven. More detailed testing is required. White-box testing (LaPlante, 1997), as it is sometimes called, involves designing the tests to exercise all possible control paths in any software module and is more logic driven.

Obviously there is a great deal more involved in the specification and design of a real-time system of any type. This is intended to give only a brief overview.

5.1.3 Real-time Image Processing Issues

Real-time image processing is a very challenging area in that it involves far more data than many real-time systems. Instead of hundreds or even thousands of sensors to process, it handles tens of thousands to millions of sensors, since every pixel is in fact an individual sensor. As such, any image processing is numerically complex and intensive because of the quantity of data. As discussed previously in Chapter 4, the goal of image processing is to recover useful information about a scene from its two dimensional projections. For real-time image processing, this is extended to recover the useful information in a manner that is numerically and computationally efficient.

Various types of operations were defined previously in Chapter 4. There are additional factors that affect the potential efficiency of these operations that are discussed next.

Point level operations have a simple one to one relationship that are easily implemented in real time. These include addition, subtraction and threshold operations.

Local level operations are generally possible in real time, although there are additional factors that are involved that can affect the computational load, such as the kernel size or neighborhood, separability, and the type of operation being performed.

For example, a simple blur filter is linearly separable, meaning that it can be separated into a combination of row operations then column operations. This separation reduces the number of times a particular pixel is actually examined, subsequently reducing the computational load. Removing any dependence of the computational load to the neighborhood size is desired, although not always possible. For a simple blur filter, further reduction in the computational load is achieved by noting that once the first element of the particular row kernel or column kernel is calculated, the next computation only requires the addition of the new pixel value and subtraction of the oldest pixel value.

A median filter is an example of another very useful local level operation for noise reduction that unfortunately is both non-linear and non-separable. Devillard (1998) compares various methods to optimize the computational load of a gray scale median filter. Judicious selection of kernel size and neighborhood type is required when using this filter to keep the computational load as low as possible.

Global level operations can be the hardest to implement in real time, but they may still be the most effective way to extract the desired information from the images. For these applications, specialized hardware has been developed. For example, 2D Fourier transform filtering is a very powerful and flexible image processing technique and as such, specialized hardware is available.

Real-time image processing is an area of intensive ongoing research, and is critical to this research. The above is an extremely brief presentation of some aspects that apply to the specific operations used in this research and discussed further in Section 5.3.1.1. Further detail and exploration are beyond the scope of this thesis.

5.1.4 Synchronization Issues

Even with the huge computational load requirement of real-time image processing, there are many systems in which additional data must be synchronized with it for it to be useful. Adding position and attitude information derived from the IMU and WADGPS, to the thermal images is a typical example of the importance of synchronization for the hot spot detection system. This information is necessary for the computation of the 3D coordinates of the extracted hot spots in real world coordinate system. The remainder of this section will discuss the different mechanisms that commonly used in synchronizing data streams in real-time systems.

Several different software and hardware mechanisms exist to facilitate the task of synchronization, inter-task communications and task switching, and are consistently defined by Douglass (1999), LaPlante (1997), and Labrosse (2002), among others. In software mechanisms, an event is any occurrence that causes the program to change flow of control. It is used to signal between tasks that a specific task has been completed and is ready for more data, or requires attention to respond to other events. In hardware mechanisms, an interrupt event is a hardware mechanism that is used to indicate that data is ready and waiting, such as when data is at the serial port or other hardware interface device. The hardware interface typically requires an immediate response so that it doesn't lose the data. Therefore, interrupt events typically have a higher priority, if not the highest priority of any events. The only mechanism that may delay or disable interrupt events would be a task which was in a critical section. Critical sections are sections of code accessing serially shared reusable resources and must be given special consideration. Critical sections should only be used when changing a few shared variables and should be kept very short. A long critical section may cause a loss of critical incoming data. Interrupt event themselves have their own event handling task, that would simply extract the data from the device into a shared data buffer that other tasks have access to for further processing. The problem is that interrupts can be very non-deterministic

depending on the data transfer mechanism and rates. Interrupt driven switching isn't necessarily the fastest task switching process.

A very effective structure to help maintain consistent and quantifiable memory use is a ring or circular buffer. It effectively appears as an infinite buffer, but is a fixed memory size where the beginning and end of valid data is tracked by a head and tail pointer. These buffers (and queues) are used to handle more complicated data passing in real time (LaPlante, 1997). The appropriate buffer sizes must be determined to allow for situations when data production can exceed data consumption for short bursts, such as high speed serial data capture and parsing. By creating these buffers in shared memory, the maximum amount of data that is processed during each periodic cycle can be software-controlled (Stewart, 2001). Another form of buffer is called a named pipe. Named pipes are another level of abstraction to a shared memory resource, with additional levels of synchronization and functionality that may be useful in certain situations. On a Windows NT operating system, named pipes allow for not only sharing data between processes on a single system, but also between remote systems.

Even with the data being available between tasks, the access to the data must be controlled, which requires signaling between tasks as to whether the data is accessible or not at a specific time. A semaphore is a mechanism that provides exclusive data access, and is an effective mechanism at protecting critical

regions. Message Mailboxes and Queues are another naming abstraction for shared memory resources for communicating between tasks in real-time systems. In this mechanism, all the data transfer and communications mechanisms are designed to work on a First in First out (FIFO) basis.

Priority inversion is the term for a scenario in which the highest-priority ready task fails to run when it should, which happens on cooperative operating systems when a lower priority thread doesn't yield to a high priority thread.

One major problem that can happen in real-time systems is the deadlock. Deadlock occurs when two tasks are unknowingly waiting for a resource controlled by the other, and is often introduced by erroneous synchronization attempts. Deadlocks can be hard to catch as it may only occur very infrequently. Careful design can prevent deadlocks, but it isn't always possible, depending on the complexity of the system. The necessary conditions for a deadlock to occur are (Douglass, 1999):

- Mutual exclusion - where each task blocks access to a resource while using it.
- No pre-emption - a task can not be interrupted by a higher priority task.
- Hold and wait - where the tasks hold on to a particular resource and wait for the additional resources it needs.
- Circular wait - where two or more tasks are waiting on resources in such a way that the tasks are waiting for each other to release a resource.

Synchronization in real-time systems is a very crucial and complex process. The efforts and approach to synchronizing the data streams for the hot spot detection system developed in thesis are presented in Section 5.2.3.

5.1.5 System Speed

A simple solution for real-time image processing could appear to be to have more system speed and processing power, and even multiple processors. In some respects this is true, in that imaging applications are well suited for parallelization and hence faster parallel architectures. Specialized architectures and hardware is even readily available for particular algorithms, as previously mentioned. There would still be important trade off's between overall performance, to image resolution and algorithm computational loads; the number of tasks to synchronization complexity; and image resolution to data storage and I/O bandwidth requirements (LaPlante, 1996). Algorithms would still need to be formulated appropriately to work on multiprocessing architectures. Finally, it could be said that faster processors and more memory than necessary tend to lead to laziness in thinking about the design (Stewart, 2001), and end up with a system much more complicated and expensive than required.

5.2 Hot Spot Detection System Development

With a background of some of the various real-time systems issues to consider, the details of the hot spot detection system development can be presented. This

will start with the original system specification and go into some hardware and issues that significantly influenced the system design. Then some general software design concepts are presented, leading into the system software design overview.

5.2.1 System Integration Overview

The main objective of this thesis is to develop a forest fire hot spot detection system that combines a thermal video camera and a georeferencing unit into a system that will automatically identify and locate forest fire hot spots to within 10 m during night and day operations. From this general objective and an evaluation of available hardware systems, the general system schematic shown in Figure 5-1 was developed.

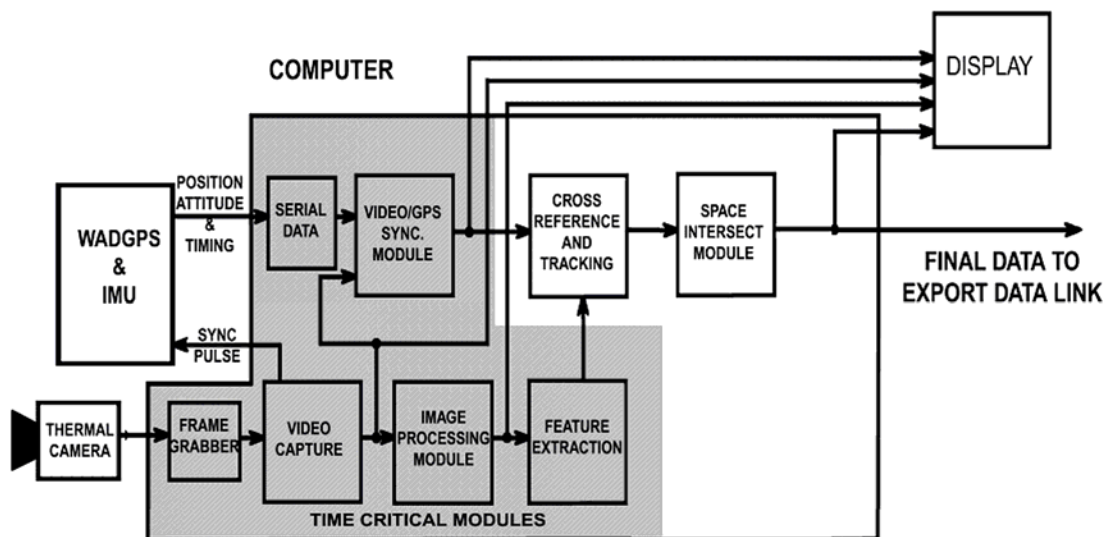


Figure 5-1: Forest Fire Hot Spot Detection System Overview

This schematic shows the system hardware and general software data flow, including the direct georeferencing subsystem, consisting of the WADGPS and IMU, the imaging subsystem consisting of the thermal camera and frame grabber, and the computer processing system.

An RS-232 serial port is the communications interface between the computer system and the georeferencing subsystem, as the frame grabber is the communications interface between the computer system and the thermal camera. Note that there is a link from the video capture module back out to the georeferencing subsystem. This is critical to the proper synchronization of the system and the accuracy of the final results. This will be discussed in more detail in Section 5.2.3.1.

The georeferencing subsystem provides the position and attitude of the imaging platform plus a synchronization time stamp. The imaging subsystem captures a continuous video signal from the thermal camera and provides the software interface providing the image data to the computer processing system.

5.2.1.1 Software Operating System

The selection of the underlying software operating system for a real-time system is critical, but not always flexible. Then an understanding of various operating system issues is required to allow for a more stable design within that system.

In this research, there was no choice in the selection of operating system. This is mainly due to the fact that the only available frame grabber for this research

comes with its proprietary software drivers that only function in a Windows operating system. This has some pros and cons as outlined next. Basically, the Microsoft Windows operating system has (for the foreseeable future) become the de-facto standard for desktop and industrial solutions. The numerous development tools available make it a simple initial choice. Unfortunately, for true real-time applications, Microsoft Windows is not considered to be real time because of the following points (O'Keefe, 2002):

- Too few thread priorities (although one of the real-time extensions to Windows mentioned next has the same number of priorities);
- Opaque and nondeterministic scheduling decisions;
- Priority inversion, particularly in interrupt processing.

Microsoft even provides technical articles that support the fact that it will not work as a real-time systems yet fortunately directs developers to partners that have developed real-time software extensions to allow for a hard real-time implementation within a Windows Environment. These include RTX (Venturcom, Inc., www.vci.com), INTime (TenAsys Corp., www.tenasys.com), and HyperKernel (Nematron Corporation, www.nematron.com). Preliminary evaluation of the capabilities of these software extensions at the initialization of this thesis suggested that they were not able to utilize the dual processor hardware system being used for this research, and therefore were not used.

An additional frustration to the use of Windows is that Microsoft has developed a multimedia framework into the Windows operating system, yet the frame grabber manufacturer does not provide a corresponding driver to function directly with the Windows Driver Model (WDM). The benefits of having a WDM driver for the hardware would have reduced programming requirements by using built-in multimedia data streaming and synchronization conventions so that system performance associated with any thread context switches among other issues does not decrease. Developing a custom WDM driver for the hardware is beyond the scope of this thesis. The software library available with the hardware does allow for storage of video, but additional software co-ordination was required to make it functional for continuous video storage. This includes the determinism of any hardware interfacing requirements. One area specifically that is troublesome is file and disk I/O. Real-time systems normally have file and disk subsystems that are designed specifically for deterministic behaviour; whereas, Windows does not. This dictated that certain design concepts be utilized in the attempt to overcome some of Windows real-time shortcomings.

For example, since Windows is considered to be a non-deterministic operating system, any dynamic memory allocation is avoided. Static shared memory between threads (such as circular buffers, queues and pipes) is used, such that dynamic allocation only occurs during the system initialization phase. This is done to limit OS intervention whenever possible. The operating system issues

can not be avoided, including any background and core threads, so an allowance in the size of the buffers to hold several seconds of data is made. Complete elimination of interrupts is not possible, but continuously polled loops are used for data capture whenever possible. This is because of unknown interrupt latencies within the system. These capture loops are given the highest priority so that they are almost always checking for data, even if other threads are in the middle of any processing. More processor overhead room than normally required for a real-time system is desirable to handle Windows tasks. A final general concept, applicable for all real-time systems, is that functional groups should be written as concurrent loops that are encapsulated within inseparable threads.

5.2.2 System Software Design

Finally specific modules within the computer processing system are presented. First, how the video and georeferencing data streams are synchronized is discussed, leading to other critical synchronization elements and finally the remaining aspects of the system. This will give a complete overview of the flow of operation of the system, with general explanations and real-time details of key modules and threads.

5.2.3 System Synchronization

Two key areas required careful programming to allow for overall system synchronization. These are the video to georeferencing data synchronization

and the storage synchronization. These two key areas will be discussed in more details next.

5.2.3.1 Video To Georeferencing Data Synchronization

The georeferencing subsystem, a Novatel Black Diamond System (BDS) has a limited mark timer rate that is slower than the potential video capture rate from the imaging module. Ideally, it would have been preferred to trigger a time mark every captured video frame and interpolate the position and attitude for every frame based on that time mark. The frame grabber has a built-in mechanism that enabled the system to trigger the time mark in hardware with minimal software overhead. Since this was not an ideal situation, an additional synchronization parameter was required; namely, a computer time mark for every captured video frame in the computer time system. The computer time and the georeferencing time are not perfectly synchronized, but by introducing this additional information, a reasonable synchronization could be done. Figure 5-2 presents this further.

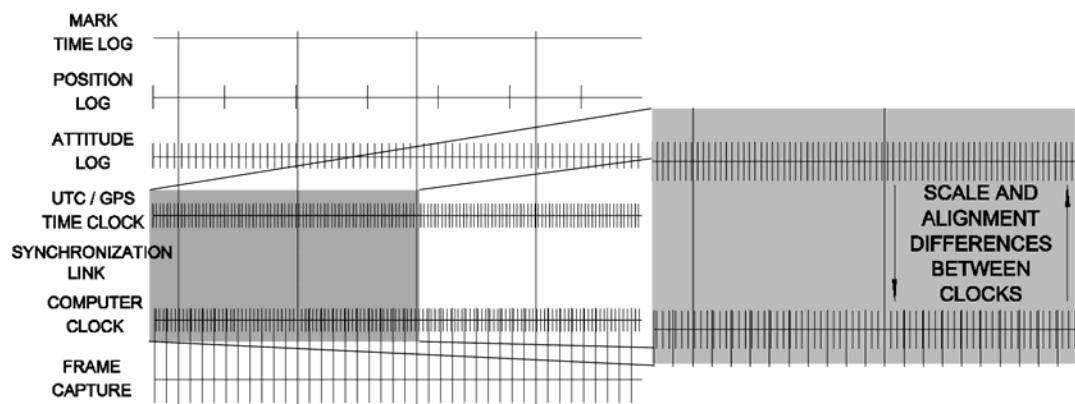


Figure 5-2: Synchronization Timing Chart

The actual mark rate possible at the time of testing allowed for a UTC time mark every 10 frames. The system position was received at 5 Hz and the attitude was received at 50 Hz, all of which are synchronized to the UTC timer. The complexity of the system was increased by the requirement to correctly correlate the georeferencing time and the computer time.

As previously discussed in Sections 5.1.4 and 5.1.5, there are several software issues that must be carefully handled to avoid any problems. Additional software overhead was required to buffer the incoming georeferencing data and to synchronize with the data transfer from the video capture. For the position and attitude information to be interpolated to the video frame timing and then merged back to the processing stream required further synchronization steps. The actual data transfer mechanism used was a data queue, in which both the captured georeferencing data and the video computer time mark used a common data queue to feed a Queue / Synchronization thread.

Figure 5-3 outlines how this thread organizes and maintains an internal list of the frame times, the position and attitude data, and the mark time data. Then this data is correlated and used to interpolate the georeferencing data into a common frame referenced data structure, which is shared with the merge thread (shown in Figure 5-7) to be merged with the frame referenced feature data. This process introduces numerous time / position discrepancies, although they are generally

less than 5 milliseconds, causing a potential horizontal positional error in the sub-meter range which is well below the potential accuracy of the WADGPS system.

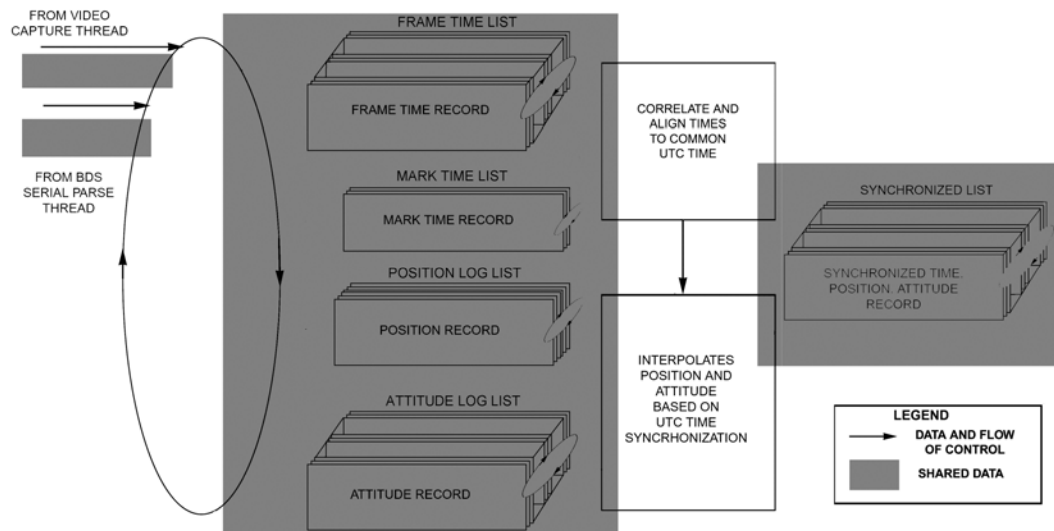


Figure 5-3: Queue / Sync. Thread Internal Structure

While the above data is being synchronized, the steps of the image processing presented in Chapter 4 are also running. This included all processing up to and including the feature extraction module shown in Figure 5-1.

5.2.3.2 Storage Synchronization

Although not shown in Figure 5-1, all received data was saved to the computer hard disk. The initial software design was to specifically capture all incoming data for the purpose of developing the remainder of the system, which also included three additional serial data streams. Therefore, the system was capturing not only the video and BDS data, but also data from two Satloc WADGPS receivers

and a Crossbow Attitude and Heading Reference System (AHRS) unit. One Satloc receiver was configured for using WAAS differential correction data and the other Satloc receiver was configured to receive and use OmniStar differential correction data. The BDS unit was internally capturing all raw GPS data for post processing purposes. The data flow and thread requirements for the BDS data capture are shown in Figure 5-4.

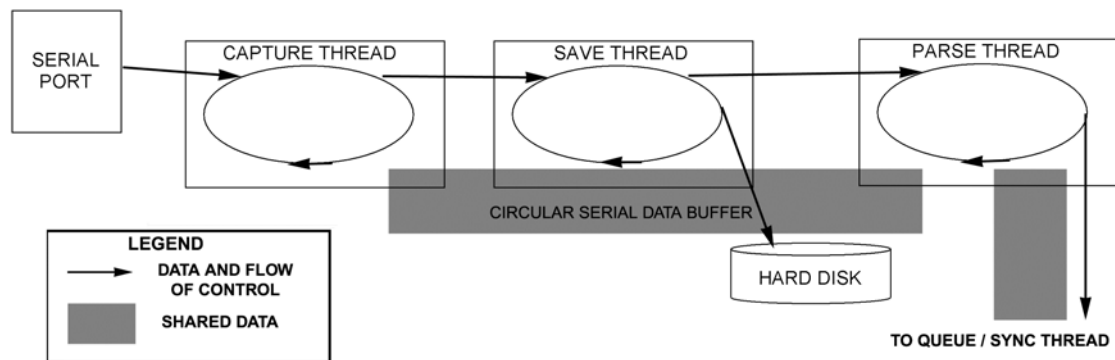


Figure 5-4: Serial Port Capture - Save - Parse Flow

The AHRS unit required a serially triggered data request to synchronize it with the video data, whereas the two Satloc receivers were not synchronized beyond the internal matching of the UTC timing to the BDS UTC time. Each of these data streams were then immediately stored to disk for later review only and used a similar thread structure as in Figure 5-4, except without the Parse thread. In order to capture all data from the serial ports, the system needed to respond or at least check the serial ports within a specific period of time, as presented in Table

5-1. The minimum check rate is how often the port must be checked to ensure no loss of data based on the buffer trigger level.

Table 5-1: Polling Rate for Serial Data

	BDS	SatLoc 1	SatLoc 2	AHRS
Comm Rate (bit/s)	230400	19200	19200	38400
Hardware Buffer	16 Byte	16 Byte	16 Byte	16 Byte
Buffer Trigger @	12 Byte	12 Byte	12 Byte	12 Byte
Min Check Rate	1920 /s	160 /s	160 /s	320 / s
Max Switch Time	1.736 ms	20.83 ms	20.83 ms	10.42 ms

There has to be significant flexibility and synchronization to allow for the BDS capture thread to be checked within 1.7 ms.

The video data required a more complex software model because of both the data rate and the proprietary software limitations. The video sequence had to be stored to disk in short frame sequences. The optimal frame storage quantity had to be determined to balance the amount of data buffered in memory to the responsiveness of the operating system and hard disk. This included a 2 Gigabyte limit on the file sizes. Tests were done to find an optimum buffer size for the storage, with results presented in Chapter 6.

5.3 System Structure and Data Flow

Each thread used in the system contained non-blocking wait functions as well as deliberate task suspension to allow for other tasks to function on a regular basis. As an example, the flow within the Capture thread is regulated and suspended as outlined in Table 5-2.

Table 5-2: Outline of Capture Thread Internal Data Flow

Wait for End of Previous Frame Grab	Allows waiting tasks to run
Thread Function: <ul style="list-style-type: none"> • Start Grab of New Frame to Buffer X • Get Frame Time and Add to Frame • Trigger Time Mark if needed • Export Frame • Transfer Buffer X data to Output Buffer • $X \neq X$ (Toggle Buffer Number) 	Double Buffering of Incoming Video: While grabbing data from one frame, Transfer other frame out of thread to Next thread.
Critical Section: <ul style="list-style-type: none"> • Increment Capture Frame Counter Leave Critical Section	Protects the synchronized data while updating it.
Release / Sleep for 1 ms	Allows waiting tasks to run
Loop back to Top	

5.3.1 Video Modules

The actual video module also consists of 6 synchronized threads (capture, prepare to save, save to disk, load from disk, play, process) as shown in Figure 5-5.

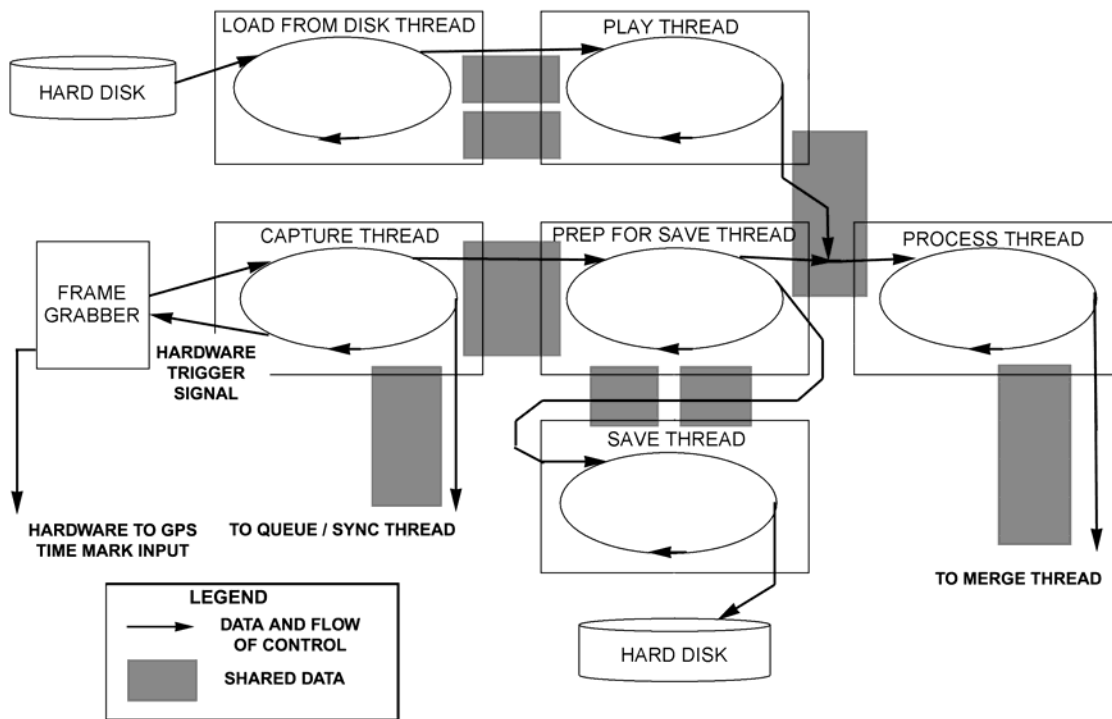


Figure 5-5: Video Module Flow

The Load from Disk and Play threads were mutually exclusive to the Capture, Prep for Save, and Save thread as they served a duplicate process of providing either stored video, or live video to the remainder of the system. The Capture thread was regulated by the incoming video signal, and the Play thread regulated the flow of the recorded video to match the recorded frame to frame times. The

Load from Disk and Prepare for Save threads either read short video sequences from disk, or organized the video into short video sequences for optimal storage size. Every video frame has one additional row of image data added to it, which is instead used to store numeric data. The frame number and computer system times are then immediately copied into this data section of each specific video frame before it was saved.

5.3.1.1 Video Processing Sub Module

The process thread encapsulates the image processing consisting of the filtering and feature tracking process initially described in Chapter 4. The final implementation of the image processing algorithms chosen was modified from this because of inherent real-time limitations of the integer or gray scale median filter used for real time, as previously presented in Section 5.1.3.

Table 5-3 lists the specific image processing functions used in the system. Note that two additional functions are included from what was presented in Chapter 4. The binary median filter function and the integer blur function were used in the final implementation due to the dramatic improvement in computational load achieved with these functions. Using the initial image processing approach outlined in Chapter 4, the computational load was proportional to the kernel filter order N and the efficiency of a Sort Operation for N^2 elements. By modifying the image processing flow as shown in Figure 5-6, the effective computational load is no longer dependent on the kernel filter order at all.

Table 5-3: Image Processing Function Computational Order

Image Processing Function	General Functional Computational Order	Optimized Functional Computational Order
Image Copy	$O(2)$	-
Image Subtraction	$O(3)$ Integer	-
Integer Median (Gray)	$O(N^2+O(\text{Sort}(N^2)))$	Dependent on Sort
Binary Median	$O(N^2)$ Logical	$O(4)$ Integer & Logical
Integer Blur	$O(N^2)$ Integer	$O(4)$ Integer
Image Thresholding	$O(2)$ Logical	-
Feature Extraction	$O(4)$ Integer & Logical	-

N - Filter Order; F - Number of Features Extracted; $O(X)$ - X pixel operations

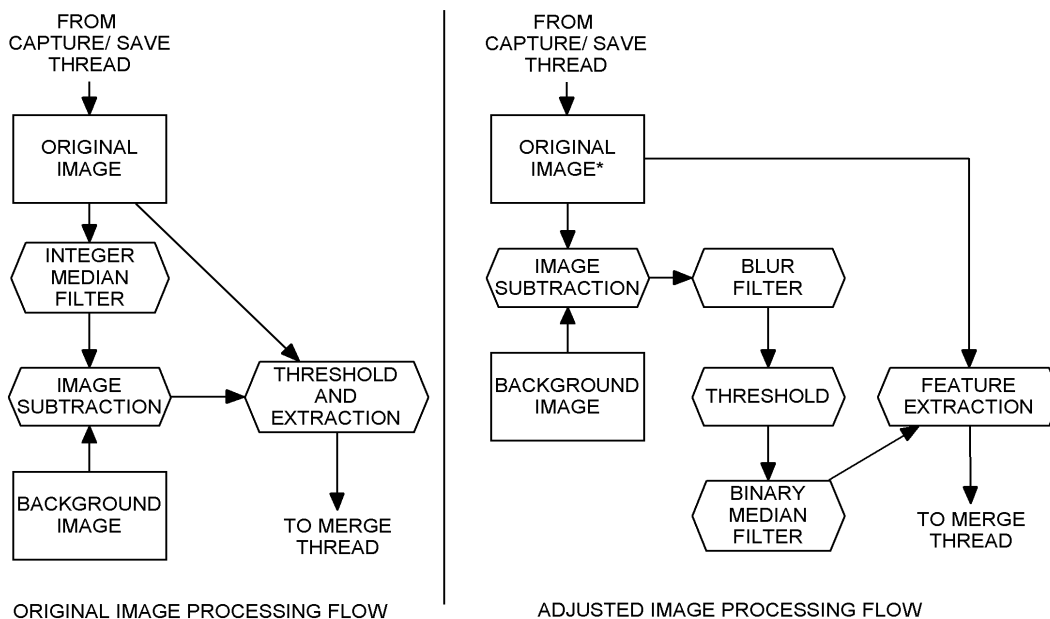


Figure 5-6: Image Processing Flow Modification

As previously discussed in Section 5.1.3, the computational order of an integer blur filter is reduced from being proportional to N^2 to having no proportionality to N at all. By changing to a binary median filter from an integer median filter, any proportionality to N is eliminated in a similar manner as with an integer blur filter. This is because it is no longer dependent on a sort operation, and is instead only counting the number of neighborhood pixels that are true. Note that by changing the local operations this way changes the final result of the image processing slightly, but in this case the change is acceptable. This makes the image processing computational load strictly dependent upon the efficiency of any programming optimizations and the processor operation speeds for logical and integer functions.

5.3.2 Remaining System Modules

The remainder of the system data flow is shown in Figure 5-7.

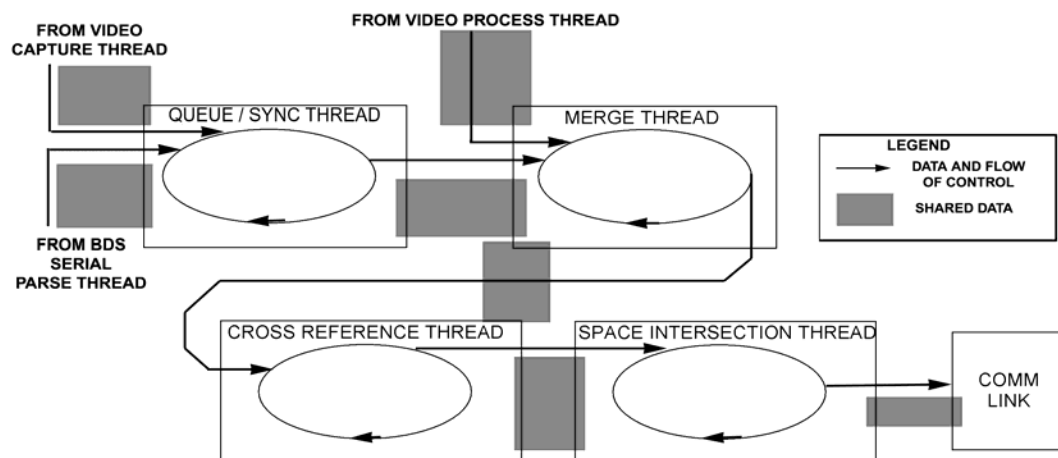


Figure 5-7: Remainder of System Data Flow Diagram

The primary difference is that the timing between these modules is not consistently required as with the previous modules, and that they will yield control to the critical modules. These modules are:

- Queue/Synchronization Thread: This thread encapsulates the entire process of merging and interpolating the position and attitude information from the BDS and the frame time information from the video capture module using the mark time data to frame time relationship as the synchronization link. It has been previously discussed in Section 5.2.3.1.
- Merge Thread: This thread, shown in Figure 5-7, simply involves matching the frame numbers, which is handled by buffering the two data streams from the video process thread and Queue/Synchronization thread through named pipes. It also includes some additional error checking to ensure that the system isn't stalled or deadlocked in this thread.
- Cross Reference Thread: This thread encapsulates the cross-referencing and tracking process previously outlined in Section 4.4.2. The internal structure of the thread is shown in Figure 5-8. Basically this thread accepts the series of possible hot spot feature data with merged position and attitude information into a frame sorted buffer to cross reference with previous feature data. Any of the features of the oldest frame cross-referenced are copied and automatically sorted into a feature track sorted buffer.

The size of the feature track buffer is a pre-allocated circular buffer that allows for a reasonable number of features. With each incoming feature for a particular track, the maximum pixel intensity is checked and recorded in the first record for that particular track. During each data import into this feature track buffer, a status count is incremented if the track did not add any new data. Once the status count exceeds a pre-set limit, there is no more data expected or possible for that particular feature track. The maximum intensity value observed for the track is tested against the minimum hot spot intensity, and any valid hot spot feature track is exported to the space intersection thread. This was previously discussed in Section 4.5.

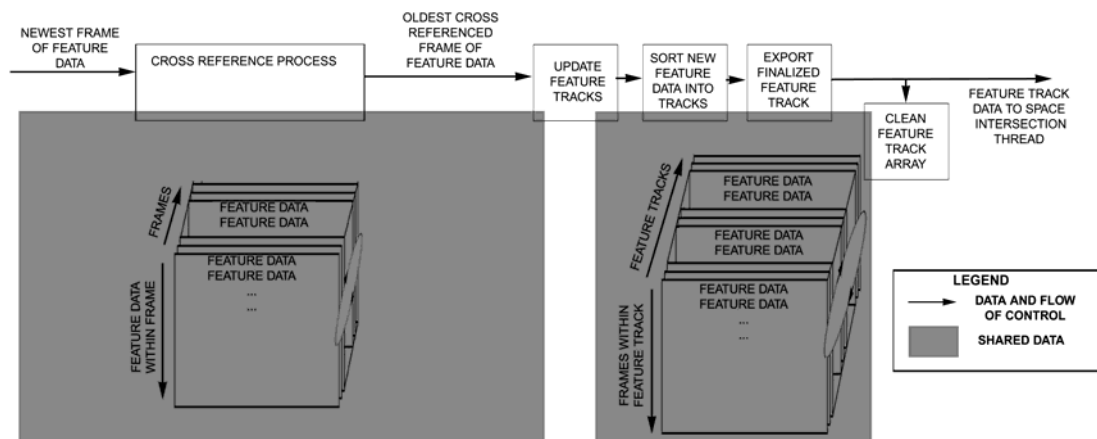


Figure 5-8: Cross Reference Thread Internal Structure

- 3D Space Intersection Thread: Once the individual hot spots have been identified, extracted, tracked and validated, the series of camera positions and image coordinates are provided to the 3D Space Intersection module

indicated in Figure 5-7. This computation has been previously presented in Section 2.4.

- **Communications Link:** The final reporting consists of maintaining a log on the system computer, and transmitting the hot spot locations via Satellite link to an internet site. This is done with a named pipe as the software transfer mechanism, such that it would be extremely easy to add this final link through an appropriate communications driver.

5.4 System Integration Summary

This chapter has presented some of the applicable terminology and background to understanding how real-time systems work, and what issues must be considered for the proper synchronization and operation of a real-time software project. Factors affecting the design of the system, such as the operating system requirement, its benefits and limitations, and the methodology selected to work with the limitations are presented. Finally, an overview of the system design is presented with a closer look at key blocks within the system to outline the operation.

Chapter 6

Tests and Results

The purpose of this research is to develop and test a real-time forest fire hot spot detection system. The various hardware and software components of the forest fire hot spot detection system have been presented previously. This chapter will provide an evaluation of the operational potential of this system, by examining the results obtained from the various subsystems. This chapter will present the system configuration and test environment, showing the equipment used, the target fires and hot spot environment. It includes an evaluation of the real-time position and attitude data to confirm the documented accuracies of the derived positions and attitude from the WAAS / OmniStar enabled WADGPS and the BDS IMU, respectively. The test results of real-time capabilities of the computer hardware and operating system will be evaluated, as well as the potential processing speed of the entire direct georeferencing process from image capture to georeferenced hot spot. Finally, this chapter will assess the accuracy of the georeferenced fires.

6.1 Equipment Configuration and Test Environment

Table 6-1 lists the hardware components utilized in the system testing and other additional hardware components. Table 6-2 lists the specifications of the

computer system used for controlling the hardware and running all the real-time software.

Table 6-1: Geo-Referencing System and Camera Mount

1: Antenna Splitter	
2: AHRS Module	
3: Mini-DV Video Camera	
4: Satloc WAAS/OmniStar Receivers	
5: Thermal Imager (10 Bit dynamic range, 320x240 image, 48.5um square pixels)	
6: The Novatel Black Diamond IMU Module	
7: The Novatel Black Diamond GPS Receiver	

Table 6-2: Critical Computer System Specifications

Dual processor 800 MHz PIII Computer: 256 Meg RAM; 80 Gig Video HDD
Matrox Genesis LC RS-422 Digital Signal Frame Grabber
Windows 2000 Professional Operating System

To test the different components and the overall accuracy of the hot spot detection system, an airborne test flight took place over controlled fires in Calgary on July 30 and 31, 2002. The controlled and monitored fires were set in

fire pits at the Bowness Park picnic area. The system was mounted in a remote sensing aircraft (aircraft and flight services provided by the Geodesy Remote Sensing Company, Calgary). Two multi-pass test flights at varying aircraft altitude took place over the test area to allow for collection of data under both day and night conditions. Table 6-3 lists the co-ordinates of the fire pits and Figure 6-1 shows two examples of the fire pits used in the test. The barbecue on the right is quite small, the pit on the left could contain a significant sized fire.

Table 6-3: Hot Spot Co-ordinates

Hot Spot	Longitude	Latitude	Height
1	-114.2215137	51.09815219	1055.507m
2	-114.221221	51.09825705	1055.594m
3	-114.2238511	51.09791932	1055.807m
4	-114.2273468	51.09760972	1056.632m
5	-114.2274524	51.09823433	1055.582m



Sample Pit: Hot Spot 1,3,4,5



Sample BBQ: Hot Spot 2

Figure 6-1: Examples of Target Hot Spots


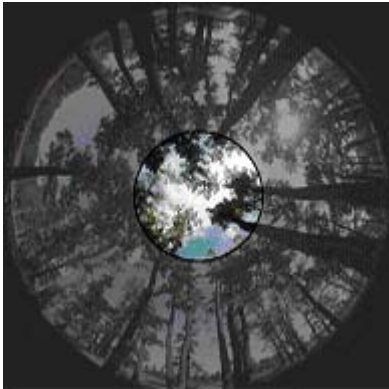
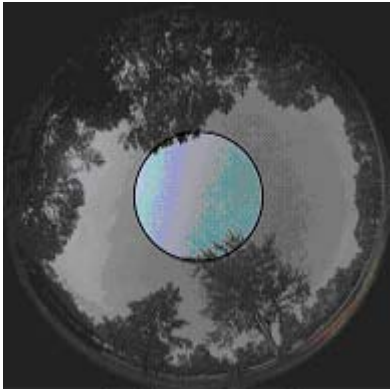
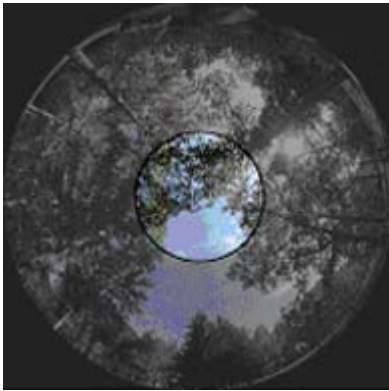
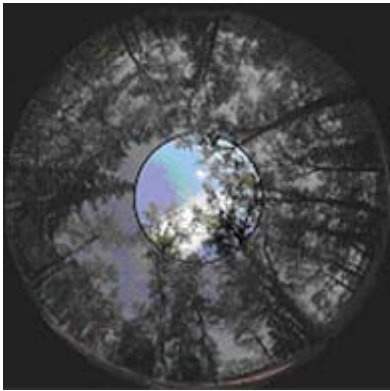
<p>These images provide a relative visualization of the overall forest canopy coverage at each hot spot observed in the tests.</p> <p>They were obtained using a 185 FOV Fisheye lens, looking straight up. Inner Black circle approximates aerial visibility and FOV.</p>	 <p>Hot Spot 1 Coverage</p>
 <p>Hot Spot 2 Coverage</p>	 <p>Hot Spot 3 Coverage</p>
 <p>Hot Spot 4 Coverage</p>	 <p>Hot Spot 5 Coverage</p>

Figure 6-2: Tree Canopy Coverage of the Test Hot Spots

The target test site was chosen for accessibility, convenience, and safety as well as to provide simple examples of obscured hot spots. Although there is some canopy coverage over all the fire pits, it is not as solid as what can occur in dense forests. Figure 6-1 shows that the targets are free of any close range coverage while Figure 6-2 shows the overall forest coverage for each possible hotspot observed in the test area. Where the sky can be seen within the inner black circle in Figure 6-2 the fire could be seen from the air.

6.2 WADGPS / IMU Results

Figures 6-3 and 6-4 show the positional accuracy of the WAAS and the OmniStar real-time positions during the two test flights. The reference trajectory for these figures is the post-processed double differenced GPS (DGPS) solution (accurate to 10 cm). The DGPS solution was derived from the University of Calgary's KINGSPAD™ software (El-Sheimy and Schwarz, 1998). The figures clearly indicate that the WAAS results are within the expected range from the WAAS system definition and other reported test results (FAA tests, 2003)(Cannon et. al., 2002). The OmniStar results are poorer than expected (OmniStar, 2003) and similar to other test results reported by Cannon (Cannon et. al., 2002).

Figure 6-5 and Figure 6-6 present the test flight trajectories in 2D indicating the different level of achieved accuracy. The most inaccurate results occur during sections of the flight with high dynamics, such as during turns. The statistical results of positional accuracies for both test flights are listed in Table 6-4. In both

flights, the WAAS derived positions were more accurate than the OmniStar results.

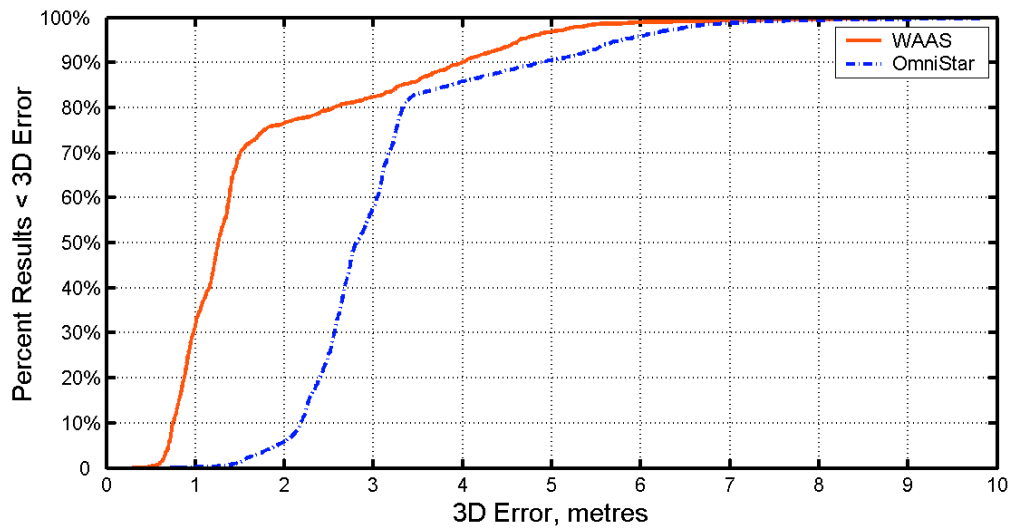


Figure 6-3: Night Flight 3D Position Error

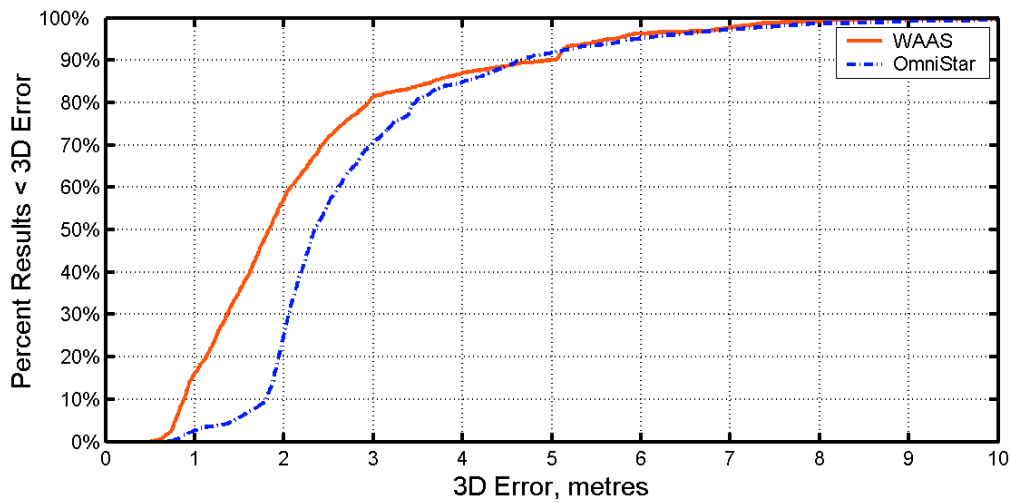


Figure 6-4: Day Flight 3D Position Error

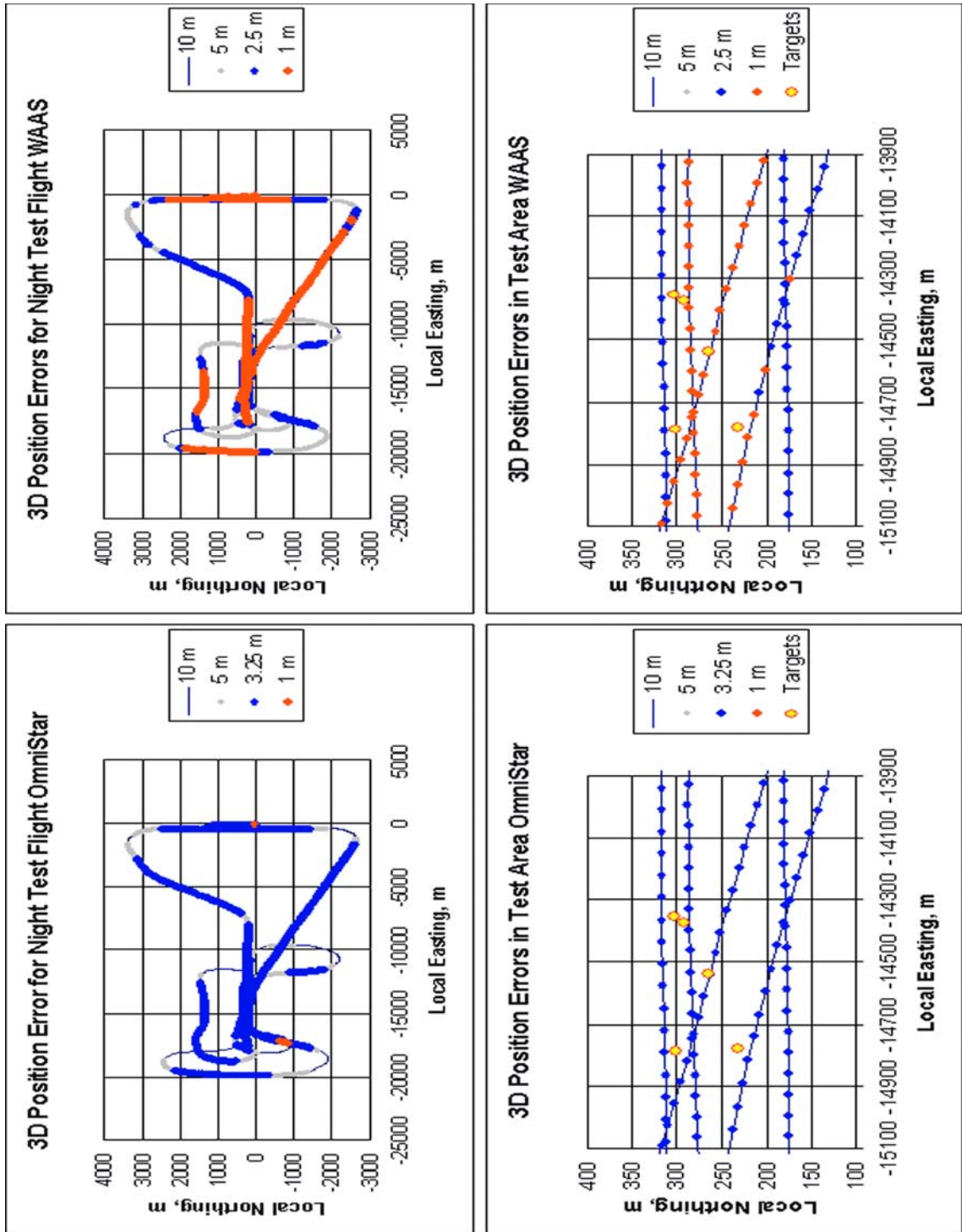


Figure 6-5: Night Test Flight Path with 3D Error Range by Location

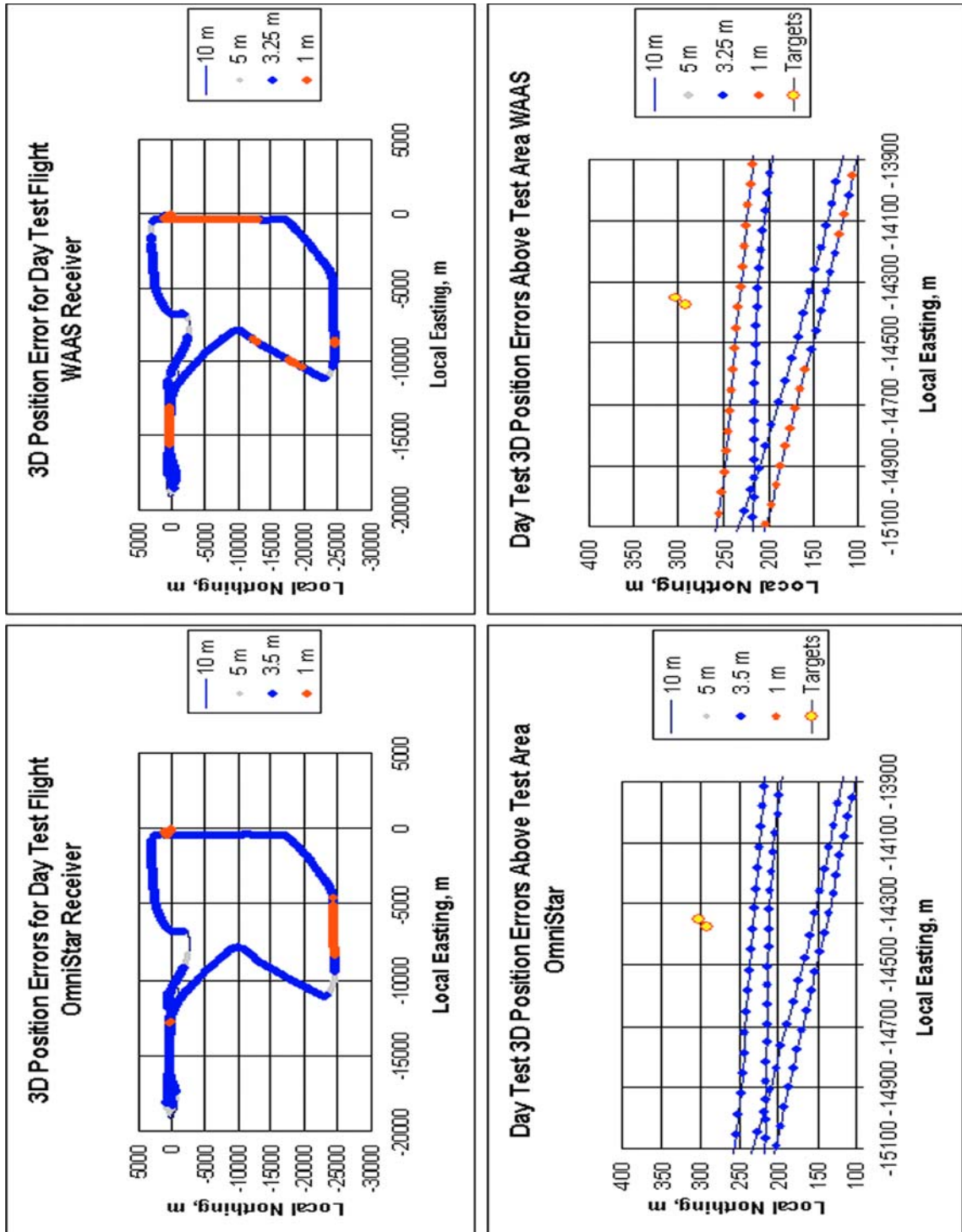


Figure 6-6: Day Test Flight Path with 3D Error Range by Location

Table 6-4: 3D Error Statistics (meter)

	Night Flight		Day Flight	
	WAAS	OmniStar	WAAS	OmniStar
Mean	1.761	3.124	2.292	2.850
min	0.294	0.715	0.504	0.706
max	8.782	10.05	12.44	12.27
Std. Dev.	1.339	1.179	1.579	1.477

Figure 6-7 and Figure 6-8 present the real-time attitude results for the two test flights. The reference attitude for these figures is the post-processed attitude derived from the University of Calgary's KINGSPAD™ software (www.kingspad.com, El-Sheimy and Schwarz, 1998). Although a first look, the real-time attitude to post-processed attitude difference is good, this is again deceptive. The actual accuracy is dependent on the quality of IMU used. These results are in fact showing how good the real-time algorithms used by the BDS system are. This is because they are so close to the post processed results.

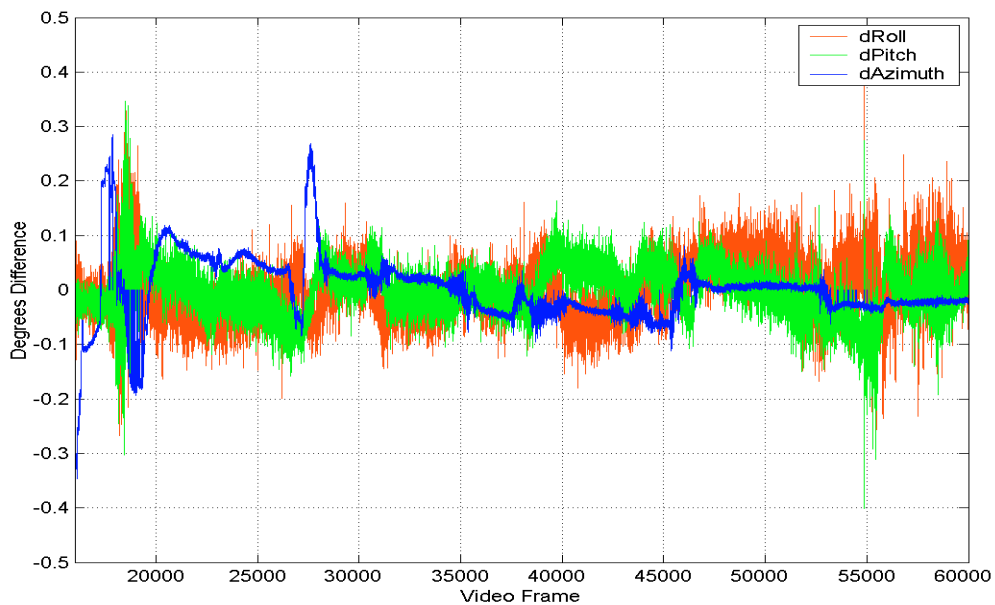


Figure 6-7: Night Flight Post Processed to Real-time Attitude Comparison

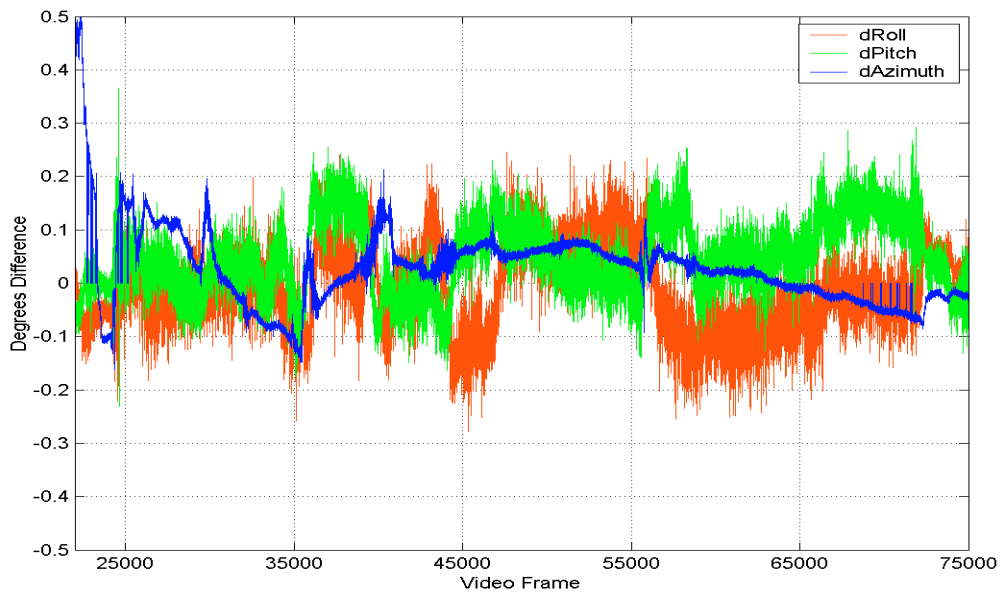


Figure 6-8: Day Flight Post Processed to Real-time Attitude Comparison

Table 6-5 lists the statistical results of the achievable attitude accuracies for both test flights. As previously mentioned, these statistics are deceptive in that they only show that the real-time attitude is close to the post-processed attitude.

Table 6-5: Attitude Error Statistics (degrees.)

	Night Flight			Day Flight		
	DRoll	DPitch	DAzimuth	dRoll	dPitch	DAzimuth
Mean	0.0007726	-0.001074	-0.0003854	-0.01007	0.04583	0.02407
Min	-0.268	-0.4011	-0.498	-0.2782	-0.2307	-0.1624
Max	0.3954	0.3471	0.2845	0.2452	0.3663	0.5495
Std. Dev.	0.4873	0.4311	0.06127	0.07139	0.06553	0.07451

6.3 Camera Geometric Calibration and Alignment Results

The process for the geometric calibration of the thermal imager was previously presented in Section 2.3.1. The standard deviation listed in Table 6-6 is deceptive, as it is dependent on the results of using the Harris corner detector to automatically detect the grid corner elements. As above, in Section 2.3.1, the calibration process uses the corner detector to pick the grid corners based on the initial input by the user, and an initial estimate of the distortion. Using the estimated distortion, the calibration software tries to determine the grid size by overlaying a grid on the image, and searches within a small range of the

estimated points to find the best corner. Where the initial estimate is off by too large a range, a false corner will be selected and used for the calibration process.

Table 6-6: Camera Calibration Results

Focal length: f:	375.9472 pixels
Principal Point: x:	151.94805 pixels
y:	118.80687 pixels
Radial Distortion Parameters:	
k1:	-0.33558
k2:	0.12022
k3:	-0.75528
Decentering Distortion Parameters:	
p1:	0.00208
p2:	0.00158

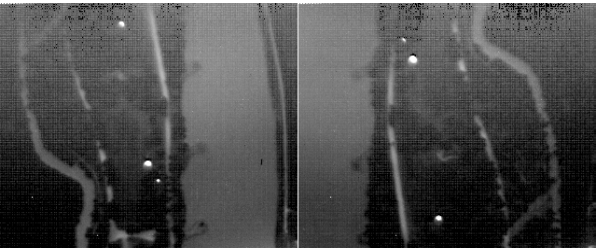
Table 6-7 lists the lever arm offset values that were determined through manual measurements.

Table 6-7: Lever Arm Offset Values

X:	Y:	Z:
-393 mm	-1130 mm	-933 mm
Measured from the GPS Antenna to the Camera		

The boresight alignment result presented in Table 6-8 was determined using images from 2 different passes over a minimum of three hot spots with known ground coordinates, using the University of Calgary's WinBundle software (Ellum, 2001). Since the targets used for this calibration are partially obscured, the actual centre of the hotspot was not readily observable. This suggests that the extracted image coordinates were not optimal. Better results can be achieved if 4 separate passes were done covering 4 quadrants of the compass, minimizing or negating the effects of any obstruction of the hot spots. However, the estimated results of the hot spots are adequate for the accuracy requirement of this research.

Table 6-8: Boresight Calibration Results with Sample Alignment Images

Roll	-177.53580 deg.	
Pitch	-0.71928 deg.	
Azimuth	-180.88616 deg.	
(41 images from 2 passes are used in the adjustment)		

A set of ground test hotspots in an open, clear area with a better geometry (points constructing either a triangle or square pattern), with 30 to 50 meters of separation would be ideal, instead of the nearly linear pattern used in this case.

6.4 Real-Time System Performance Results

The discussion presented in Chapter 5 suggests that Windows is not an appropriate OS platform for a real-time system. Nonetheless, for testing the feasibility of the forest fire hot spot detection system it proved to be adequate. Evidence supporting this will be presented below.

6.4.1 Video Sub-System Performance

Figure 6-9 shows the result of testing the time required for capturing and saving the video frames. This information is used to determine the optimum number of video frames to store during a save operation. The linearized value for the minimum storage time for the given number of frames suggests that there is a minimum start up time to save the images to the hard disk, with a relatively low amount of time needed for each frame. This indicates that a true real-time operating system would be able to achieve this storage time result with the current hardware configuration.

The Per Frame trace shown in Figure 6-9 is an average result of the testing. Although this trace is generally decreasing as the frames per save buffer increases, it also has a somewhat random behaviour. The maximum storage time trace in Figure 6-10, identifies the non-deterministic nature of Windows, in that the maximum storage time went up to nearly 10 seconds. At higher number of frames per save buffer values, the minimum save time becomes more erratic

and less deterministic. This test indicates that the hardware could support the video frame rate (29.97 frames/second) with a true real-time operating system.

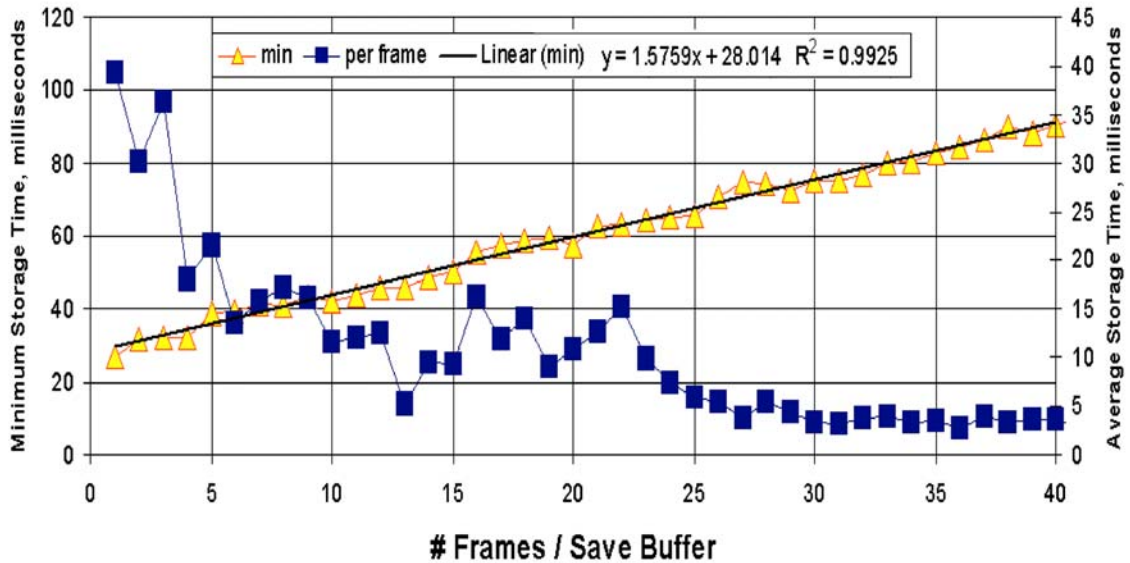


Figure 6-9: Multi-Frame Storage Test Results

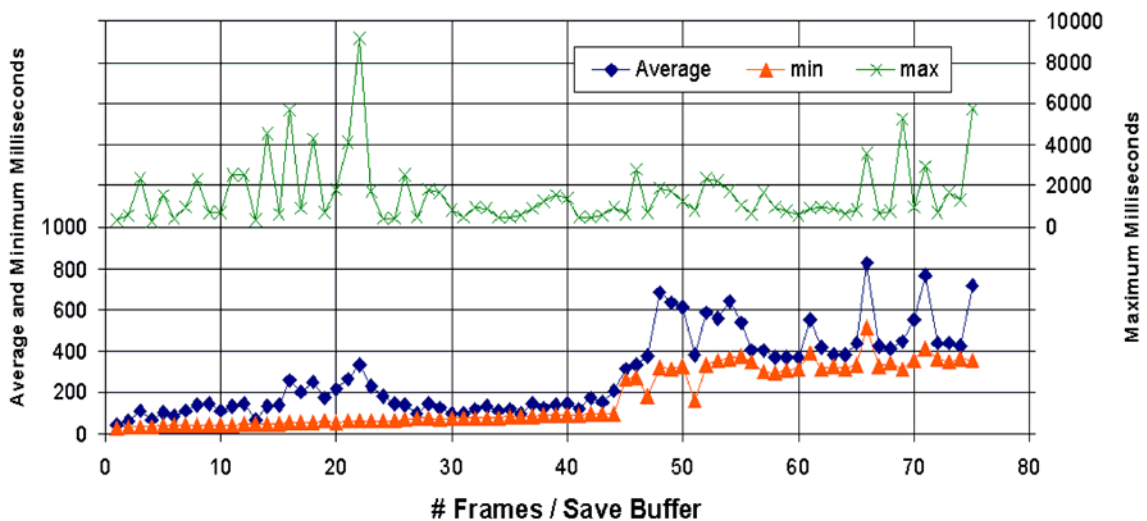


Figure 6-10: Storage Non Deterministic Behavior

The next component of this research tested the frame rate at which the system was capable of recording. Figure 6-11 highlights specific intervals during which the actual capture process was delayed. Every time a mark time signal was triggered, the actual time that the capture thread took to complete its loop exceeded the time for a single video frame. Thus, for every 10 frames, one field of the NTSC based video frame was lost. When the system was saving data, additional video fields were lost. The above two effects don't show up as a lost frame, because the computer time stamp is not applied unless a frame is captured.

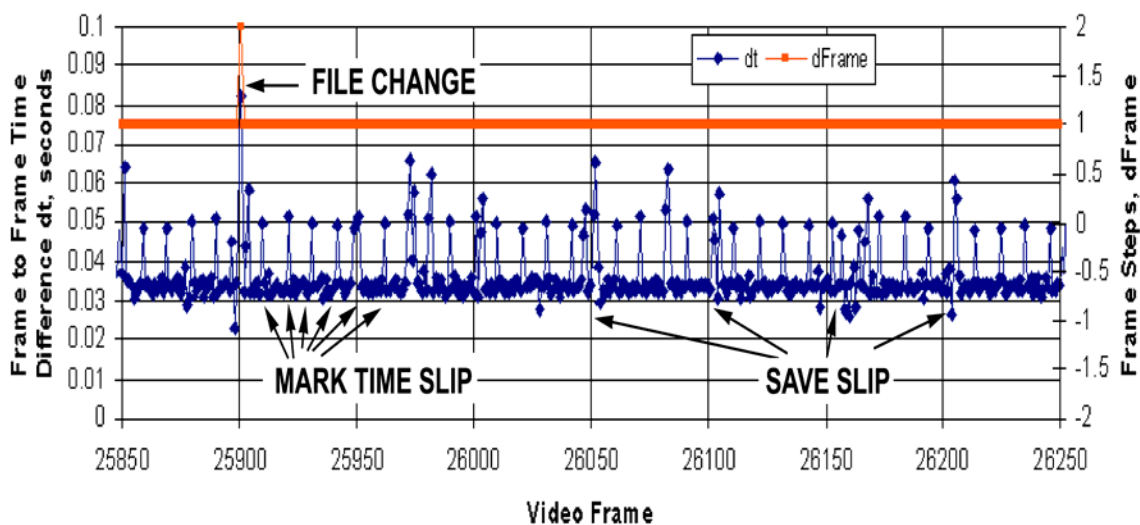


Figure 6-11: Actual Frame Times and Video Slips

Another problem that appeared was from a limitation in the software library. The video file size could not exceed 2 gigabytes. Therefore a new file was created every time the file size reached 2 gigabytes, which occurs every 12800 frames,

or just over 7 minutes. The loss of a frame when a new file is created is shown in Figure 6-11.

Figure 6-12 highlights another effect on the initial system performance of the non-deterministic behaviour of Windows. During the initial start up of the capture and save process, the system was very slow and appears to stall. Although the data was actually captured, the storage buffer was overwritten before the data was saved.

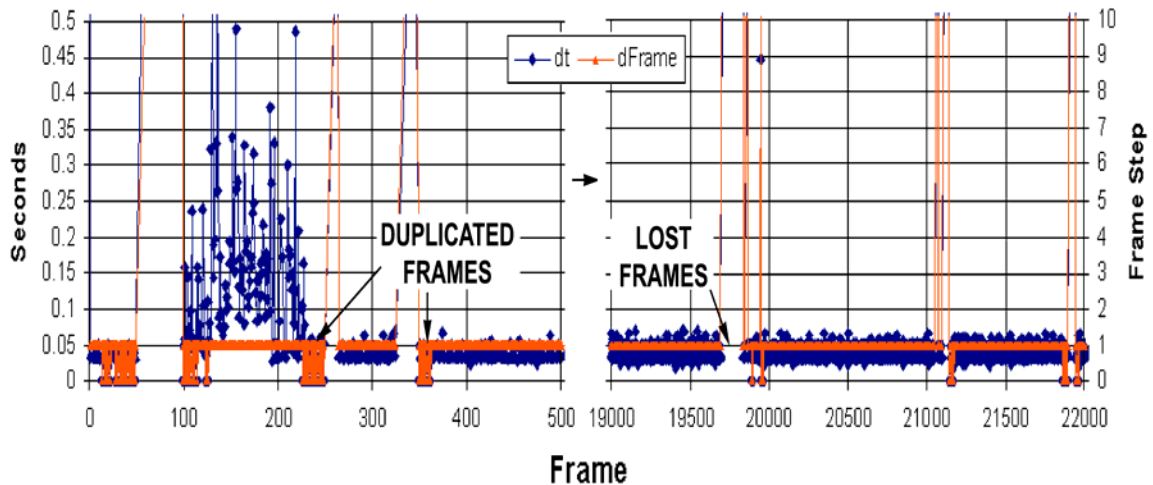


Figure 6-12: Lost and Duplicated Video Frames

This may be due to a priority inversion occurring in the Windows system, or incorrect signaling between the different modules, as the system process loading appeared to be low. The net effect of this stall is shown in Table 6-9, which lists the number of frames captured, the number lost, and the largest gap.

Table 6-9: Video Capture and Save Statistics

	Night Test Flight	Day Test Flight
Captured Frames	60999	78449
Lost Frames	393	210
Largest Gap	147	128

This inconsistent timing and capture does not represent a system failure. The mark signal was consistent which still allows for synchronization. As a result the feasibility of the system can be evaluated.

6.4.2 WADGPS/IMU Georeferencing Sub-System Capture Performance

Table 6-10 presents the capture statistics for the georeferencing data. The mark time (MT), IMU Attitude (ATT), WAAS and OmniStar (OMNI) position logs used the same time base and are automatically synchronized. The video timing signal (VTS) is based on computer time, which is different from the UTC or the GPS time. The critical link is the MT data and the VTS, as presented in Section 5.3.1.1. The MT data was the only loss that must be detected, corrected and adapted for. The WAAS, OMNI, and ATT logs are readily checked, as they are all scheduled logs. The MT must be correlated with the VTS to determine if it was lost, or if there were longer than expected intervals for the video frames.

Table 6-10: Georeferencing Sub-System Capture Statistics

	Night Test Flight (lost/total)	Day Test Flight (lost/total)
WAAS Position Log	13/2178	22/2798
OmniStar Position Log	15/2089	27/2842
IMU Attitude Log	6/111040	0/141134
Mark Time (MT) Log	0*/6106	4/7846
Video Timing Signal	393/60999	210 / 78448
* 1 MT log duplicated during Night Test when bad log received.		

As can be seen in Table 6-10, data logs of every type used by the system were lost, including the critical MT log. With appropriate error checking between the VTS and the MT Log, the lost or incorrect data is readily detectable as shown in Figure 6-13 and Figure 6-14.

When MT data is lost, it causes a dramatic offset in the difference between the GPS time and computer time relationship, as shown in Figure 6-13. The frame to frame difference of differences in Figure 6-14 becomes significantly uncorrelated, as indicated by the noise and difference between the Pre Correction and Post Correction traces. When the MT data loss is corrected for, as shown in Figure 6-13 by the Post Correction trace, the correlation of the frame to frame differences is much stronger, as indicated by less noise in the Post Correction trace.



Figure 6-13: Comparison between Video Timing Signal and GPS Mark Time

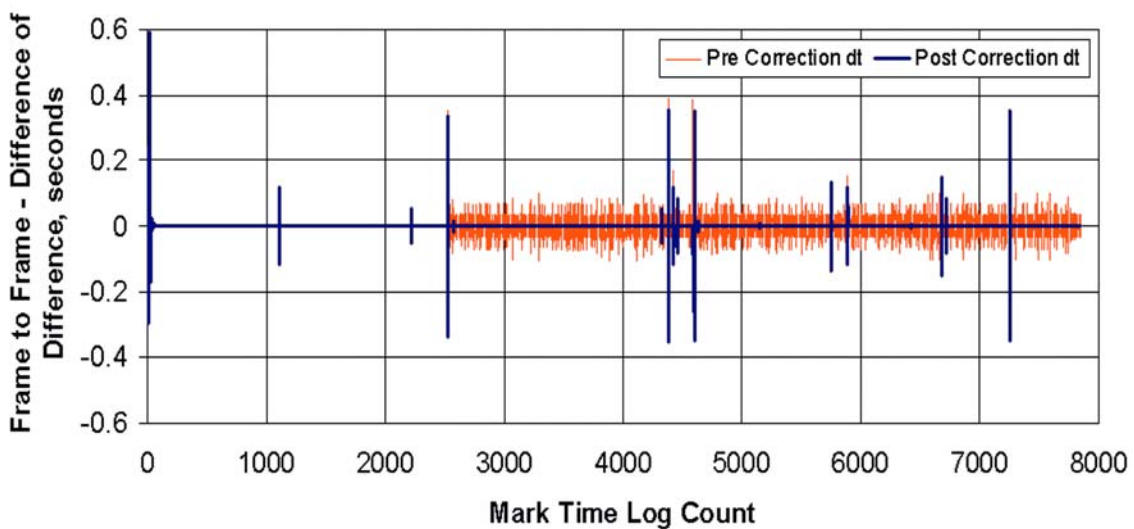


Figure 6-14: Comparison between VTS Frame to Frame Time Difference and
MT Frame to Frame Time Difference

There are also corresponding positive - negative differences in Figure 6-14 that are indications of further momentary synchronization errors; these are immediately corrected through the internal timing. The errors and subsequent corrections are possibly due to a task switch between the start of a frame capture and the triggering of the mark pulse. This delays the mark for the duration of the task switch. It causes a momentary timing and synchronization error that can be corrected, but does not appear to cause a significant error for testing the feasibility of the system.

If both MT data and the VTS data were lost during the same time frame, there would be no simple way to cross-reference and synchronize the timing signals. The timing values would need to be cross-correlated over a series of frames and MT data logs to find an offset time that matches the differences correctly. This should be avoidable in a true real-time system, and has not been tested.

6.5 Image Processing Performance

The actual image processing results presented here were generated after the test flights. They provide a reliable indicator of the performance of the hardware used. The test flights were done with the capture and save functionality as well as the threshold and feature extraction modules of the image processing active. This was to ensure the test video data was captured, as the data was needed to develop the appropriate image processing flow. Table 6-11 lists the average

image processing times for the various functions. Note that the performance tests were done using a single processor on the target system with 100% load.

Table 6-11: Image Processing Performance

Processing Function	Average ms	Processing Function	Average ms
Copy	1.958	Threshold	2.821
Basic Statistics	3.033	Binary Median Filter	10.074
Subtract Images	4.083	Feature Extraction	10.608
Blur Filter	12.669		
		Total	44.067 ms

With the implementation of the optimizations outlined in Chapter 5, the performance of the blur and binary median filter functions are completely independent of the filter order. The image processing has a significant major impact on the overall processing time. The process times in Table 6-11 demonstrates what the system's capabilities would be when the data capture modules and processing modules are integrated into a single program. This data is relevant, despite the utilization of a dual processor for the target system.

Table 6-12 lists the tracking and georeferencing software performance. Most of these functions are dependent upon the number of features involved, and have an inverse relationship to the amount of filtering in the image-processing module.

As expected, the tracking and 3D space intersection function (SI) modules have a wide variance in their time requirements. These results also suggest areas where further optimization work can be done. This is particularly true in the data cleanup function, which is keeping the memory buffers properly organized. Also, the first number of the space intersection timing result presented in Table 6-12 is an average result over every frame during that test. The function is not called at every frame, but only called when a valid hot spot feature track is identified. The second number in the Space Intersection results is the average of the result over the number of times that it was actually called. For the test pass with minimal blur and median filtering in the image processing module, the SI module was called only 63 times over the 1600 frames.

Table 6-12: Tracking and Georeferencing Performance (millisecond)

Processing Function	Min. ms	Max. ms	Average ms
Cross Referencing	1.070	4.909	2.054
Data Cleanup	4.257	9.029	5.988
Space Intersection*	1.236 / 35.333	2.392 / 60.744	1.663 / 43.694
Misc. Functions	1.660	2.227	1.841
Total	8.222	18.556	11.545

These results do not indicate how long each feature track takes to process, rather, they are looking at the average performance from minimal blur or median

filtering to strong filtering of a test sequence with both long and short feature tracks.

6.6 3D Space Intersection Results

This section will present the space intersection results generated by the system through the previous processing stages as well as the boresight alignment values determined by the method discussed in Section 2.3.2. The results in Table 6-13 for the space intersection process are extremely promising.

The results are divided into two values; a 2D horizontal error component and a vertical component to highlight the issue discussed in Section 2.3.3, related to the geometric issues on the accuracy of the estimated height. The vertical error component is generally several times larger than the 2D horizontal component. For the purpose of this system, only the 2D horizontal component is required. There are some blank cells in Table 6-13. These are due to the particular target hotspots not being detected during that pass. This is an expected result in pass 3 and 4, as their altitudes are much higher than passes 1,2 and 5. The results are divided into two values; a 2D horizontal error component and a vertical component to highlight the issue discussed in Section 2.3.3, related to the geometric issues on the accuracy of the estimated height. The vertical error component is generally several times larger than the 2D horizontal component. For the purpose of this system, only the 2D horizontal component is required. There are some blank cells in Table 6-13. These are due to the particular target

hotspots not being detected during that pass. This is an expected result in pass 3 and 4, as their altitudes are much higher than passes 1,2 and 5.

Table 6-13: Night Test Calculated Position Errors, meters Using Post Processed Georeferencing Data.

Target	Error Type	Pass				
		1	2	3	4	5
1	2D Horz.	1.8	0.4	2.8	5.3	0.1
	Vertical	7.4	7.6	16.0	16.4	9.4
2	2D Horz.	1.3	0.3 / 1.2			1.4
	Vertical	5.4	7.2/8.8			6.1
3	2D Horz.	1.4	0.6	2.7	4.7	0.5
	Vertical	7.1	6.3	18.6	18.3	6.2
4	2D Horz.	1.1	1.2			0.8/0.4
	Vertical	5.3	5.7			-2.9/-2.0
5	2D Horz.	1.5	0.8			0.9
	Vertical	7.5	2.9			3.1
Altitude		404 m	359 m	942 m	961 m	364 m

There are also results in Table 6-13 with multiple numbers. These are examples of when the target was obstructed by the trees and not seen for several frames. Therefore the second result occurred when the targets were treated as a new

feature. The actual number of frames that features were tracked across was 10 frames. This may be too low, but there is a trade off between the number of frames that features are cross-referenced, and the speed of the cross-referencing and tracking module. This is an area in which more testing and research is needed.

To evaluate the combined errors of possible boresight misalignment, the entire data set is reprocessed using the University of Calgary's WinBundle bundle adjustment software (Ellum, 2001). The boresight alignment results listed in Table 6-8 were obtained from using images which contained three or more hot spot points from the first two passes. The results in Table 6-14 use the same control points as used previously in Table 6-13 plus a set of image points from pass 5, where 3 or more hot spots were also visible. The remaining image point sets were also included, but treated as unknown tie points.

Table 6-14: Re-Calibrated Boresight Alignment

Roll	-177.559 deg.
Pitch	-0.76371 deg.
Azimuth	-180.986 deg.

The largest change was with the azimuth alignment, although it is only different by 0.1 degree. Using these new numbers for the boresight alignment does not improve the overall results for the space intersection, as shown in Table 6-15.

Some of the results listed in Table 6-15 are slightly better than the results in Table 6-13, such as Target 1 in pass 1; and some are slightly worse, such as Target 3, pass 5.

Table 6-15: Night Test Calculated Position Errors, meters Using Post Processed Georeferencing Data and Re-Calibrated Boresight.

Target	Error	Pass				
		1	2	3	4	5
1	2D Horz.	1.6	0.8	3.3	5.4	1.0
	Vertical	7.7	7.6	16.1	17.1	10.6
2	2D Horz.	1.6	0.6 / 1.5			1.1
	Vertical	5.5	7.3 / 8.7			7.3
3	2D Horz.	1.3	0.9	3.3	4.6	1.2
	Vertical	7.8	6.3	19.1	18.8	7.6
4	2D Horz.	0.9	1.4			1.6 / 1.1
	Vertical	6.0	5.7			-1.9 / -0.9
5	2D Horz.	1.3	1.2			1.2
	Vertical	7.9	3.0			4.7

Also, there is a significant difference in the accuracy of the vertical component for the results in Table 6-15 as in Table 6-13.

The final test results presented in Table 6-16 and Table 6-17 were determined using the real-time WAAS position and IMU attitude georeferencing data. The

results in Table 6-16 indicates that there is minimal effect by using the real-time WAAS positioning data and attitude data on the final space intersection results. In some cases the results are better than those obtained from the post processed data.

Table 6-16: Night Test Calculated Position Errors, meters Using WAAS Georeferencing Data and Re-Calibrated Boresight

	Pass				
Target	1	2	3	4	5
1	1.6	0.8	3.5	5.6	0.5
2	1.3	0.6 / 1.5			1.3
3	1.2	0.9	3.5	4.9	0.8
4	0.8	1.4			1.0 / 0.4
5	1.3	1.2			1.1

These results are expected as per the ground size of the pixels, which is function of the image scale. At the flying heights of the conducted tests, the image scale ranges from 1:19689 for pass 2 to 1:52705 for pass 4. At these scales, the pixel size on the ground is 0.955 m² for pass 2 and a 2.556 m² for pass 4. The estimated positioning results are similar to the pixel ground size in passes 1,2 and 5. This indicates that the results are quite good, both for the feature extraction process and the georeferencing system. The slightly larger difference

between the pixel ground size and the positioning errors during passes 3 and 4 may suggest small errors in the geometric calibration of the thermal camera.

The last component of the evaluation is the effectiveness of the system to detect hot spots during daytime operations. The initial results are a qualified success based on the two test hot spots utilized. Table 6-17 lists the test results during a day test flight. The results are again on the same level as with the night flight, and also require an additional comment. Two target fires were set in the test area, one in the small BBQ sample shown in Figure 6-1. This fire was deliberately very small and not observable with the system during this test. This confirms an expectation that a small or smouldering fire would be difficult, or impossible to detect from the air. A lower altitude test flight would have been desirable to test this further, but was not possible as the test area was within the city limits and a minimum flying height had to be maintained.

Table 6-17: Day Test Calculated 2D Horizontal Position Errors, meters

	Pass			
	6	7	8	9
Post Processed	2.4	1.7	2.1	0.5
Real-time WAAS	1.9	2.6	1.8	1.7
Altitude, m	393 m	368 m	358 m	358 m

6.7 Testing and Results Summary

This chapter has presented the results of testing the various components that comprise the forest fire hot spot detection system, under less than ideal operating conditions. Even so, the results are extremely promising. The evaluation of operating the system during the day was unfortunately limited, yet the initial results support expectations that it will work. The thermal images during other parts of the daytime test flight appear to be insensitive to reflections. Nonetheless, further testing and evaluation is needed.

Chapter 7

Summary and Recommendations

Forest fires cause extensive human and financial loss. The purpose of this research was to develop technology aimed at improving the detection of, and subsequent response times to, forest fires. The research investigated the feasibility of a real-time forest fire hot spot detection system and identified the types of fires that can be detected with a thermal imager from an airborne platform. The detection system consists of a WADGPS receiver, a strap down IMU, a thermal imager and a computer based multimedia capture system. The system allowed for the acquisition of georeferenced thermal imagery over controlled fires. The data permitted the development of effective image processing algorithms to accurately identify and locate the controlled fires. Large and small (or low-level) hot spots were observable in real time with this hardware. A simple and practical method for geometrically calibrating the thermal imager was also described and tested.

Since the initiation of this research, computer and thermal imaging technology has dramatically improved. Such improvements support the feasibility of a system to detect and georeference forest fire hotspots in real time using 30 Hz thermal video.

7.1 Conclusions

The prototype system allowed for the successful evaluation of several system components yielding several conclusions.

- WADGPS Applicability to Real-Time Georeferencing.

The WAAS and OmniStar wide area differential systems provide a simple way to achieve real-time georeferencing of video imagery to within 2 m accuracy. With speed of response more critical than absolute accuracy, these positioning systems provide the accuracy without any need for differential GPS base stations.

- Automatic Identification and Tracking of Hotspots

With careful image processing and by monitoring the spatial and temporal characteristics of hot features extracted from thermal video sequences, small hot spots can be effectively identified and tracked leading to robust and accurate real-time georeferencing of forest fire hot spots to within 2 m.

- Use of Windows 2000 Operating System for a Real-time System

It was shown that Windows 2000 definitely is not suitable for a hard real-time system. Even with its limitations, a decent evaluation for the potential real-time performance of the hot spot detection system was possible without investing in dedicated real-time operating system.

7.2 Specific Contributions

The contributions of this research are primarily in the proof of concept and feasibility for the real-time detection and georeferencing of forest fire hot spots.

7.3 Recommendations

The hot spot detection system as implemented in this thesis is very near to being functional in its current state. Once the final integration is complete, the following testing and investigations are required.

- System Repeatability and Performance

Although the testing done in this research has provided promising results, further testing is required to ensure the system can provide consistent and repeatable results and daytime hot spot detection. One factor that needs to be evaluated is the effect of large temperature variations from day to night.

- Image Processing Algorithms

Further testing and acquisition of thermal video of actual forest fires is required to finalize the actual image processing algorithms. Although the implemented image processing works very well, improvements may be possible using Fourier Transform filtering algorithms to eliminate low level image noise, and then possibly detect even lower level hot spots.

References

- ASRD Forest Protection, 2004. Alberta Sustainable Resource Development Forest Protection web page. Last retrieved from <http://www3.gov.ab.ca/srd/wildfires/fpd/index.cfm> May 21, 2004
- ASRD Wildfire Detection, 2004. Alberta Sustainable Resource Development Wildfire Detection web page. Last retrieved from http://www3.gov.ab.ca/srd/wildfires/fpd/fw_wd.cfm May 21, 2004
- ASRD Wildfire Behaviour, 2004. Alberta Sustainable Resource Development Wildfire Behaviour web page. Last retrieved from http://www3.gov.ab.ca/srd/wildfires/fpd/fw_wb.cfm May 21, 2004
- Benning, W. and Aussems, T., 1998. "Mobile mapping by a car driven survey system (CDSS)", last retrieved from http://www.gia.rwth-aachen.de/Service/download.php?fileTag=9804_iag.pdf May 21, 2004
- Blaho, G. and Toth, C., 1995. "Field experiences with a fully digital mobile stereo image acquisition system", Proceedings of 1995 Mobile Mapping Symposium, pp. 97-104, Columbus, OH, USA.
- Bouquet, J., 2004. "Camera Calibration Toolbox for Matlab", Last retrieved from May 21, 2004.
- Bouquet, J., 1999. "Visual Methods for Three-Dimensional Modeling", Ph.D. Thesis, California Institute of Technology, Pasadena, California, USA. Last retrieved from <http://www.vision.caltech.edu/bouquetj/thesis/thesis.html> May 21, 2004.
- CNFDP Area Statistics, 2003. "Area Classification by Class and Province/Territory, 1991", Canadian National Forestry Database Program, Last retrieved from http://nfdp.cfm.org/cp95/data_e/tab11e_1.htm May 21, 2004
- CNFDP Economic Statistics, 2003. "Economic Profile of the Forest Sector, 1990-2002", Canadian National Forestry Database Program. Last retrieved from http://nfdp.cfm.org/cp95/text_e/tab82em.htm May 21, 2004.
- CNFDP Expenditure Statistics, 2003. "Total Expenditures on Forest Management by Activity and Province/Territory, 1977-2002 Updated:

11/07/03", Canadian National Forestry Database Program, Last retrieved from http://nfdp.ccfm.org/cp95/data_e/tab72e_1.htm May 21, 2004

CNFDP Forest Fire Statistics, 2003. "Forest Fire Statistics by Province / Territory / Agency, 1970-2002", Canadian National Forestry Database Program. Last retrieved from http://nfdp.ccfm.org/cp95/data_e/tab31e_1.htm May 21, 2004.

Cannon, M., S. Skone, Y. Gao, Y. Moon, K. Chen, S. Crawford, G. LaChapelle, 2002. "Performance Evaluation of Several Wide-Area GPS Services", Proceedings of ION GPS-02 Conference, The Institute of Navigation, Portland, Oregon, USA, pp.1716-1725.

Douglass, Bruce Powel, 1999. "Doing Hard Time: Developing Real-Time Systems with UML, Objects, Frameworks, and Patterns". Addison-Wesley-Longman.

Ellum, C.M. and El-Sheimy, N., 2001. "A Mobile Mapping System for the Survey Community", Proceedings of The 3rd International Symposium on Mobile Mapping Technology (MMS 2001), On CD-ROM, Cairo, Egypt.

Ellum, C.M. and El-Sheimy, N., 2001. "Land Based Mobile Mapping Systems", Journal of Photogrammetric Engineering & Remote Sensing, Vol. 68, Number 1, January 2002 pp. 13 - 18.

Ellum, C., 2001. "The Development of a Backpack Mobile Mapping System", M.Sc. Thesis, Department of Geomatics Engineering, University of Calgary, Calgary, Alberta, Canada.

El-Sheimy, N., 1996. "The Development of VISAT - A Mobile Survey System for GIS Applications", Ph.D. Thesis, Department of Geomatics Engineering, University of Calgary, Calgary, Alberta, Canada.

El-Sheimy, N and Schwarz, K.P. 1998. "User Manual For KINGSPAD™ (KINematic Geodetic Software for Position and Attitude Determination) GPS/INS software". Last retrieved from <http://www.uti.ca/kingspad-manual-20-07-2000.pdf> May 21, 2004.

El-Sheimy, N., 1999. "Mobile Multi-sensor Systems: The New Trend in Mapping and GIS Applications", Geodesy Beyond 2000: The Challenges of the First Decade, Springer-Verlag Berlin., pp. 319-324. International Association of Geodesy, Symposia Volume 120.

El-Sheimy, N., 2000. "ENGO431: Analytical Photogrammetry Course Notes". Department of Geomatics Engineering, University of Calgary, Calgary, Alberta, Canada.

FAA, 2003. "WAAS Web Site". Last retrieved from <http://gps.faa.gov/Programs/WAAS/waas.htm> May 21, 2004.

FAA Tests, 2003. "Wide-Area Augmentation System Performance Analysis Report", William J. Hughes Technical Center, Atlantic City, NJ, USA. Last retrieved from <ftp://ftp.nstb.tc.faa.gov/pub/archive/REPORTS/waaspan6.pdf> May 21, 2004.

Farrell, J.A. and Barth, M., 1999. "The Global Positioning System & Inertial Navigation", McGraw-Hill, Inc., New York, New York. USA.

Graefe, G., Caspary, W., Heister, H., Klemm J., and Sever, M., 2001. "The road data acquisition system MoSES - determination and accuracy of trajectory data gained with the Applanix POS/LV", Proceedings of The 3rd International Symposium on Mobile Mapping Technology (MMS 2001), On CD-ROM, Cairo, Egypt.

Harris, C. and M. Stephens, 1988. "A combined corner and edge detector", pp. 147-151, Proceedings of Fourth Alvey Vision Conference, Manchester, UK.

Heikkilä, J. and Silven, O., 1997. "A Four Step Camera Calibration Procedure with Implicit Image Correction", IEEE Computer Society Conference on Computer Vision and Pattern Recognition (CVPR'97), pp. 1106-1112, San Juan, Puerto Rico, USA.

Holtz, Gerald C., 2001. "Common Sense Approach to Thermal Imaging". Vol. PM86. SPIE Press, Bellingham, Washington USA.

Hunter, A., 2002. " Mobile GIS as if Field Users Mattered: Small is Ubiquitous but can Speech be Recognized? " M.Sc. Thesis, Department of Geomatics Engineering, University of Calgary, Calgary, Alberta, Canada..

Jain, R., R. Kasturi, B.G. Schunck, 1995. "Machine Vision". McGraw-Hill, Inc. New York, New York.

Martell, D.L., 2001, " Chapter 15: Forest Fire Management" from "Forest Fires: Behavior and Ecological Effects", Johnson, E. A., Miyanishi, K. - Editors, Academic Press, San Diego, CA.

Krabill, W.B., Wright, C.W., et al., 2000. "Airborne Laser Mapping of Assateague National Seashore Beach", Journal of Photogrammetric Engineering & Remote Sensing, V. 66, No. 1, pp. 65-71, ASPRS.

Labrosse, Jean J., 2002. "MicroC/OS-II - The Real Time Kernel". CMP Books, Lawrence, Kansas.

LaPlante, Phillip A., A. D. Stoyenko. Editors, 1996. "Real Time Imaging: Theory, Techniques, and Applications". IEEE Press, IEEE, New York, New York.

LaPlante, P. A., 1997. "Real-Time Systems Design and Analysis - An Engineer's Handbook". 2nd Ed., IEEE Press, IEEE, New York, New York.

Li, Q., B. Li, J. Chen, Q. Hu, and Y. Li., 2001. "3D Mobile Mapping System for Road Modeling", Proceedings of The 3rd International Symposium on Mobile Mapping Technology (MMS 2001), On CD-ROM, Cairo, Egypt.

Mikhail, E. M., J.S. Bethel, J.C. McGlone, 2001. "Introduction to Modern Photogrammetry". John Wiley and Sons, Inc. New York, New York.

Morin, K. and El-Sheimy, N., 2002. "Post-mission Adjustment Methods of Airborne Laser Scanning Data.", Proceedings of the FIG/ASPRS Annual Conference, On CD-ROM, Washington, D.C., USA.

Mostafa, M., 1999., "Georeferencing Airborne Images from A Multiple Digital Camera System by GPS/INS", Ph.D. Thesis, Department of Geomatics Engineering, University of Calgary, Calgary, Alberta, Canada.

Nematron, 2003. "HyperKernel - Windows NT for Real Time Control", Last retrieved from <http://www.nematron.com/Software/HyperKernel.shtml> May 21, 2004.

O'Keefe IV, J.A. 2002., "Venturecom RTX Enabling Microsoft Windows Windows XP and Windows XP Embedded for Hard Real-Time", Last Retrieved from www.vci.com/community/RTXWhitePaper.pdf May 21, 2004.

OmniStar, 2003. "OmniSTAR: Worldwide DGPS Service". Last accessed at <http://www.omnistar.com/home.html> May 21, 2004.

Perry, S.W., Wong, H., Guan, L., 2001. "Adaptive Image Processing, A Computational Intelligence Perspective", CRC Press, Boca Raton, Florida, USA.

Petrovello, M., Cannon, M., Lachapelle, G., 2003. "Quantifying Improvements from the Integration of GPS and a Tactical Grade INS in High Accuracy Navigation Applications". Presented at ION NTM-03, Anaheim, California, USA.

Rogalski, A and Chrzanowski, K., 2002. "Infrared Devices and Techniques", Opto-Electronics Review 10(2), pp. 111-136, Warsaw, Poland.

Rothermel, R.C., 1993. "Mann gulch fire: a race that couldn't be won", General Technical Report INT-299, 10 pages, United States Department of Agriculture, Forest Service, Intermountain Research Station, Ogden, Utah, USA.

Russ, John C., 2002. "The Image Processing Handbook". 4th Ed., CRC Press, Boca Raton, Florida, USA.

Ryan, R. 2002, "Methods for LWIR Radiometric Calibration and Characterization", ISPRS WG 1/2 Calibration and Characterization: Proposed Standard Processes Technical Session, ISPRS Commission 1 Symposium, November 10-15, 2002, Denver, CO.

Salychev, O., Voronov, V., Cannon, M., LaChapelle, G., 2000. "Low Cost INS/GPS Integration: Concepts and Testing", Institute of Navigation National Technical Meeting, Anaheim, California, USA.

Shin, E.H. and El-Sheimy, N., 2002. "Accuracy Improvement of Low Cost INS/GPS for Land Applications", The US Institute of Navigation 2002 National Technical Meeting, On CD-ROM, San Diego, California, USA.

Škaloud, J., 1999. "Optimizing Georeferencing of Airborne Survey Systems by INS/DGPS", Ph.D. Thesis, Department of Geomatics Engineering, University of Calgary, Calgary, Alberta, Canada.

Škaloud, J., 1999. "Problems in Direct-Georeferencing by INS/DGPS in the Airborne Environment", Invited Paper at ISPRS Workshop on Direct versus

indirect methods of sensor orientation, Commission III, WG III/1, Barcelona, Spain.

Smith, S.M. and Brady, J.M., 1997. "SUSAN - A New Approach to Low Level Image Processing." *Int. Journal of Computer Vision*, Vol. 23(1), pp. 45-78.

Stewart, David B., 2001. "Twenty Five most Common Mistakes with Real Time Software Development", *Proceedings of 2001 Embedded Systems Conference*, San Francisco, CA, USA. Last retrieved from <http://www.embedded-zone.com/esc/mistake.pdf> May 21, 2004.

Stewart, David B., 2001. "Measuring Execution Time and Real Time Performance", *Proceedings of 2001 Embedded Systems Conference*, San Francisco, CA, USA. Last Retrieved from <http://www.embedded-zone.com/esc/mezexec.pdf> May 21, 2004.

West, L and Gregor, P, 1999."Uncooled Microbolometer Focal Plane Array Technology", *Machine, Plant & Systems Monitor*, Jan/Feb 1999, Coxmoor Publishing Company, UK

Zhang, Z., 2002. "A Flexible New Technique for Camera Calibration", *Technical Report MSR-TR-98-71*, Microsoft Research, Redmond, Washington, USA.